UNIVERSIDADE DE CAXIAS DO SUL
ÁREA DE CONHECIMENTO DE CIÊNCIAS DA VIDA
INSTITUTO DE BIOTECNOLOGIA
PROGRAMA DE PÓS GRADUAÇÃO EM BIOTECNOLOGIA

PAULA SARTORI

DESIGN AND DEVELOPMENT OF ANTIVIRAL AND ANTIMICROBIAL FILTER ELEMENTS

CAXIAS DO SUL
2025

DESIGN AND DEVELOPMENT OF ANTIVIRAL AND ANTIMICROBIAL FILTER ELEMENTS

being a thesis submitted for the degree of

Doctor of Philosophy

by

Paula Sartori

Based on a research carried out under the supervision of

Dr. Janaina da Silva Crespo

Dr. Declan M. Devine

Dr. Marcelo Giovanela

CAXIAS DO SUL

2025

Dados Internacionais de Catalogação na Publicação (CIP)
Universidade de Caxias do Sul
Sistema de Bibliotecas UCS - Processamento Técnico

S251d Sartori, Paula
Design and development of antiviral and antimicrobial filter elements [recurso eletrônico] / Paula Sartori. – 2025.
Dados eletrônicos.

Tese (Doutorado) - Universidade de Caxias do Sul, Programa de Pós-Graduação em Biotecnologia, 2025.
Orientação: Janaina da Silva Crespo.
Coorientação: Declan M. Devine, Marcelo Giovanela.
Modo de acesso: World Wide Web
Disponível em: https://repositorio.ucs.br

1. Nanopartículas. 2. Prata. 3. Grafeno. 4. COVID-19. I. Crespo, Janaina da Silva, orient. II. Devine, Declan M., coorient. III. Giovanela, Marcelo, coorient. IV. Título.

CDU 2. ed.: 620.3

Catalogação na fonte elaborada pela(o) bibliotecária(o)
Márcia Servi Gonçalves - CRB 10/1500

PAULA SARTORI

DESIGN AND DEVELOPMENT OF ANTIVIRAL AND ANTIMICROBIAL FILTER ELEMENTS

A thesis submitted in partial fulfillment of the requirements for the degree of Doctor of Philosophy in a collaborative research project between the Department of Polymer, Mechanical and Design of the Technological University of the Shannon: Midlands Midwest (TUS), Ireland, and the Biotechnology Graduate Program of Universidade de Caxias do Sul (UCS), Brazil.

Examiners:

_____

Dr. Daniel Teixeira

NTC Company, Brazil

_____

Dr. Declan Colbert

Technological University of the Shannon: Midlands Midwest, Ireland

_____

Dr. Paula Cristina Rodrigues Pascoal Faria

Instituto Politécnico de Leiria, Portugal

_____

Dr. Sidnei Moura e Silva

Universidade de Caxias do Sul, Brazil

Acknowledgements

I would like to thank Fundação de Aperfeiçoamento de Pessoal de Nível Superior (CAPES), Conselho Nacional de Desenvolvimento Científico e Tecnológico (CNPq) and the Government of Ireland International Education Scholarships (GOI-IES) for the financial support that made this research possible.

To my supervisors, Dr. Janaina da Silva Crespo, Dr. Declan M. Devine and Dr. Marcelo Giovanela, thank you for your guidance, patience and shared knowledge. I am extremely grateful for your support and the opportunities you have given me.

To NTC Company, especially Mr. Luis Augusto Steffen and Dr. Daniel Teixeira, thank you for supplying the PA6, for the technical support and partnership in this project.

To Dr. Renan Demori, thank you for all your help in the beginning of this research.

To my parents, Alcides and Rosina, you are the most selfless and strong people I have ever known, thank you for your unconditional support. Also, thank you to my sisters, Fernanda and Renata, for always being there for me.

To my partner Michel, I could not have done this without you, thank you from the bottom of my heart.

To my colleagues and dear friends, Luiza, Aline, Danielle, Jordana, Keilla, Michele and Vitória, thank you for your friendship and all the fun.

ABSTRACT

The widespread use of facemasks became a necessity during the COVID-19 pandemic caused by the SARS-CoV-2 virus. Even with the onset of vaccination, the use of masks was recommended for an additional two to ten weeks after achieving global vaccination coverage of 70-90%, due to the emergence of new variants of the virus. Facemasks are typically composed of one or more partially filtering materials, and the World Health Organization recommends a filtration efficiency of at least 95%. An added feature to enhance protection is the incorporation of antimicrobial materials, such as graphene oxide (GO) and silver nanoparticles (AgNPs), which provide additional defense against fluids potentially carrying the SARS-CoV-2 virus. Within this context, this study aimed to develop an antiviral and antimicrobial filter element for application in masks and respirators. Different polyamide 6 (PA6) formulations containing graphene oxide (GO) and silver nanoparticles (AgNPs) were prepared and processed into microfibers by solution blow spinning technique for its use as a filter element in face respirators. The resulting samples were then characterized by field emission gun-scanning electron microscopy (FEG-SEM), energy dispersion spectroscopy (EDS), ultraviolet–visible diffuse reflectance spectroscopy (UV–Vis DRS), water contact angle analysis (WCA), thermogravimetric analysis (TGA), respirability testing, and antibacterial, antiviral and cytotoxicity assays. Microbiological analyses demonstrated antibacterial activity against *Escherichia coli* and *Staphylococcus aureus*, with inhibition zones of up to 4.0 mm in disk diffusion assays and growth inhibition in liquid medium assays for the samples containing AgNPs. The samples with GO did not present antibacterial activity and were discontinued. Antiviral tests revealed efficacy against the betacoronavirus MHV-3, achieving up to a 99.9% reduction in viral particles. Additionally, cytotoxicity assays indicated initial cytotoxic effects on days 1 and 2, while some extracts exhibited no cytotoxicity by day 7, suggesting cellular adaptation to the culture medium. In general, the microfibers exhibited good dispersion and uniform AgNPs distribution, a hydrophilic character, and thermal stability, with a maximum weight loss of 2.9% attributed to the water evaporation. The sample produced with a silver nitrate concentration of 10 mmol L^{-1} (A) showed respirability levels within the expected standards established by technical regulations. Based on the dataset and the simplicity of the microfiber fabrication process, this material demonstrates suitability as a filter element for face respirators, with potential applications not only as a preventive measure in future pandemics but also in other products requiring antibacterial or antiviral performance, such as air-conditioning filters, water filters, hospital textiles, and medical dressings.

Keywords: solution blow spinning; microfibers; graphene oxide; silver nanoparticles; antiviral activity; antimicrobial activity.

LIST OF FIGURES

LIST OF TABLES

LIST OF ABBREVIATIONS AND ACRONYMS

°C – Celsius degree

AATCC – American Association of Textile Chemists and Colorists

Ag – Silver

AgNPs – Silver nanoparticles

AgNW – Silver nanowires

BUNV – Bunyamwera virus

c^* – Overlap concentration

C_∞ – Characteristic ratio

CFU – Colony forming units

CLSI – Clinical and Laboratory Standards Institute

cm – centimeter

CuNPs – Copper nanoparticles

DMEM – Dulbecco's Modified Eagle's medium

DMF – *N*,*N*-dimethylformamide

DNA – Deoxyribonucleic acid

DTG – Derivative thermogravimetry

EDS – Energy dispersive spectroscopy

EDX – Energy-Dispersive X-Ray Spectroscopy Fluorescence

EVA – Polyethylene-co-vinyl acetate

FBS – Fetal bovine serum

Fe_2O_3NPs – Iron oxide nanoparticles

FEG-SEM – Field emission gun scanning electron microscopy

GO – Graphene oxide

h – Hour

HEPA – High efficiency particulate air

HIV – Human immunodeficiency virus

ICTV – International Committee on Taxonomy of Viruses

ISO – International Organization for Standardization

kV – kilovolt

l – Bond length.

L – Liter

m – Meter

M_0 – Molecular weight of the monomer

MERS – Middle East respiratory syndrome

mg – Milligrams

MH – Mueller Hinton

MHV-3 – Murine hepatitis virus-3

MICs – Minimum inhibitory concentrations

min – Minute

mL – Milliliter

mm - Millimeter

mmol – Millimole

MPa – Megapascal

MTT – 3-(4,5-dimethylthiazol-2-yl)-2,5-diphenyltetrazolium bromide assay

M_w – Molecular weight

N_a – Avogadro's number

NaCl – Sodium chloride

NBR – Brazilian Standards (Normas Brasileiras)

NH_2 – Amino group

nm – Nanometer

P/S – penicillin/streptomycin

Pa – Pascal

PA6 – Polyamide 6

PAN – Poly(acrylonitrile)

PC – Polycarbonate

PEO – Polyethylene oxide

PLA – Poly(latic acid)

PP – Polypropylene

PPE – Personal protective equipment

PVA – Poly(vinyl alcohol)

PVDF – Polyvinylidene fluoride

R^2 – Mean-square end-to-end distance for the polymer solvent system

RNA – Ribonucleic acid

rpm – Revolutions per minute

SARS – Severe acute respiratory syndrome

SBS – Solution blow spinning

SSD – Silicon drift detector

$TCID_{50}$ – Tissue culture infectious dose

TEM – Transmission electron microscopy

TGA – Thermogravimetric analysis

UV – Ultraviolet

UV-Vis DRS – Ultraviolet-Visible diffuse reflectance spectroscopy

v/v – Volume per volume

WCA – Water contact angle

WHO – World Health Organization

wt – Weight

XRD – X-ray diffraction

ZnONPs – Zinc oxide nanoparticles

α – Flory temperature expansion coefficient

μL – microliter

μm – micrometer

SUMMARY

1 INTRODUCTION

Face masks and respirators have long been recognized as effective tools in protecting against environmental hazards. These pieces of personal protective equipment (PPE) help safeguard the respiratory system from droplets and aerosols that may carry viral particles or pollutants. The filtration efficiency of different masks against aerosols can vary significantly, as viral particles differ in size, shape and properties (TCHARKHTCHI *et al.*, 2021).

The pandemic caused by the SARS-CoV-2 virus has infected millions of people worldwide. The virus primarily spreads through respiratory fluids, prompting the World Health Organization (WHO) to recommend the use of face masks as the most effective method to reduce the risk of transmission (FORMENTINI *et al.*, 2021).

However, if masks are not resistant to microorganisms, they may pose a risk to the wearer (HIRAGOND *et al.*, 2018). Since virus-laden droplets and aerosols can settle on the mask surface, combined with the temperature and humidity conditions created during the respiratory cycle, the penetration of virus into the masks can be accelerated (TCHARKHTCHI *et al.*, 2021).

One way to enhance the protective capabilities of masks is by incorporating nanomaterials with antimicrobial properties. Among the various nanoparticles studied, such as copper (CuNPs) (MORENO-SAMANIEGO *et al.*, 2024), zinc oxide (ZnONPs) (LAHOTI; CARROLL, 2025) and iron oxide (Fe_2O_3NPs) (SHANMUGAM *et al.*, 2025), silver nanoparticles (AgNPs) are the most commonly used due to their unique physicochemical and biological properties (HIRAGOND *et al.*, 2018). Recently, graphene oxide is also being studied as a very promising antimicrobial and antiviral agent (RHAZOUANI *et al.*, 2021; SEIFI; REZA KAMALI, 2021). To preserve their reactivity and minimize their environmental release, the nanomaterials are often embedded within a matrix.

Over the past decade, techniques for manufacturing polymeric microfibers have been

significantly advanced, making them easier to scale up. Additionally, other nanoscale materials can be integrated into these microfibers to create hybrids or composites with more interesting properties. Among emerging technologies, the solution blow spinning process stands out for its cost-effectiveness and speed (DADOL *et al.*, 2020).

The solution blow spinning technique can be used to produce microfiber membranes that effectively capture micro and submicron particles. When graphene oxide (GO) and/or silver nanoparticles (AgNPs) are incorporated into these membranes, they impart antimicrobial properties, making them suitable for applications in face masks and respirators.

In view of all these aspects, the methodology proposed in this project focuses on a strategy for preventing viral and bacterial contamination, which can later be adapted for a wide range of products, including air conditioning filters, water filters, hospital textiles (such as sheets and lab coats), and even medical dressings. Therefore, this work not only presents an effective approach for developing antiviral and antimicrobial filter elements but also seeks to expand the scope of research in this field, paving the way for other innovative antiviral and antimicrobial protection systems.

1.1 GENERAL OBJECTIVE

To develop a hybrid material for use as an antiviral and antimicrobial filter element in masks and face respirators through the solution blow spinning process.

1.1.1 Specific objectives

To achieve the general objective, the following specific objectives have been defined:

a) determine the optimal concentration of polyamide 6 (PA6), graphene oxide (GO) and silver nanoparticles (AgNPs) for the production of antiviral and antimicrobial microfibers;

b) evaluate the formation of AgNPs using transmission electron microscopy (TEM);

c) produce microfibers using the blow spinning process, based on the defined composition;

d) evaluate the antimicrobial activity of the microfibers through bactericidal tests in both semi-solid and liquid media;

e) assess the antiviral activity of the microfibers;

f) investigate the cytotoxicity of the microfibers using the 3-(4,5-dimethylthiazol-2-yl)-2,5-diphenyltetrazolium bromide (MTT) assay and cell adhesion tests;

g) confirm the presence of AgNPs in the microfibers through a UV-vis reflectance spectroscopy;

h) analyze the morphology of microfibers using the field emission gun-scanning electron microscopy (FEG-SEM);

i) determine the hydrophilic or hydrophobic character of microfibers using the water contact angle (WCA) technique;

j) assess the thermal stability of the microfibers using the thermogravimetric analysis (TGA);

k) evaluate the breathability of the microfibers;

l) evaluate the performance of aging samples with antimicrobial and cytotoxic assays.

2 LITERATURE REVIEW

2.1 VIRAL INFECTIONS

Viruses are infectious intracellular parasites whose genomes consist of deoxyribonucleic acid (DNA) or ribonucleic acid (RNA). These viral genomes are responsible for their own replication and the synthesis of other viral components, using the cellular systems of host cells. Viruses depend on host cells for the biosynthesis of proteins and other macromolecules. A minimal virus consists of a genome, which contains an origin of replication, and a protein coat, known as a capsid (PELLETT; MITRA; HOLLAND, 2014).

According to the International Committee on Taxonomy of Viruses (ICTV, 2022), viruses can be categorized into two mains on their genomic content: those with RNA genomes and those with DNA genomes. Further divisions are made according to the size and structure of the capsid (icosahedral, helical or complex), whether the capsid is enveloped, and the nature of the genome (single- or double-stranded, linear or circular, segmented or unsegment). This taxonomic classification provides a framework to define the main groups of genetically distinct viruses across families (PELLETT; MITRA; HOLLAND, 2014).

Figure 1 presents a simplified diagram of the viral replication cycle. The cycle begins with entry of the virus into the host cell, which consists of several steps. Attachment proteins on the surface of virions (the infectious form of viruses) recognize and bind to specific receptors on the host cell surface. In the penetration stage, the viral envelope fuses with the host cell membranes, enabling the virus to enter. Once inside host cell, the viral capsid is degraded, releasing the viral nucleic acid, which is then available for replication and transcription (PELLETT; MITRA; HOLLAND, 2014).

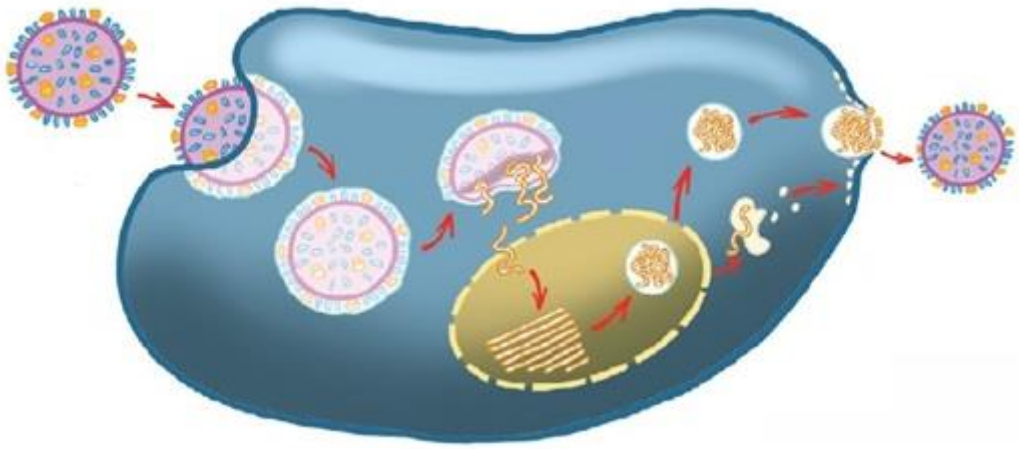

Figure 1 – Schematic representation of the viral replication cycle, illustrating the key steps from host-cell entry to release of newly assembled virions (Nogueira; Ponce, 2021)

Infectious diseases caused by viruses pose serious risks to public health and economic stability. Viral epidemics and pandemics have been recurring events throughout human history, underscoring the vulnerability of societies to such threats (ALBUQUERQUE *et al.*, 2022). Examples of notable outbreaks include the severe acute respiratory syndrome (SARS) in 2003, the H1N1 influenza pandemic in 2009, the Ebola epidemic in 2013, and most recently, the COVID-19 pandemic. These events have been classified as public health emergencies of international concern (HAN *et al.*, 2022; NGUYEN; KANNEGANTI, 2022; SONI; DINDA; KUMAR, 2022).

2.1.1 SARS-CoV-2

Viral infections pose significant threats to human health due to their widespread dissemination and ability to evolve through genetic mutations. The Coronaviridae family, commonly referred to as coronaviruses (CoVs), consists of two subfamilies: *Coronavirinae* and *Torovirinae*. Infection with a member of the *Coronavirinae* subfamily can lead to various diseases, including reproductive disorders, pneumonia, polyserositis, enteritis, hepatitis,

encephalomyelitis, nephritis, or sialodacryoadenitis (NIKAEEN; ABBASZADEH; YOUSEFINEJAD, 2020). In humans, coronaviruses are associated with a broad spectrum of illnesses, ranging from the common cold to severe respiratory diseases such as Middle East respiratory syndrome (MERS), severe acute respiratory syndrome (SARS), and novel coronavirus infections.

Recent coronavirus epidemics emerged unexpectedly and spread easily, posing significant threats to global health and socio-economic stability. For example, the SARS-CoV epidemic in 2003 infected more than 8,000 individuals and caused approximately 900 deaths worldwide. Similarly, MERS-CoV, first identified in 2012, has infected 2,494 individuals by June 2019, with a mortality rate of 34.4% (ALIZADEH; KHODAVANDI, 2020; BARTOSZKO *et al.*, 2020). In late 2019 and early 2020, cases of a novel coronavirus infection were reported. On January 7, 2020, China confirmed the discovery of a new coronavirus, later named SARS-CoV-2, responsible for causing the coronavirus disease known as COVID-19. The structure of SARS-CoV-2 is shown in

Figure 2.

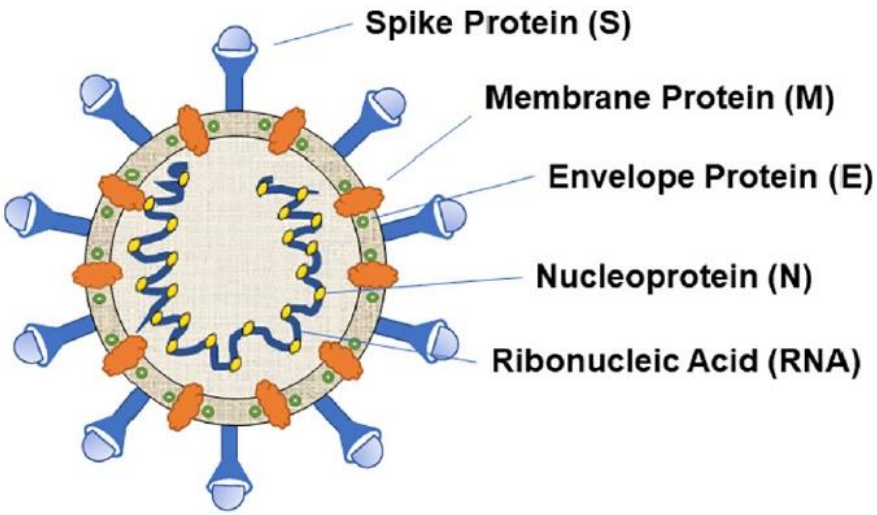

Figure 2 – Schematic representation of the SARS-CoV-2 structure, highlighting its major

structural components (Naqvi *et al.*, 2020)

On March 11, 2020, the WHO declared the SARS-CoV-2 outbreak a pandemic. Although the pandemic officially ended in May 2024, new cases and deaths continued to occur. By June 2025, over 775 million cases and more than 7.1 million deaths had been reported globally due to COVID-19 (WHO, 2024). The highest number of cases and deaths were recorded on the American and European continents. **Figure 3** illustrates the number of deaths reported to WHO between March 2020 and October 2024.

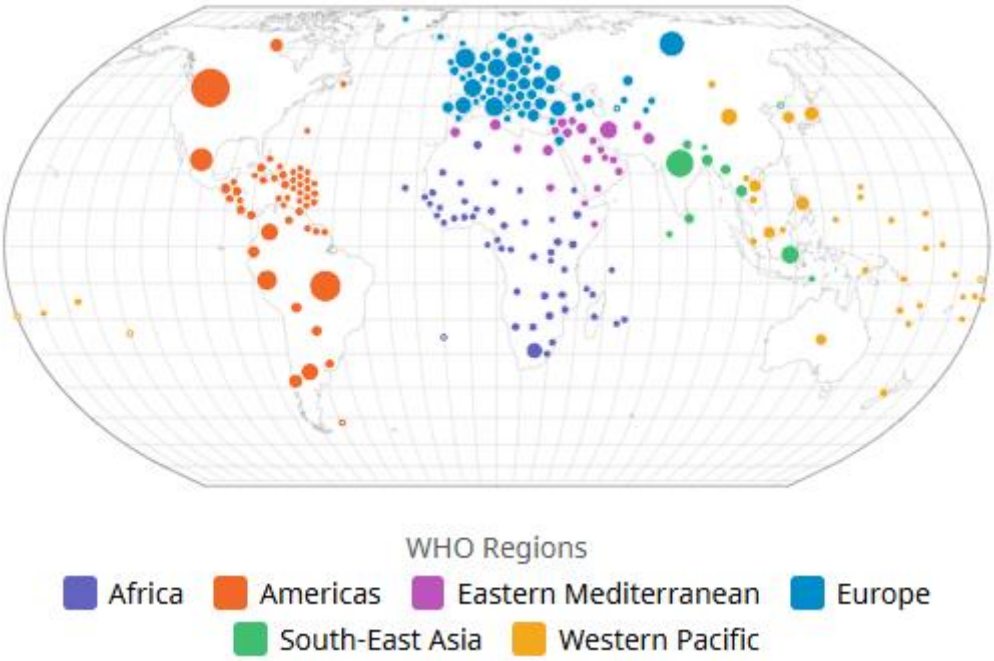

Figure 3 – Number of COVID-19 deaths reported to WHO from March 2020 to October 2024

Some precautions became essential to prevent the spread of the virus and protect healthcare professionals as well as the general population. These measures included frequent hand hygiene, social distancing, and the use of face masks. Even after the vaccines became available, a significant portion of the population did not complete their vaccination schedules.

By December 2023, 67% of the global population had received a complete primary series of a COVID-19 vaccine (**Figure 4**), while 32% has received at least one booster dose (WHO, 2024). Consequently, the use of personal protective equipment (PPE), such as face masks, remained crucial for a prolonged period, even for vaccinated individuals.

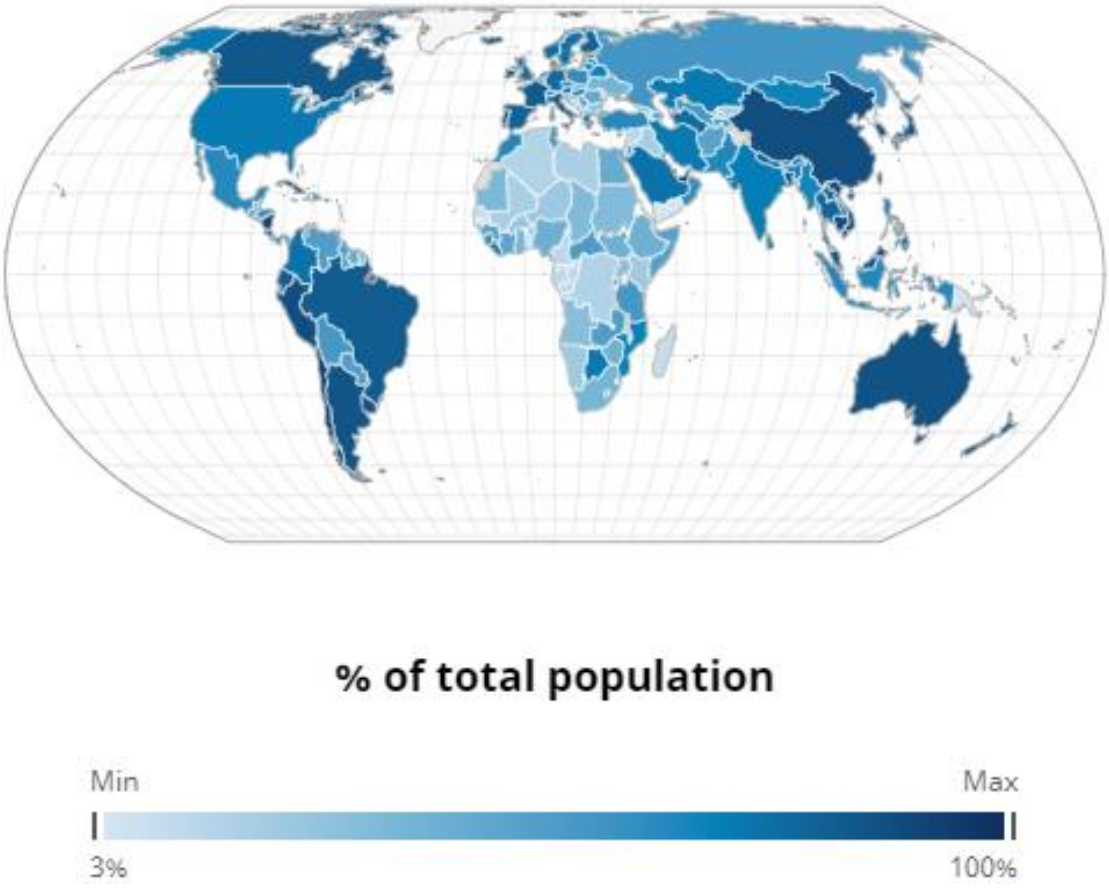

Figure 4 – Percentage of the world population vaccinated with a complete primary series of a COVID-19 vaccine by December 2023

A study using computer modeling highlighted the importance of continuing face mask use for 2 to 10 weeks after achieving the target of complete vaccination coverage (70-90%). The study considered factors such as the cost-benefit of mask usage compared to hospital and insurance costs and emphasized the reduction in hospitalization and mortality rates through the continued use of masks. Additionally, emergence of new variants, which may be more

transmissible and potentially diminish vaccine effectiveness, underscores the critical role of masks in mitigating the spread of infection (BARTSCH *et al.*, 2022).

2.2 FACE MASKS

The use of face masks significantly contributes to controlling infectious diseases such as COVID-19 (MA *et al.*, 2020; MORAIS *et al.*, 2021). They serve dual purposes: preventing healthy individuals from contracting the virus and limiting transmission from infected individuals (WHO, 2022).

Different types of face masks are classified according to their filtration efficiency. Respiratory protection devices, commonly known as N95 or PFF2 masks, offer the highest filtration capacity. These masks are designed to filter at least 95% of airborne particles and fit snugly to the user's face. Typically, they comprise four layers: a non-woven layer that filters particles as small as 0.5 μm, an activated carbon layer that removes chemicals, and a cotton layer that filters particles up to 0.3 μm, and another non-woven fabric layer (LI *et al.*, 2021).

Surgical masks, on the other hand, are intended to block large respiratory particles during routine procedures but are less effective against smaller particles. These masks usually consist of three layers, with a filter layer placed between two non-woven fabric layers (LI *et al.*, 2021; PALMIERI *et al.*, 2021). A metal or plastic nose clip at the top allows adjustment around the nasal bridge, minimizing gaps between the mask and the user's face to reduce particle entry and leakage (LI *et al.*, 2021).

For non-professional use, fabric masks and other improvised options became widespread, particularly during the early stages of the COVID-19 pandemic when N95 and surgical masks were in short supply. Although these masks are less effective against aerosols, their use still plays an important role in reducing virus spread, especially when combined with preventive measures such as social distancing and frequent hand washing (LI *et al.*, 2021).

The filtration efficiency of different masks available in Brazil was assessed by Morais

et al. (2021). **Table 1** summarizes the key findings from their study. Some of these masks are presented in **Figure 5**.

Table 1 – Filtration efficiency of different masks available in Brazil

Type of mask	Filtration efficiency (60-300 nm)
N95	0.98
Surgical masks	0.89
Non-woven masks	0.78
Non-woven masks (3 layers)	0.87
Non-woven masks (5 layers)	0.91
Cotton	0.40
Combined fabrics	0.83
Neoprene	0.78
Laminated polyurethane foam	0.25
Microfiber	0.51
70% polyester, 30% resin	0.12

Figure 5 – Different types of face masks: N95 (A), surgical (B), cotton (C) and neoprene (D)

One study found that many N95-type face masks tested were not water-repellent, significantly reducing their protective effectiveness when moistened by accidental splashes of patients' blood, bodily fluids, sweat, or respiratory droplets. If the surface of the mask becomes contaminated with infectious agents, microorganisms can penetrate the protective layers along with droplets (LI *et al.*, 2006).

Respiratory droplets vary in size, with aerosols specifically comprising droplets smaller than 5 μm. Larger droplets (> 5 μm) tend to settle within 1–2 m due to gravitational forces, whereas aerosols, being smaller and lighter, can remain airborne for extended periods, increasing the likelihood of viral transmission (EL-ATAB *et al.*, 2020). Consequently, the use of face masks acts as a physical barrier, reducing exposure to respiratory droplets. However, inadequate filtration properties can compromise their protective efficacy.

The SARS-CoV-2 virus, classified as betacoronavirus, has an elliptical or spherical shape with a size range of 60–140 nm (EL-ATAB *et al.*, 2020; ZERAATI *et al.*, 2021), which confirms the need for developing masks with enhanced filtration capabilities to effectively block viral particles of this scale.

In response to the COVID-19 pandemic, substantial research has been conducted to improve mask performance by incorporating nanoparticles. These innovations aim to enhance antiviral activity, filtration efficiency, and breathability (PALMIERI *et al.*, 2021). Nanoscale materials are of particular interest due to their antiviral properties, which are primarily attributed to their high surface-to-volume ratio and multivalent interactions. These characteristics enable them to interfere with viral binding, block viral entry into cells, or deactivate viral particles (CHEN; LIANG, 2020; CHEN *et al.*, 2016).

In this context, Nanotechnology has attracted significant attention across various fields, including medicine, agriculture, and biosensing. Its applications in medical science are extensive, ranging from gene therapy, controlled drug delivery systems, and imaging to

artificial implants and biosensors for detecting pathogens. Additionally, nanotechnology is being used to treat or diagnose cancer and develop potent agents against viral, bacterial, and fungal infections (HUSSAIN *et al.*, 2019; NIKAEEN; ABBASZADEH; YOUSEFINEJAD, 2020; USKOKOVIĆ, 2020).

Silver nanoparticles (AgNPs) have demonstrated antimicrobial efficacy against bacteria and viruses, attributed to their high surface-area-to-volume ratio and distinctive chemical and physical properties. Studies have confirmed the antiviral activity of AgNPs against a range of viruses, including human immunodeficiency virus (HIV), hepatitis B virus, herpes simplex virus type 1, respiratory syncytial virus, monkeypox virus, Tacaribe virus, and influenza A virus (WIELER *et al.*, 2023). The antiviral mechanism of AgNPs involves physical interactions with viral particles, where nanoparticles bind to and deactivate viruses, thereby blocking their activity or entry into host cells (ALLAWADHI *et al.*, 2021; WIELER *et al.*, 2023). Several factors influence the antiviral efficacy of AgNPs, such as their size, shape, and the capping agents used in the synthesis. Previous studies indicates that AgNPs smaller than 10 nm are most effective, with spherical shape particles outperforming tubular or aggregated forms (CHEN *et al.*, 2016).

Another nanomaterial that has stood out is graphene oxide (GO). GO-based nanomaterials have emerged as promising candidates for a wide range of applications, particularly in the medical and electronic fields, due to their unique physicochemical characteristics. These include a high surface-to-volume ratio, surface charge, size, shape, and notable optical, electronic, and biological properties. GO's strong negative surface charge enables interactions with positively charged viruses, which contributes to its notable antiviral activity. Furthermore, both GO and graphene are capable of neutralizing viruses through several mechanisms, such as inhibiting viral attachment, promoting photodegradation, causing electrostatic trapping, and directly inactivating viral particles (RHAZOUANI *et al.*, 2021;

SEIFI; REZA KAMALI, 2021).

The integration of graphene-based materials with AgNPs has emerged as a powerful strategy in the development of multifunctional nanocomposites for biomedical applications (UNNIKRISHNAN *et al.*, 2024). The antibacterial activity of GO arises from a combination of physical interactions, including membrane disruption caused by its sharp edges, and chemical mechanisms associated with oxidative stress mediated by reactive oxygen species (ROS) (BADONI; PRAKASH, 2024). However, these effects can be significantly enhanced by anchoring metallic nanoparticles, especially silver or silver oxide, onto GO sheets. The combination not only prevents nanoparticle agglomeration but also mitigates GO restacking, preserving the physicochemical properties of both components (CHAUDHARY *et al.*, 2024; UNNIKRISHNAN *et al.*, 2024).

The integration of AgNPs into GO matrices results in nanohybrids with enhanced antibacterial activity compared to either AgNPs or GO alone, due to enhanced ROS generation, physical membrane disruption, and sustained release of silver ions (BENTEDLAOUTI; BELOUATEK; KEBAILI, 2024; CHAUDHARY *et al.*, 2024). These synergetic effects have been confirmed by significantly reduced minimum inhibitory concentrations (MICs) and larger inhibition zones in comparison to GO or AgNPs alone. For instance, Sharma *et al.*, (2021) demonstrated that GO/AgNP-impregnated polyacrylonitrile nanofibers exhibited effective antibacterial activity and potential use in filtration devices due to their high surface interaction with microbes. Similarly, Saeidi *et al.* (2024) found that Ag/$Co_3V_2O_8$-GO nanocomposites exhibited enhanced efficacy against multidrug-resistant strains such as *Pseudomonas aeruginosa* and *Staphylococcus aureus*, further confirming the utility of GO as a delivery platform for metallic antimicrobials. In summary, the convergence of GO and AgNPs results in a multifunctional, biocompatible, and highly efficient antibacterial platform. The combined mechanical robustness of GO and the potent antimicrobial activity of silver nanoparticles hold

significant promise for applications ranging from wound healing dressings to biomedical device coatings and air filtration membranes (CHAUDHARY *et al.*, 2024; SHARMA *et al.*, 2021; UNNIKRISHNAN *et al.*, 2024).

To optimize the application of AgNPs and GO, they are typically embedded within a matrix, which enhances their reactivity and reduces the risk of environmental release. Such release could pose environmental and health hazards. For face masks, polymeric microfiber matrices serve as ideal supports due to their high porosity. This structural feature promotes greater contact between AgNPs, GO and airborne particles, enhancing the overall filtration efficiency and antiviral effectiveness.

2.3 POLYMERIC MICROFIBERS

Polymeric microfibers have attracted much attention due to their advantageous properties, including lightweight construction, small diameters, controllable porous structures, and a high surface-to-volume ratio. These characteristics make them ideal for various applications, such as sensors, functional materials, tissue engineering, protective clothing, and filtration systems (MONSORES *et al.*, 2022).

Polymeric micro and nanofibers can be produced from synthetic and natural polymers, giving them a wide range of tunable physicochemical properties. When associated with functional nanocomponents, such as metal nanoparticles, metal oxides, or organic compounds with biological activity, these fibers become promising platforms for applications that require continuous antimicrobial and antiviral action, such as face masks, hospital gowns, air filters, and smart dressings (EL-SEEDI *et al.*, 2023; MALISZEWSKA; CZAPKA, 2022). The morphology and properties of the fibers are highly dependent on parameters such as polymer concentration, solution viscosity, relative humidity, and ambient temperature. Modifications in the equipment configuration, such as the use of multiple needles and rotating collectors, have

been explored to improve the uniformity, alignment, and production rate of the fibers (EL-SEEDI *et al.*, 2023; MILAZZO *et al.*, 2020; PALANI *et al.*, 2024).

The polymers used in the production of micro and nanofibers can be classified into two broad categories: natural and synthetic. Natural polymers, such as gelatin, chitosan, collagen, cellulose and their derivatives, are widely used due to their biocompatibility, biodegradability and intrinsic biological activity. However, their processability can be limited by factors such as solubility and thermal stability (CHEAH *et al.*, 2023). On the other hand, synthetic polymers such as poly(lactic acid) (PLA), poly(caprolactone) (PCL), polyurethane (PU), and polyethylene oxide (PEO) present excellent processability and stability, but may lack biological functionality (ALOSAIMI *et al.*, 2023; PALANI *et al.*, 2024).

Vitchuli *et al.* (2010) developed protective clothing material against chemical and biological warfare agents using electrospinning PA6 fibers supported directly on nylon or cotton fabrics. The resulting material demonstrated aerosol filtration efficiency on the micrometric scale exceeding 250% when the PA6 fiber layer was deposited on the fabric.

Lee (2009) produced polypropylene (PP) fibers embedded with zinc oxide nanoparticles via electrospinning, supported on cotton fabric. The resulting laminated fabrics provided bacterial protection and ultraviolet radiation shielding, achieving a UVA and UVB protection level of 40.

Zhang *et al.* (2020) created multilayer poly(vinyl alcohol) (PVA) membranes by electrospinning, achieving filtration efficiency between 99.3% and 99.9% for NaCl and 99.4% to 99.8% for bis(6-methylheptyl) decanedioate aerosols. These membranes also exhibited lower airflow resistance compared to N95 face masks commonly used by healthcare professionals.

Wang *et al.* (2022) developed a nanofiber membrane for face masks using electrospinning with a highly diluted poly(lactic acid) (PLA) solution. The material was designed for high porosity, small pore size, good mechanical properties, and hydrophobicity.

Compared to commercial masks, it showed superior filtration efficiency (99.996%) and reduced weight. Furthermore, the membrane was biodegradable, fully decomposing within 150 days in soil.

Park *et al.* (2021) fabricated poly(acrylonitrile) (PAN) microfibers via electrospinning and incorporated silver nanowires (AgNW) using electrospray, creating an air filter with antimicrobial properties. The resulting product demonstrated filtration efficiencies of 98.3% and 99.6% and significant antimicrobial activity against various bacteria.

Cheng *et al.* (2018) produced films with PP, PA6 and AgNP microfibers using electrospinning. The AgNPs were evenly distributed throughout the microfibers, providing up to 100% inhibition of Gram-negative and Gram-positive bacterial growth, depending on the AgNP concentration. Similarly, Shi *et al.* (2011) developed PA6 nanofibers with AgNPs, observing analogous antimicrobial effects.

One of the most promising strategies in the development of advanced polymeric fibers is the incorporation of functional nanocomponents with antimicrobial and antiviral properties. These nanomaterials can be introduced into the polymer matrix by different routes, such as direct dispersion in solution, post-production surface immobilization, or by hybrid methods that combine chemical and physical functionalization (ALOSAIMI *et al.*, 2023; MALISZEWSKA; CZAPKA, 2022; PALANI *et al.*, 2024).

The use of nanofibers with antiviral activity has proven particularly relevant in response to recent pandemics, such as COVID-19, where barrier materials with active properties against respiratory viruses have become essential. Fibers containing nanoparticles of silver, copper or metal oxides showed significant reduction in viral load as well as antimicrobial properties (KUBO *et al.*, 2022; SALAM *et al.*, 2021).

Although electrospinning is widely recognized as the most established technique for the production of polymeric micro and nanofibers, it has limitations that may restrict its application

in industrial contexts, such as low productivity, the need for a high electric field, and restrictions on the use of polymers and solvents with certain dielectric properties. In view of this, alternative methods have been proposed, with emphasis on the solution blow spinning (SBS) process, which has established itself as a promising technology due to its simplicity, versatility, and potential for large-scale production (RODRIGUES *et al.*, 2024).

2.3.1 Blow spinning process

Medeiros *et al.* (2009) were the first to develop and report the blow spinning process as an alternative method to obtain polymeric micro- and nanofibers compared to those obtained by the electrospinning and melt blowing techniques. Since then, the blow spinning process has emerged as a promising microfiber production technique due to its simplicity, high productivity, and versatility. The conventional setup for blow spinning, illustrated in **Figure 6**, consists of concentric nozzles with an infusion pump, a pressurized gas source, and a collector (DOS SANTOS *et al.*, 2020).

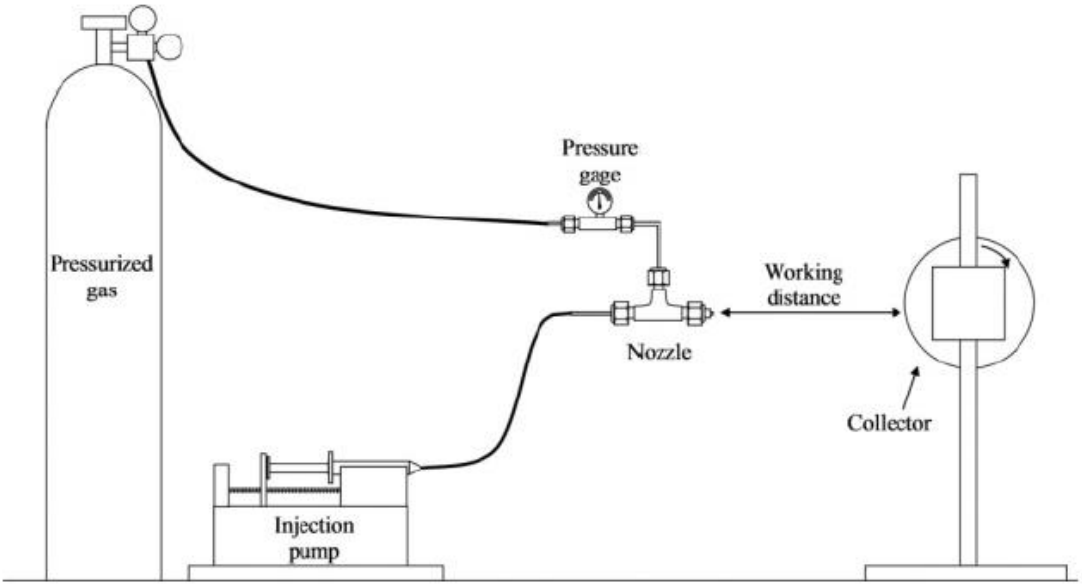

Figure 6 – Basic configuration of the solution blow spinning process (Medeiros *et al.*, 2009)

This technique relies on two parallel concentric fluid flows: a polymer solution dissolved in a volatile solvent and a pressurized gas surrounding the polymer solution. These flows are efficiently combined using a commercial airbrush, offering a cost-effective and accessible approach (DADOL *et al.*, 2020; DARISTOTLE *et al.*, 2016).

During the process, the polymer solution is delivered through the inner nozzle, forming a droplet at its tip. A high-pressure gas flows through the external nozzle, stretching the droplet. Once the aerodynamic forces exceed the surface tension of the polymer solution, the droplet is released and elongated, while the solvent rapidly evaporates. This results in the formation of a web of microfibers that can be deposited on virtually any target substrate (DADOL *et al.*, 2020; DARISTOTLE *et al.*, 2016; DOS SANTOS *et al.*, 2020).

The formation of polymeric fibers with the blow spinning technique is explained by the entanglement of polymer chains, which requires a minimum concentration of the solution, known as the overlap concentration (c^*). When this concentration is reached, the viscosity of the solution is increased due to the interaction between the polymer chains and can overcome the surface tension (DADOL *et al.*, 2020; DARISTOTLE *et al.*, 2016; GAO *et al.*, 2021). c^* can be estimated with **Equation 1**.

$$c^* = \frac{6^{3/2} M_w}{8 N_a \langle R^2 \rangle^{3/2}} \quad \textbf{(1)}$$

M_w is the molecular weight, N_a is the Avogadro's number and R^2 the mean-square end-to-end distance for the polymer solvent system. R^2 can be calculated with **Equation 2**.

$$R^2 = \alpha^2 C_\infty \left(\frac{2M_w}{M_0}\right) l^2 \quad \textbf{(2)}$$

α is the Flory temperature expansion coefficient, C_∞ is the characteristic ratio, M_0 is the molecular weight of the monomer and l is the bond length.

According to Daristotle et al. (2016), if the actual work concentration (c) is equal to or very close to c*, one can expect the formation of fibers with a "beads on a string" morphology. When c > c*, the formation of continuous, defect-free fibers is favored due to the stabilization of the polymer jet.

The blow spinning technique offers several advantages over extrusion and electrospinning methods. Fibers produced by the extrusion technique typically have larger diameters, and the process involves high energy consumption due to the elevated temperatures required to melt the polymers. In contrast, the electrospinning technique, while capable of producing finer fibres, has a low yield and is limited to certain types of polymers. This limitation arises from the need for specific solution conductivity to maintain the process, which relies on high voltage. Additionally, electrospinning requires specialized collectors, which can restrict its versatility. Blow spinning, on the other hand, provides high performance in a shorter time frame. Since it does not rely on an electrostatic field or high temperatures, this technique allows fibers to be collected on a wide variety of surfaces with greater safety and flexibility compared to the other techniques mentioned (GAO *et al.*, 2021).

The blow spinning process is relatively simple; however, it is essential to fine-tune certain parameters in advance. According to Gao et al. (2021), the formation and morphology of polymeric fibers obtained by blow spinning is altered by the type of polymer and its concentration, in addition to factors inherent to the process, such as gas pressure, the distance between the airbrush tip and the collector, the airbrush opening diameter and factors related to the environment, such as atmospheric pressure, temperature and humidity.

J Gonzalez et al. (2017) observed that the gas pressure and the working distance

presented a great influence in the production, diameter and distribution of fibers obtained from solutions of polyethylene oxide (PEO), polyethylene-co-vinyl acetate (EVA) and polyvinylidene fluoride (PVDF). Nicolau et al. (2022) evaluated different concentrations to obtain polycarbonate (PC) nanofibers by SBS and found that the increase in the concentration of the solution directly influences the formation of nanofibers, and that at low concentrations it was not possible to obtain nanofibers. As the concentration increased, the formation of fibers with a large number of droplets was observed, until they obtained the ideal concentration, producing homogeneous fibers without the presence of droplets that formed a nanoporous mat. The solution concentration is also one of the most important parameters to evaluate in the electrospinning processes; low concentrations can generate an electric spray phenomenon, while high concentrations increase the viscosity of the solution and can cause the obstruction of the nozzle equipment (XU et al., 2025).

The attributes of the blow spinning technique enables the exploration of non-woven materials in a broad range of applications (DARISTOTLE *et al.*, 2016). Microfibers, which are gaining significant market potential, stand to benefit from this technique, which could emerge not only as an alternative but also as an enhanced method for producing high-performance fibers for various industrial uses (DADOL *et al.*, 2020).

Despite the advantages of the SBS process, it also presents challenges. One of the main ones is the precise control of fiber diameter and uniformity, which can be influenced by fluctuations in gas pressure and instabilities of the polymer jet. In addition, the choice of solvents must consider not only their volatility, but also operator safety and environmental impact, since large volumes of solvents can be released during the process (GAO *et al.*, 2021).

3 MATERIALS AND METHODS

3.1 MATERIALS

The polymers used in this study were poly(vinyl alcohol) (PVA, Sigma-Aldrich, 85,000 – 124,000 Da), polypropylene (PP, Sigma-Aldrich, 250,000 Da), poly(vinylidene fluoride) (PVDF, Sigma-Aldrich, 534,000 Da), polyamide 6 (PA6, LANXESS, 30,000 Da) and natural rubber latex (NRL, RubberSul, 60% wt. in aqueous solution). PVA was solubilized in deionized water, while PP and PVDF were dissolved in *N*,*N*-dimethylformamide (DMF, C_3H_7NO, Sigma-Aldrich). PA6 was solubilized using a mixture of methanoic acid (98 – 100%, CH_2O_2, Merck) and ethanoic acid (100%, $C_2H_4O_2$, Merck). All materials were used as received, without further purification.

Graphene oxide (GO) was obtained from BoomaTech Company (São Marcos, Brazil). The dispersion of GO in ethanoic acid was performed by the company, using an ultrasonic tank (CTA do Brasil). The concentration of the obtained dispersion was 30 mg mL^{-1}.

Silver nitrate ($AgNO_3$) was synthesized from silver recovered from discarded Ag_2O button cells.

3.2 METHODOLOGY

3.2.1 Characterization of Graphene Oxide

Graphene oxide characterization was performed by UCSGRAPHENE (Embrapii unit), before dispersing the sample in ethanoic acid. The sample was dried in an oven (Thermo Scientific) at 105 °C for 24h before analysis. Scanning electron microscopy with a field emission gun (SEM-FEG) and energy dispersive spectroscopy (EDS) tests were performed using a TESCAN MIRA 3 electron microscope. The X-ray diffraction (XRD) was obtained in a Shimadzu XRD-6000 instrument, scanning from 5 to 90° in steps of 0.02° per second, using CuKα radiation (λ = 1.54056 Å), voltage of 40.0 kV and current of 30.0 mA. The XRD

diffractogram was evaluated with QualX software and PowCod database (ALTOMARE *et al.*, 2015).

Raman spectroscopy was performed on a Horiba LabRAM HR Evolution spectrometer, according to ISO TS 21356-1:2021, from 500 cm^{-1} to 3000 cm^{-1} and acquisition time of 10 s.

Fourier transform infrared spectroscopy (FTIR) analysis was performed on a Perkin Elmer Spectrum 400 equipment. The spectral range comprised 400 and 4000 cm^{-1} and a resolution of 4 cm^{-1}. After moisture removal, GO was incorporated into potassium bromide (KBr) and pressed into a tablet.

Thermogravimetric analysis (TGA) was performed using a Netzsch STA 449 F3 equipment, according to adaptations of ASTM C561-16 and ISO 11308:2020 standards. To evaluate the ash content, the sample was heated from room temperature to 910 °C, with a heating rate of 8 °C min^{-1} to 500 °C, 2 °C min^{-1} to 750 °C and 3 °C min^{-1} to 910 °C, maintaining this temperature for 1 min. To evaluate the carbon purity, the sample was heated from room temperature to 1010 °C, with a heating rate of 5 °C min^{-1}. Both tests were performed in an alumina crucible under air.

Atomic force microscopy (AFM) images were obtained with a Shimadzu SPM 9700HT equipment.

3.2.2 Synthesis and Characterization of Silver Nitrate

The process began by collecting material from the cathodes of spent batteries, which was then subjected to an acid digestion process. A copper wire was submerged in the resulting solution to precipitate metallic silver. The recovered silver was further digested with nitric acid (HNO_3 65% PA) in a water bath at 90 °C. After the digestion process, the solution was cooled to room temperature, allowing the $AgNO_3$ to crystallize completely. The salt was then characterized by Energy-Dispersive X-Ray Spectroscopy Fluorescence (EDX), in a Shimadzu

EDX-7000 device under vacuum using a 10 mm collimating beam for 100 s. XRD was obtained in a Bruker D8 Advance equipment, from 20 to 100 ° in steps of 0.05° with 5 s per step, CuKα radiation (λ = 1.54056 Å), voltage of 40 kV and current of 30.0 mA. EDS analysis was performed using a silicon drift detector (SSD) using a TESCAN MIRA 3 electron microscope.

3.2.3 Obtaining PA6-GO-AgNPs microfibers

To obtain the PA6-GO-AgNPs microfibers, a PA6 solution with a concentration of 15% *wt* was initially prepared by dissolving the polymer in a mixture of ethanoic acid and methanoic acid in a of 2:1 (v/v) ratio. The solution was stirred at 100 rpm in a shaker-type incubator (Novatecnica, model 715D) at 50 °C for 6 h. Subsequently, different concentrations of GO and $AgNO_3$ (as shown in **Table 2**) were added to the polymeric solution. The mixture was then stirred at 100 rpm in the incubator for an additional 24 hours at room temperature, facilitating the formation of AgNPs.

Table 2 – Nomenclature of the samples and the different concentrations of GO and $AgNO_3$ evaluated during the preparation of PA6-GO-AgNPs microfibers

Sample	**GO (mL)**	**[$AgNO_3$] (mmol L^{-1})**
A	0.0	10.0
B	1.0	10.0
C	1.0	0.0
D	0.0	20.0
E	2.0	20.0
F	2.0	0.0
G	0.0	0.0

The solutions containing only $AgNO_3$ were analyzed using TEM, to evaluate the formation of AgNPs. PA6-AgNPs solutions were diluted in ethanoic acid, and a drop of the

solution was placed on a holey carbon grid for analysis. TEM analysis was conducted on a MORGAGNI 268 D microscope (FEI Company) at an acceleration voltage of 80 kV. The size of the AgNPs was determined using ImageJ software.

Subsequently, all the polymeric solutions underwent the blow spinning process (**Figure 7**), using an airbrush with a nozzle diameter of 0.3 mm, a compressed air pressure of 0.5 MPa, a collector distance of 30 cm, and a process duration of 20 min.

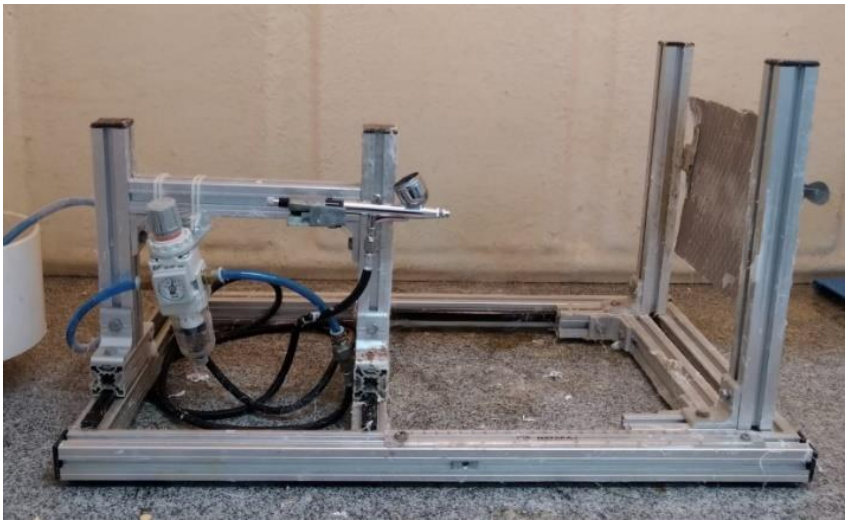

Figure 7 – Photograph of the experimental setup used for the solution blow spinning (SBS) process

The microfibers obtained after the solutions underwent the blow spinning process were analyzed through antimicrobial assays in semi-solid and in liquid medium. These assays served as guidelines for the continuation of the research, since only the samples that showed antimicrobial activity continued to be analyzed.

3.2.4 Sample sterilization

Prior to conducting the antimicrobial and cytotoxic assays, the samples were sterilized under UV light. Different exposure times of 1, 4 and 8 h, with half of the exposure time applied to each side of the sample. To assess the effectiveness of the sterilization process, the samples

were immersed in thioglycolate medium for 7 days. After this incubation period, the medium was inspected for any turbidity. In addition, a Gram stain test was performed. Samples that did not cause turbidity in the medium and that did not indicate the presence of bacteria in the Gram stain test were considered successfully sterilized.

3.2.5 Antimicrobial assays

3.2.5.1 Semi-solid medium

Antimicrobial tests in semi-solid medium were performed according to the CLSI M2-A8 (disc diffusion) and AATCC 147 (striation) standards. Gram-negative *Escherichia coli* (*E. coli*) and Gram-positive *Staphylococcus aureus* (*S. aureus*) were used at a concentration of 1.0×10^6 colony forming units (CFU) mL^{-1}.

In the disc-diffusion assay, bacteria were evenly plated on Mueller Hinton (MH) agar medium in Petry dishes, after which the samples were placed over the plates. For the striation test, bacteria were plated in five parallel streaks on the MH agar, with samples positioned perpendicularly to the streaks. Petry dishes were incubated at 37°C for 24 h. Following incubation, the formation of inhibition halos around the samples was evaluated, as the presence of these halos indicates the inhibition of bacterial growth.

3.2.5.2 Liquid medium

For tests in liquid medium, *E. coli* and *S. aureus* were used at a concentration of 1.0×10^4 CFU mL^{-1}. Samples were placed in a 24-well plate, each submerged in 600 μL of MH culture medium and 30 μL of bacterial solution. Culture medium alone served as the negative control, while culture medium with bacteria was used as the positive control. All plates were incubated at 37 °C for 24 h. After incubation, small aliquots were collected and inoculated onto Petry plates containing MH agar medium to assess whether the samples exhibited bactericidal

or bacteriostatic effects. Bacterial growth was also evaluated by adding 30 μL of resazurin to each well and gently stirring at 37 °C for 1 h. Resazurin is a dye that indicates cell viability by changing color from blue to pink due to the chemical reduction associated with aerobic respiration during cell growth.

3.2.6 Antiviral assays

The antiviral assay was performed at the Núcleo Vitro laboratory (Porto Alegre, RS, Brazil) in accordance with ISO 18184:2019. Betacoronavirus MHV-3 was used at a concentration of 1.0×10^5 tissue culture infectious dose ($TCID_{50}$). Virus aliquots were diluted in cell culture medium, and the samples were soaked in closed tubes for 2 h. The samples were then inoculated onto a monolayer of L929 cells, in quadruplicate to evaluate viral multiplication. Cellular changes, including the cytopathogenic effects induced by the viruses, were assessed. Control group comparisons were made through imaging and viral titration, which indicated the reduction in the number of infectious viral particles, expressed as logarithmic reductions in accordance with ISO 18184:2019.

3.2.7 Cytotoxic assays

3.2.7.1 MTT assay

Cell viability was assessed using the MTT assay. Microfibers were sterilized under UV light for 8 h, with half the exposure time for each side. The samples were then submerged (6.0 $cm^2\ mL^{-1}$) in in Dulbecco's Modified Eagle's medium (DMEM, Sigma Aldrich), supplemented with 10% fetal bovine serum (FBS, Gibco BRL, Life Technologies) and 1% penicillin/streptomycin (P/S, Sigma Aldrich), and incubated for 24 h at 37 °C (ISO 10993-12:2012). Dilutions of 10, 50, and 90% (v/v) of the extracts were prepared.

L929 cells were seeded at a density of 1.0×10^5 cells mL^{-1} in 96-well plates, each well

containing 100 µL of DMEM medium supplemented with 10% FBS and 1% P/S. After 24 h, the cells were exposed to the sample extracts for 1, 2, and 7 days. The negative control consisted of DMEM medium, and the viability was assessed by adding 100 µL of MTT (1.0 mg mL^{-1}) to each well. After 2h of incubation at 37 °C, the MTT solution was removed, and the formazan crystals were solubilized with 100 µL of dimethylsulfoxide. The optical density was measured at 570 nm using a spectrophotometer (Max190 Spectra, Molecular Devices, USA). Results were expressed as a percentage of cell viability, with the negative control equating to 100% viability. A sample was considered cytotoxic if cell viability fell below 70%, according to ISO 10993-5:2009.

Statistical analysis was performed using ANOVA followed by a post hoc Tukey test, with statistical significance set at 5% ($p \leq 0.05$).

3.2.7.2 Cell adhesion

Cell adhesion on the samples was evaluated by seeding L929 cells in 12-well plates at a density of 5.0×10^4 cells mL^{-1} for 1, 2, and 7 days. After incubation, the cells were fixed with 3% glutaraldehyde solution in PBS (v/v) for 15 min, followed by dehydration with ethanol solutions (30, 50, 70, 90, and 100% (v/v) for 10 min. The samples were then analyzed by FEG-SEM. FEG-SEM micrographs were obtained using the same operating conditions described in Section 3.2.2.

3.2.8 Characterization of PA6-GO-AgNPs microfibers

The microfibers were characterized using several techniques: field emission gun-scanning electron microscopy (FEG-SEM) to assess morphology; energy dispersive X-ray spectroscopy (EDS) to evaluate silver distribution on the samples; UV-Vis diffuse reflectance spectroscopy (UV-Vis DRS) to confirm the presence of AgNPs; WCA measurements to

determine the hydrophilic or hydrophobic nature of the samples; TGA to evaluate thermal stability; breathability tests to assess airflow during inhalation and exhalation; microbiological assays to evaluate antibacterial and antiviral properties; and cytotoxicity tests.

FEG-SEM micrographs were obtained using a Tescan MIRA3 electron microscope with a secondary electron detector. The samples were mounted on stubs with carbon tape and then covered with a thin layer of gold. The voltage used to obtain the micrographs was 10.0 kV.

EDS spectra were acquired immediately following the FEG-SEM analysis, maintaining the same operational conditions. The silicon drift detector (SSD) from Oxford Instruments was used for the analysis.

UV-Vis DRS analysis was performed using a Shimadzu UV-2600 spectrophotometer, covering a range of 250 to 700 nm with a step size of 1.0 nm. The sample was placed in a specific holder for solids protected by quartz glass, with barium sulfate used as the reference sample.

WCA measurements were carried out using an SEO Phoenix 150 device. The sessile drop method was applied, where 100 μL of distilled water was deposited on the sample, which was fixed on a flat surface, and the photographic record of the water drop on the sample was captured using the equipment's software.

TGA was performed on a Shimadzu TGA 50 instrument. The samples were heated from room temperature to 310 °C in a platinum crucible at a heating rate of 20 °C min^{-1} under a nitrogen atmosphere with a flow of 50 mL min^{-1}.

Breathability tests were conducted by the Falcão Bauer laboratory (São Paulo, Brazil) following the NBR 13698:2022 standard. The test measured the resistance to inhalation at continuous airflows of 30 L min^{-1} and 95 L min^{-1}, and to exhalation at a continuous airflow of 160 L min^{-1}. The pressure drop should remain as low as possible, not exceeding 70, 240, and 300 Pa, respectively.

3.2.9 Evaluation of the aging samples

To assess the stability of the samples over time, antimicrobial tests with *E. coli* and the MTT assay were performed on one-year-old samples.

4 RESULTS AND DISCUSSION

This chapter presents the results obtained from the analysis of the data collected during the research, in accordance with the methodology described in the previous chapter. The organization of the results follows the specific objectives of the study, as presented in the introduction.

First, the characterization tests of graphene oxide and silver nitrate are presented. Next, the procedures for determining the process parameters leading to the production of microfibers are described. These microfibers are then subjected to microbiological and characterization tests.

The results are discussed as they are presented, based on the scientific literature.

4.1 GRAPHENE OXIDE CHARACTERIZATION

The morphology of the graphene oxide sample can be observed in the SEM images presented in **Figure 8**.

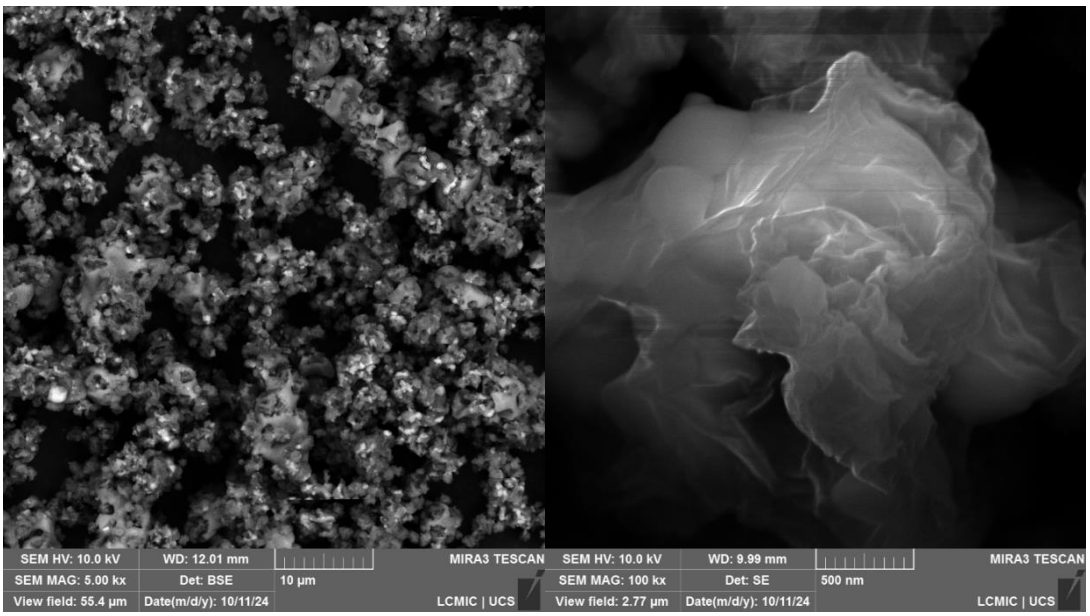

Figure 8 – FEG-SEM micrographs of graphene oxide sample

It is possible to observe the presence of different interconnected and stacked layers. The image with 100 kx magnification shows very wrinkled GO sheets, similar to what was observed in other studies (FARIVAR *et al.*, 2021).

The EDS test (**Figure 9**) revealed the presence of carbon (47.5%) and oxygen (27%), constituents of GO, in addition to impurities such as sodium (12.2%), sulfur (6.2%), chlorine (5.9%), potassium (0.6%) and manganese (0.6%). **Figure 9** also shows that these elements are uniformly distributed in the sample, and are not isolated contaminations. The presence of these elements is possibly due to residues related to the production process or to impurities present in the raw materials used. It is important to note that in the datasheet presented by the manufacturing company (Annex A), the composition of the material is different, being carbon (49-56%), oxygen (41-50%) and the observed impurities are hydrogen (1-2%), nitrogen (0-1%) and sulfur (2-4%).

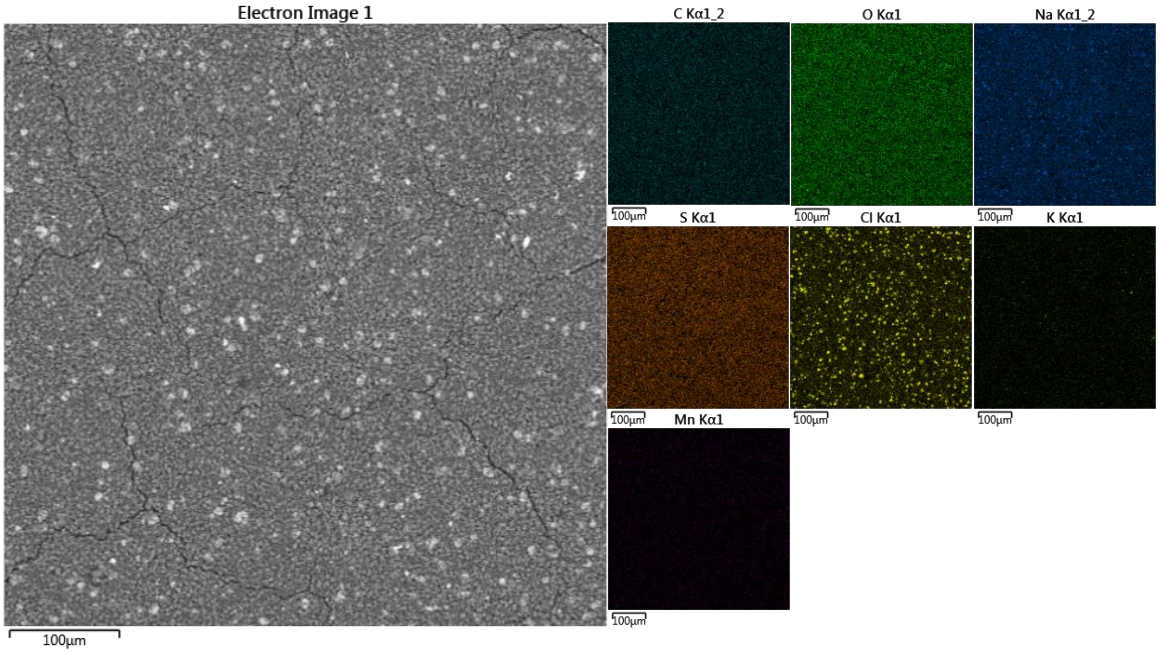

Figure 9 – EDS composition maps of graphene oxide sample

The diffractogram shows the presence of several diffraction peaks (**Figure 10**). GO is

characterized by an intense peak at approximately 10° (PERUMBILAVIL *et al.*, 2015). Graphene and graphite, in turn, present peaks in the same position, at ~26°, with a difference in intensity (FARIVAR *et al.*, 2021). The obtained diffractogram was analyzed in the QualX software, where a search was performed in the PowCod database, and it was not possible to relate the peaks to any standard. This occurred due to the presence of impurities observed in the EDS test.

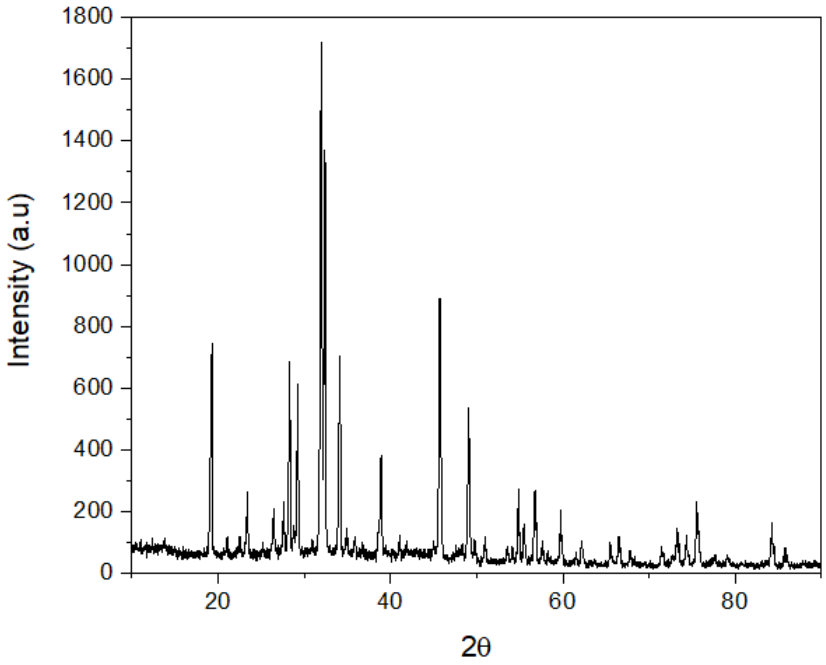

Figure 10 – X-ray diffraction pattern of graphene oxide sample

Raman spectroscopy analysis (**Figure 11**) identified peaks at 1339 cm^{-1}, 1580 cm^{-1} and 2670 cm^{-1}, corresponding to the D, G and 2D bands respectively. According to ISO TS 21356-1:2021, the presence of these bands identifies a graphitic material. The D band is known as the disorder band and is associated with structural imperfections derived from sp^3-type bonds. The G band is associated with sp^2-type bonds between carbons and the 2D band is used in the identification of graphene (PERUMBILAVIL *et al.*, 2015; YE *et al.*, 2015).

The intensity ratio between bands D and G (I_D/I_G) determines the oxidation and the level

of structure disorders in carbonaceous materials (ANUAR *et al.*, 2024). Also, the I_D/I_G correlates to lateral size of graphene or GO flakes (ISO TS 21356-1:2021). Larger ratios typically indicate smaller lateral dimensions. The I_D/I_G measured for the GO sample is 0.68, which implies a lower level of oxidation and structure disorders and large lateral dimensions.

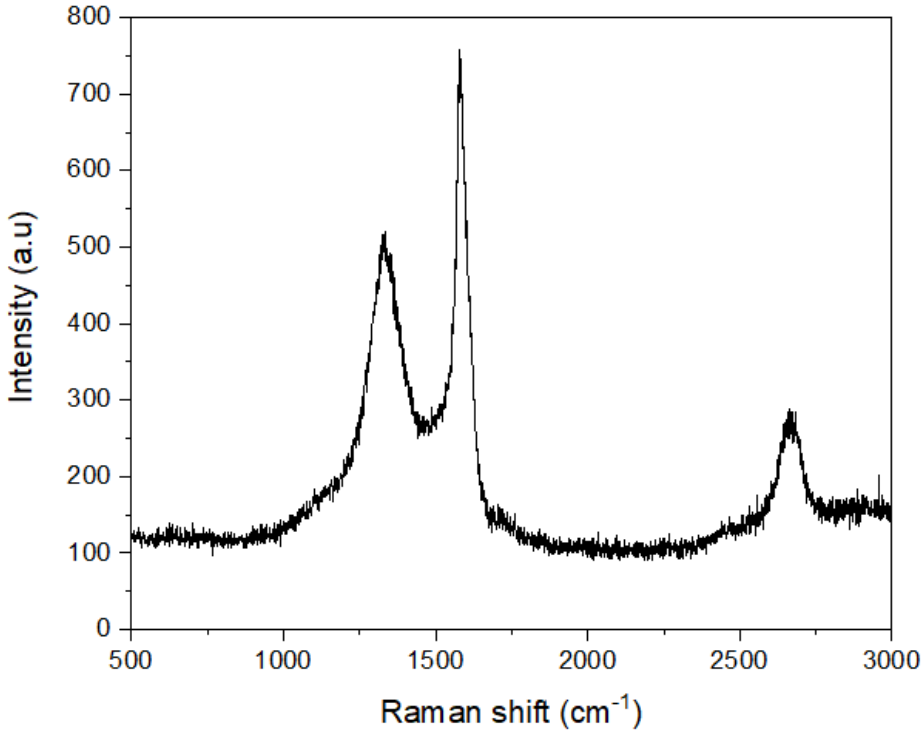

Figure 11 – Raman spectra of graphene oxide sample

The FITR spectra of the graphene oxide sample is shown in **Figure 12** and showed distinct absorption bands corresponding to O–H stretching vibrations at 3413 and 1637 cm^{-1}, C=C stretching at 1618 cm^{-1}, C–O vibrations at 1115 cm^{-1}, and C–S bonds at 616 cm^{-1}. The broad O–H band and its associated bending mode are indicative of hydroxyl and adsorbed water groups, commonly observed in oxidized carbon materials (ANUAR *et al.*, 2024, BENTEDLAOUTI; BELOUATEK; KEBAILI, 2024, ZIKALALA *et al.*, 2024). The band at 1618 cm^{-1} is consistent with aromatic C=C stretching, suggesting the partial retention of the sp^2-hybridized carbon network within the GO structure (ANUAR *et al.*, 2024, ZIKALALA *et*

al., 2024). The C–O vibration detected at 1115 cm^{-1} aligns with signals typically attributed to epoxy or alkoxy functional groups, confirming the presence of oxygenated functionalities introduced during oxidation (BENTEDLAOUTI; BELOUATEK; KEBAILI, 2024, ZIKALALA *et al.*, 2024). Notably, the presence of a C–S vibration at 616 cm^{-1} suggests that sulfur-containing species may have been incorporated during the synthesis of GO, contributing to a modified surface chemistry. Compared with literature data, which frequently show stronger signals in the 1700–1725 cm^{-1} region due to carboxylic C=O groups, the absence of this feature in the present sample implies a lower abundance or absence of such groups, potentially influencing the material's reactivity and compatibility with further functionalization.

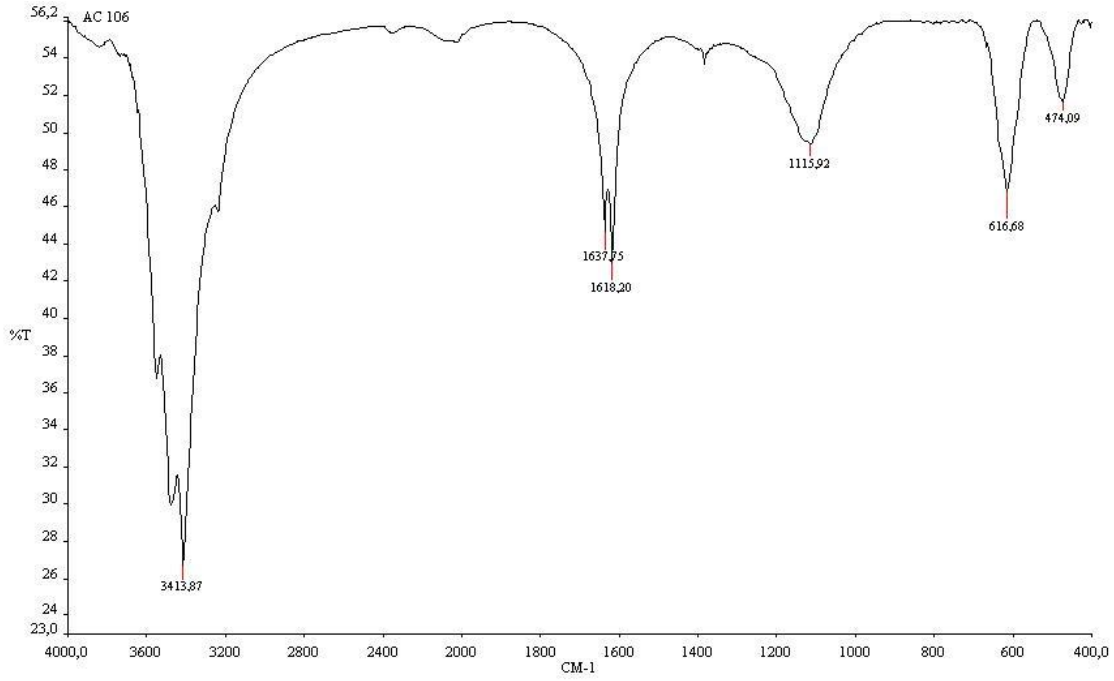

Figure 12 – FTIR spectra of graphene oxide sample

Thermogravimetric analysis (**Figure 13**) sought to evaluate the ash content and carbon purity. The mass loss of GO occurs in three temperature ranges: up to 100°C, related to water evaporation; between 100 and 360°C, the removal of oxygenated functional groups occurs; and

from 360 to 1000°C, oxidative pyrolysis of carbon occurs (FARIVAR *et al.*, 2021). It was observed that, in the test based on the ASTM C561-16 standard, the ash content was 41.65%. Generally, it is observed that pure GO samples have an ash content of less than 10% (FARIVAR *et al.*, 2021; ZIKALALA *et al.*, 2024). Regarding the carbon purity test, the value observed was 49.77%, which, according to ISO 11308, classifies this sample as poor in relation to carbon purity, since the residual mass is greater than 20%.

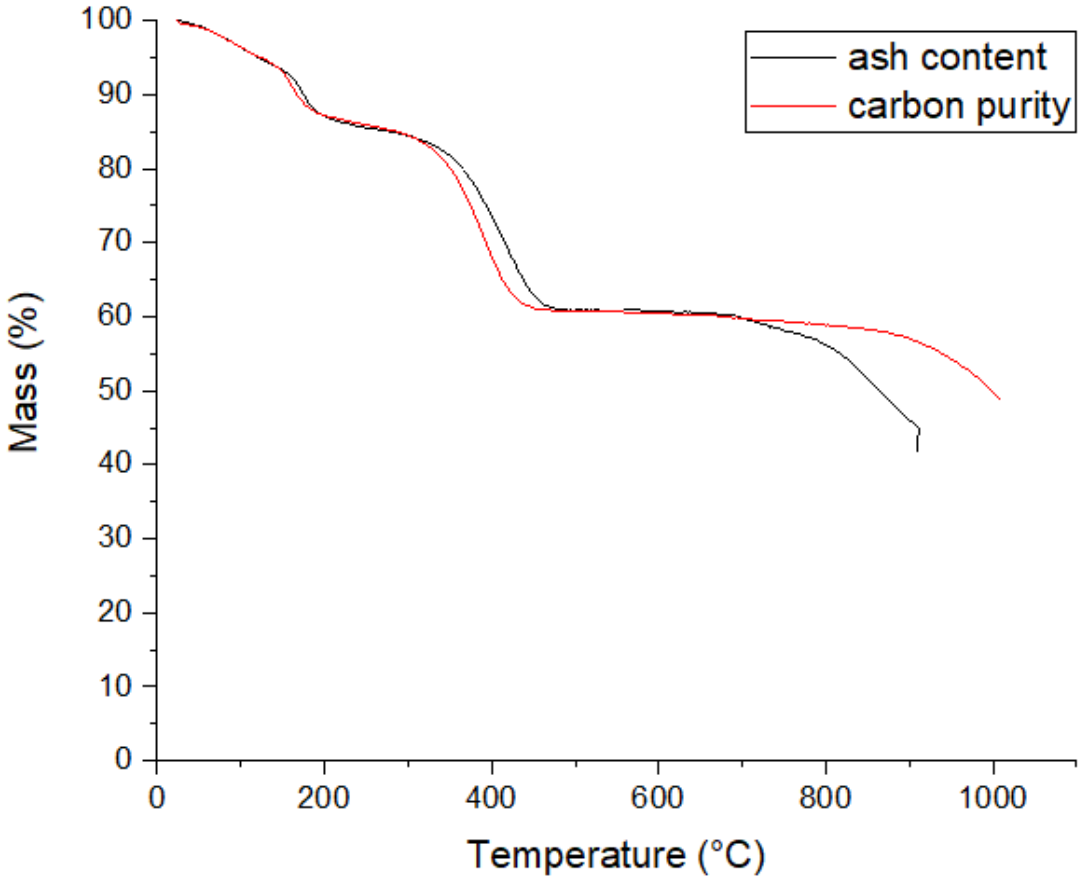

Figure 13 – Thermogravimetric analysis of graphene oxide sample

The AFM image shown in **Figure 14** shows that the material analyzed contains dirt with a thickness of approximately 80 nm, as shown in the profile presented in **Figure 15** which made it impossible to obtain measurements to determine the number of layers and obtain the histogram.

In general, the tests demonstrated that the material analyzed is a carbonaceous sample that presents characteristics similar to graphene oxide, but contains a high content of impurities, in addition to being a sample considered poor in relation to carbon purity.

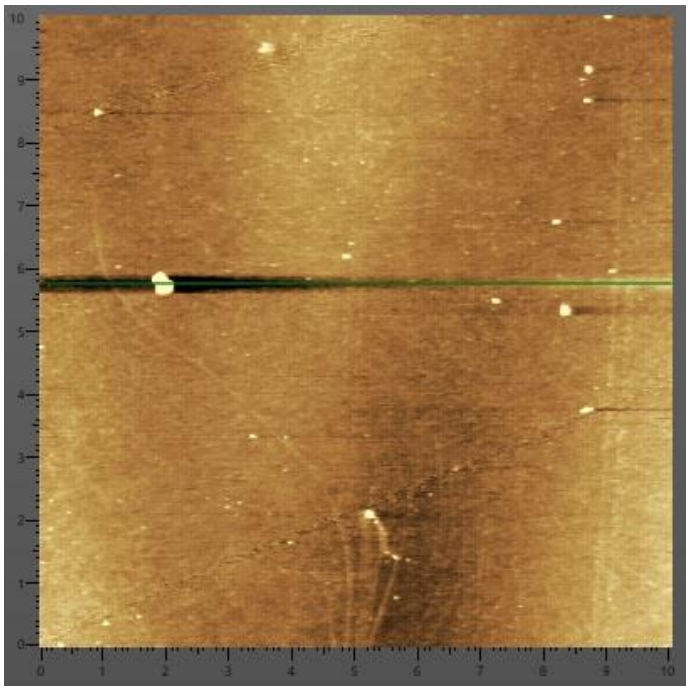

Figure 14 – AFM image of graphene oxide sample with a scan area of 10 × 10 μm

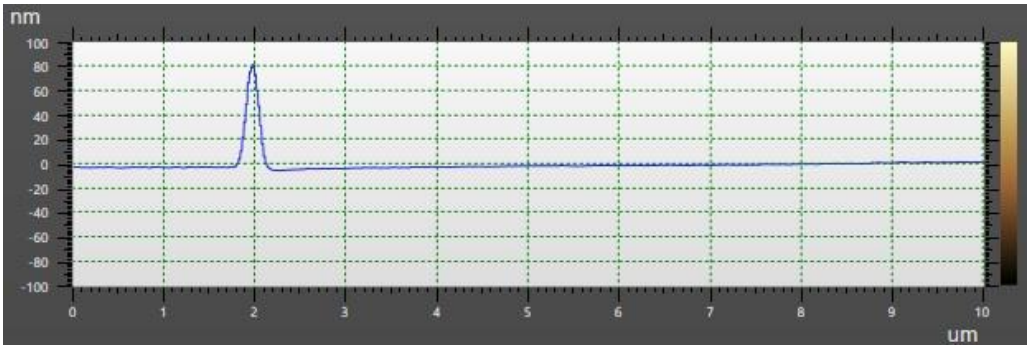

Figure 15 – AFM profile of graphene oxide sample

4.2 SYNTHESIS AND CHARACTERIZATION OF SILVER NITRATE

The methodology used to obtain silver nitrate from silver recovered from batteries is

outlined in **Figure 16**.

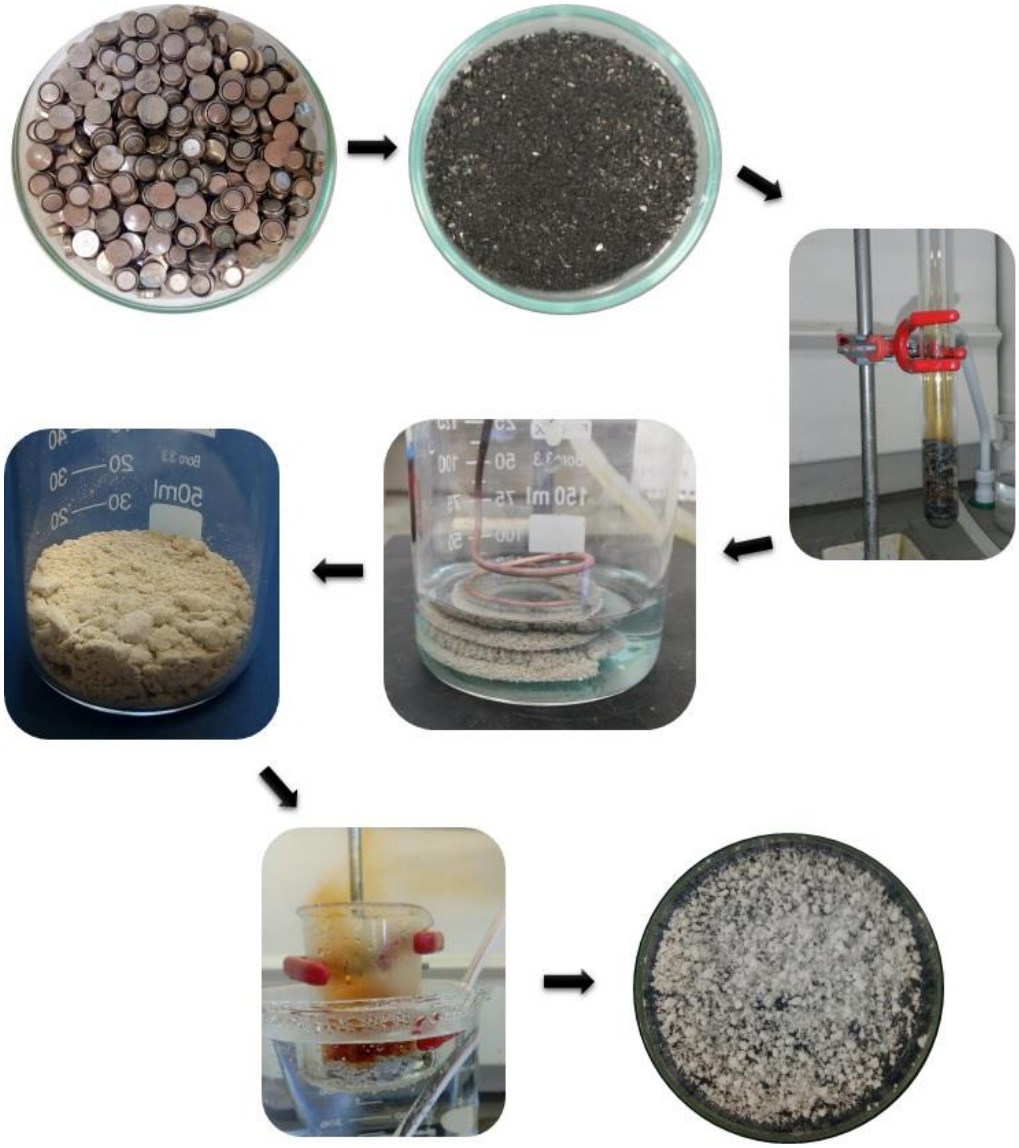

Figure 16 – Methodology of silver recovery and silver nitrate synthesis

Basically, the batteries were opened and the residue containing silver was collected, which was then leached with nitric acid. Then, the solution obtained was filtered and a copper wire was inserted into it, where the precipitation of silver was observed due to the oxidation-reduction reaction, reducing Ag^{1+} ions to Ag^{0}. The silver obtained was diluted in nitric acid at a controlled temperature, then the solution was cooled to room temperature, promoting the

crystallization of silver nitrate. This process was developed in a previous work, where it is widely discussed (SARTORI *et al.*, 2020).

The XRF analysis demonstrated that the silver nitrate was highly pure (>99.4%), which was confirmed by the XRD diffractogram (**Figure 17**), in which all the peaks observed were related to silver nitrate. The XRD diffractrogram of silver nitrate is known for presenting several intense and cristaline peaks (AZIZ *et al.*, 2017; BAKR *et al.*, 2022). The obtained diffractogram was related to the letter 00-150-9468 from the PowCod database.

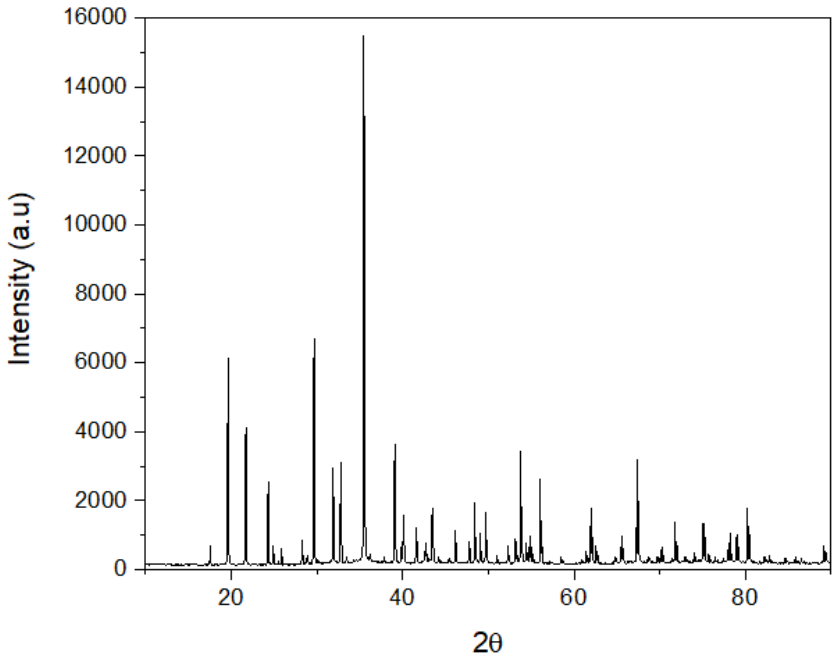

Figure 17 – X-ray diffraction pattern of silver nitrate sample

The EDS test (**Figure 18**) confirmed the purity of the material, with only the presence of silver, nitrogen, oxygen and carbon being observed, the latter being related to the tape used to fix the sample.

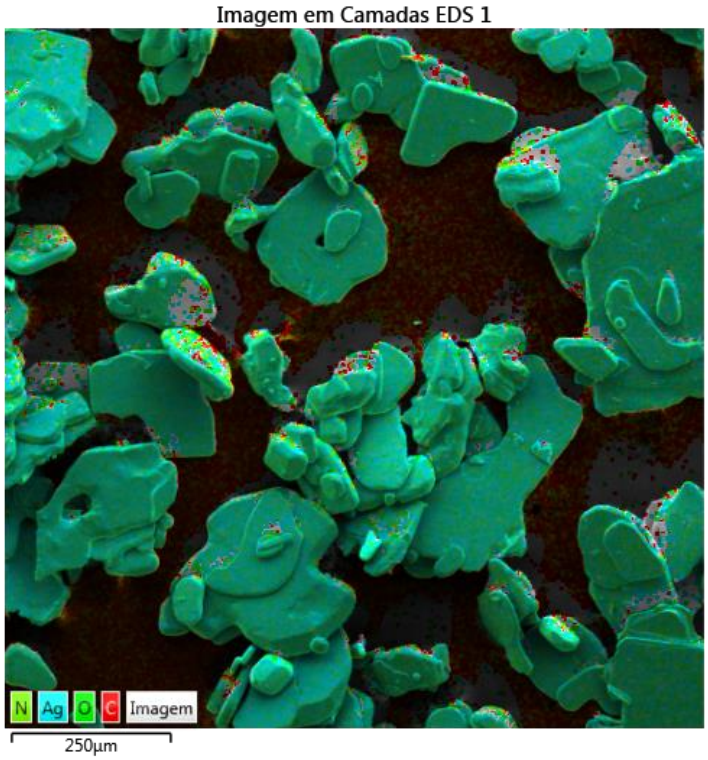

Figure 18 – EDS composition map of silver nitrate

In addition to the characterization performed to demonstrate the purity of the synthesized silver nitrate, the material was tested in the synthesis of AgNPs in a previous study. The AgNPs were synthesized by a chemical route, using sodium citrate and sodium borohydride, at different pHs (2.0 - 13.0). The obtained AgNPs were characterized and, after verifying that pH 10.0 was more favorable to the formation of smaller and stable nanoparticles, they were incorporated into a chitosan solution to obtain hybrid pellets that were used in the treatment of industrial wastewater, inhibiting the growth of *E. coli*. In the study, the synergistic action that occurred between chitosan and AgNPs was clearly demonstrated (SARTORI *et al.*, 2023).

4.3 DETERMINATION OF BLOW SPINNING PROCESS PARAMETERS

In this study, the parameters were evaluated in such a way that no form of environmental

control was required. Accordingly, the different polymers selected for testing were assessed, and it was found that microfibers of PP, PVA, and PVDF could only be obtained when controlling the temperature of the solution and/or the environment, as well as the humidity. In the case of NRL, it was not possible to produce microfibers even under controlled conditions. PA6, on the other hand, yielded microfibers without any type of environmental control and with the solution kept at room temperature; therefore, PA6 was selected as the polymer of choice for this work.

Several tests were conducted to optimize the process parameter. It was observed that with low compressed air pressure, microfibers failed to form, and only droplets were produced. Conversely, at high pressure, some microfibers were initially formed but were subsequently degraded. The PA6 concentration plays a crucial role in determining the viscosity of the solution. Solutions with low viscosity resulted in difficulty forming fibers, and when fibers did form, the solvent did not evaporate completely. On the other hand, solutions with high viscosity could not flow through the airbrush nozzle, preventing microfiber formation. Furthermore, the distance between the airbrush nozzle and the collector must be adjusted to ensure that all solvents have sufficient time to evaporate during the movement between from one point to the other. After several iterations of optimizing these parameters, the initial following conditions were established as optimal for obtaining microfibers: a PA6 solution concentration of 15% *wt*, a compressed air pressure of 0.5 MPa, and an airbrush-to-collector distance of 30 cm.

The experimental concentration (c), in g mL^{-1}, was compared with the theoretical overlap concentration (c*), calculated from equations 1 and 2. The values used for the calculations are presented in **Table 3**.

Table 3 – Parameters used to calculate c*

Parameter	Value
M_w	30000 g mol^{-1}
N_a	6.022×10^{23} mol^{-1}
α	1.3
C_∞	9.5
M_0	113.16 g mol^{-1}
l	1.54×10^{-8} cm

After solving the equations, a value of c* = 0.0319 g mL^{-1} was obtained. The working concentration is 0.218 g mL^{-1}, therefore the relationship between the concentrations is given by c/c* = 6.83. This value, according to Daristotle *et al.* (2016), indicates the possible formation of uniform fibers.

4.3.1 Proportion of solvents

The 15% *wt* PA6 solutions were initially prepared using two solvent ratios of ethanoic acid and methanoic acid: 1:1 and 2:1 (v/v). During the microfiber production process, it was observed that the 2:1 solvent ratio lead to better microfiber formation, with higher yield and productivity. The solvent evaporated more easily, and the resulting fibers exhibited improved process stability and flexibility compared to those produced with the 1:1 solvent ratio. The microfibers formed with the 1:1 ratio displayed greater mechanical fragility and became brittle during handling.

Figures 19 and **20** show that, in both solutions, the fibers are randomly arranged, and droplet formation occurs in both samples. However, droplet formation is more pronounced in the 1:1 solvent ratio, which seemingly results in a higher fiber packing density.

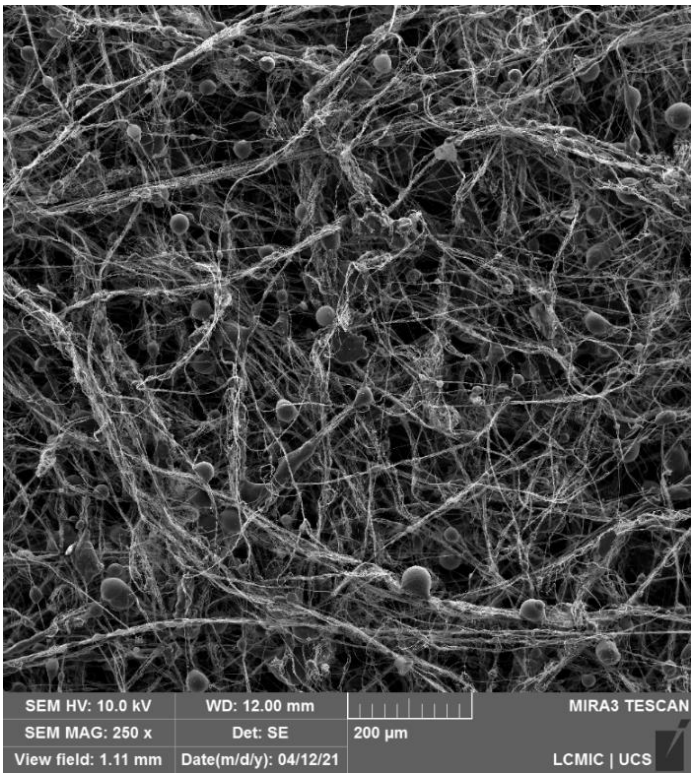

Figure 19 – Microfibers obtained from 15% wt PA6 solution with 2:1 solvent ratio

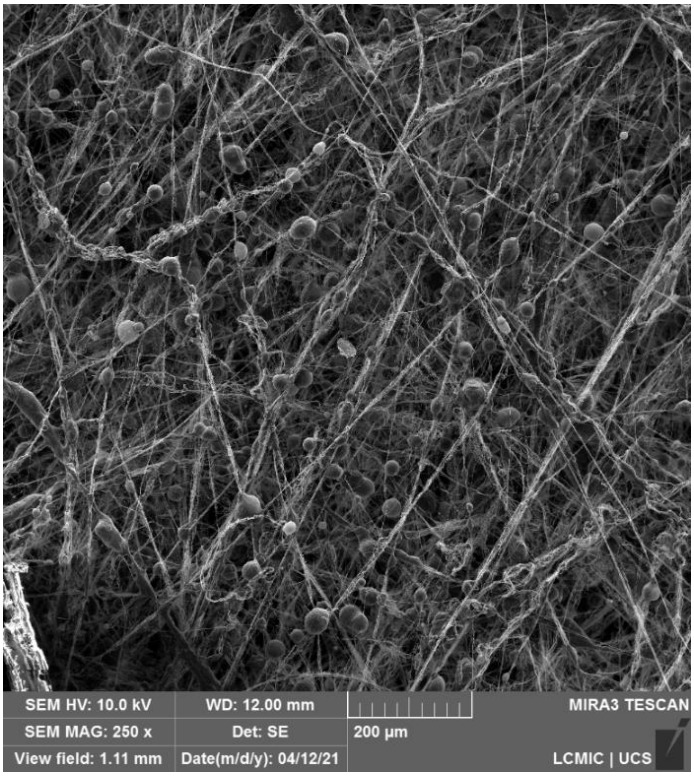

Figure 20 – Microfibers obtained from 15% wt PA6 solution with 1:1 solvent ratio

The difference in droplet formation helps explain the variation in mechanical properties between the two samples. Based on these observations, the study proceeded with the fabrication of microfibers using the 15% *wt* PA6 solution with a 2:1 (v/v) solvent ratio.

4.3.2 Airbrush diameter opening

The diameter of airbrush opening significantly influences the morphology of the fibers. A smaller opening results in larger droplets. Additionally, the airbrush opening diameter affects the packing density of the fibers, which is particularly important for applications like filter elements, where high packing density is required. Samples obtained using two airbrush opening diameters, 0.2 mm (**Figure 21**) and 0.3 mm (**Figure 22**), were evaluated.

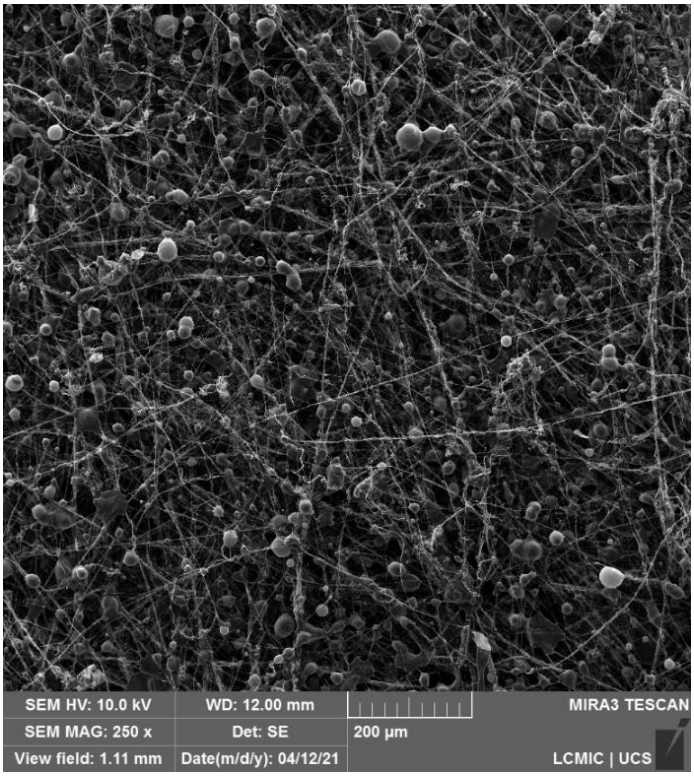

Figure 21 – Microfibers obtained with airbrush diameter opening of 0.2 mm

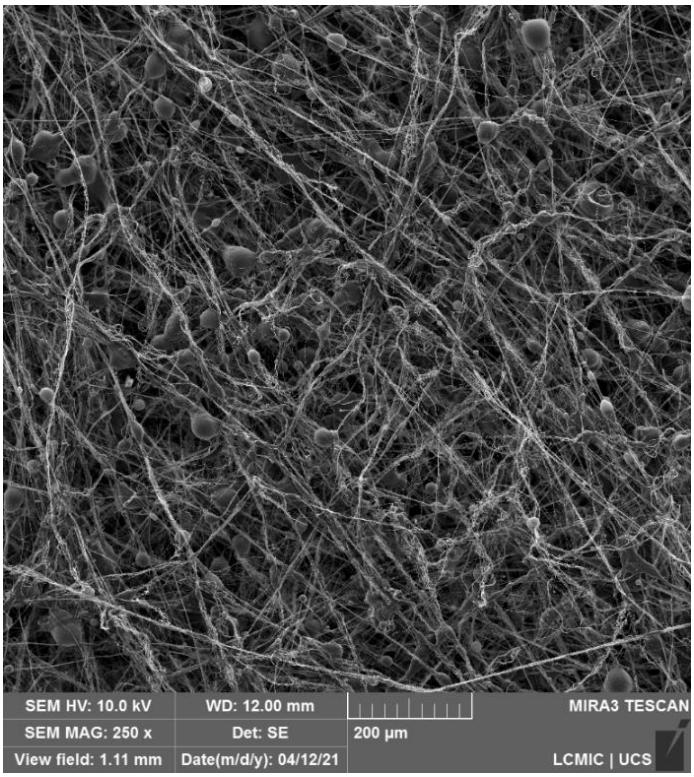

Figure 22 – Microfibers obtained with airbrush diameter opening of 0.3 mm

It was observed that the samples formed with a 0.2 mm diameter opening exhibited greater droplet formation compared to those obtained a 0.3 mm diameter opening. Although the droplets are slightly smaller in the fibers obtained with the 0.2 mm diameter opening, the higher concentration may negatively impact the performance of the samples. Therefore, the 0.3 mm diameter opening was found to be more suitable for the production of microfibers.

4.3.3 Spinning time

The spinning time is a critical parameter, as it must be sufficient to produce samples with adequate mechanical resistance for handling and subsequent characterization, while avoiding excessive fiber deposition. If the spinning time is excessively long, an overproduction of fibers may occur, leading to increased material consumption, economic losses, and alterations in membrane properties, such as reduced breathability.

In this study, spinning times of 10 and 20 min were evaluated. The initial spinning time of 10 min was selected because it corresponded to the onset of homogeneous membrane formation. However, samples produced with a 10-minute spinning time exhibited low mechanical resistance and were difficult to handle, as they deformed easily, rendering them unsuitable for further evaluation. In contrast, samples prepared with a 20-minute spinning time showed improved mechanical integrity and were easier to manipulate.

Based on these observations, a spinning time of 20 min was established as the working condition, as it ensured the production of mechanically stable and manageable samples. Although only two spinning times were investigated in this work, a more detailed evaluation of intermediate and longer spinning durations may be explored in future studies to further optimize membrane properties and process efficiency.

4.4 SYNTHESIS OF AGNPS IN THE PA6 SOLUTION

Upon the addition of $AgNO_3$ to the polymeric solution, it was observed that it acquired a yellow-gold color, characteristic of AgNPs (FU *et al.*, 2021). This color change suggests successful nanoparticle formation, which is further supported by the findings of Shi et al. (2011), who noted that methanoic acid, in addition to its role in solubilizing PA6, acts as a reducing agent due to the presence of its carbonyl groups. During the reduction of AgNPs, the aldehyde group of methanoic acid is oxidized, forming carboxylic acid, which rapidly dissociates into carbon dioxide and water (**Figure 23**). AgNPs remain stable in solution, as PA6 molecules act as stabilizing agents, preventing aggregation of the nanoparticles. According to Hasan *et al.* (2020), this occurs due to the interaction of Ag^+ ions with the amino group ($-NH_2$) in PA6.

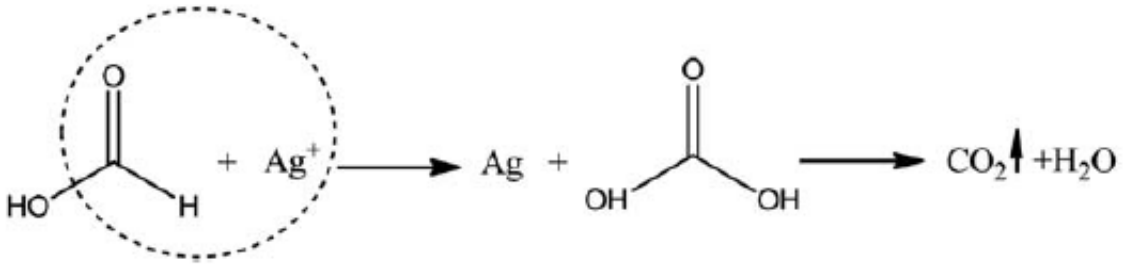

Figure 23 – Reduction mechanism of AgNPs by methanoic acid (Shi et al., 2011)

The incorporation of AgNPs into polymeric microfibers to impart antimicrobial properties has been widely reported in the literature. However, this typically involves multiple steps: the synthesis of AgNPs followed by their incorporation into the polymeric solution or the already formed fibers (ALJOHANI *et al.*, 2021; HUANG; LIN; SU, 2024; KUMAR *et al.*, 2023; LV *et al.*, 2021). The direct synthesis of AgNPs within the polymeric solution, as demonstrated in this study, offers several advantages. Not only does this process eliminate the need for an additional step to introduce nanoparticles into the microfibers, but it also ensures a more homogeneous distribution of AgNPs throughout the sample, which is crucial for the uniformity of antimicrobial activity. Furthermore, the release of Ag^+ ions from AgNPs is lower when the synthesis is performed in situ. Cheng et al. (2018) observed that AgNPs are effective in inhibiting bacterial growth even with an extremely low Ag^+ ion release rate.

In the TEM micrographs (**Figures 24 and 26**), the formation of spherical nanoparticles is clearly observed. The histograms shown in **Figures 25** and **27** indicate that the nanoparticles in both solutions exhibit sizes ranging from 3 to 14 nm.

As expected, sample D demonstrated a higher concentration of AgNPs; however, no agglomeration due to increased concentration was observed. This observation aligns with the findings of Alahmadi et al. (2018), who also reported that varying the concentration of $AgNO_3$ during the formation of AgNPs did not significantly affect their size or shape.

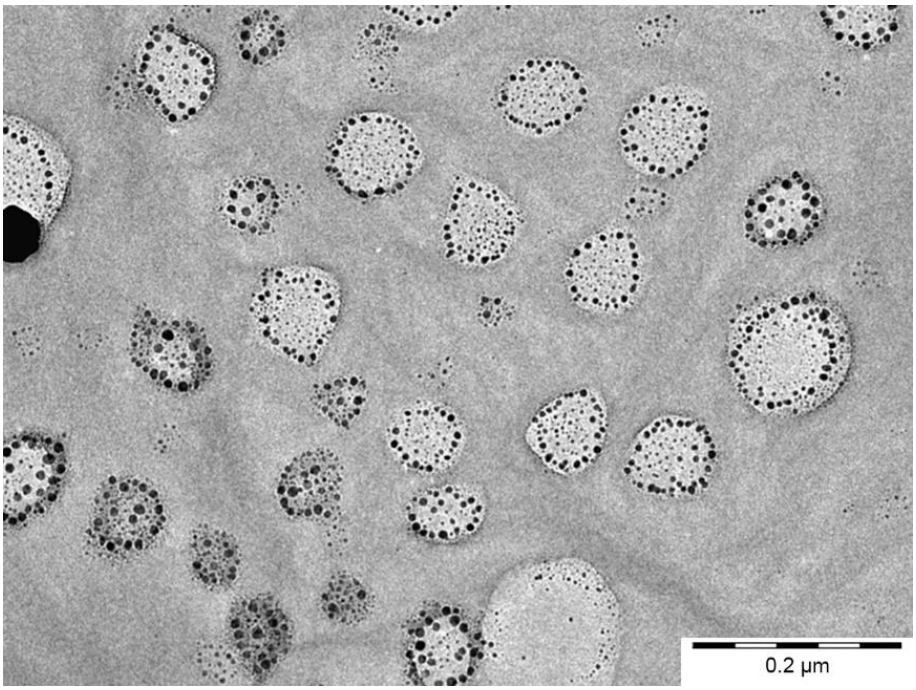

Figure 24 – Transmission electron microscopy micrograph of sample A

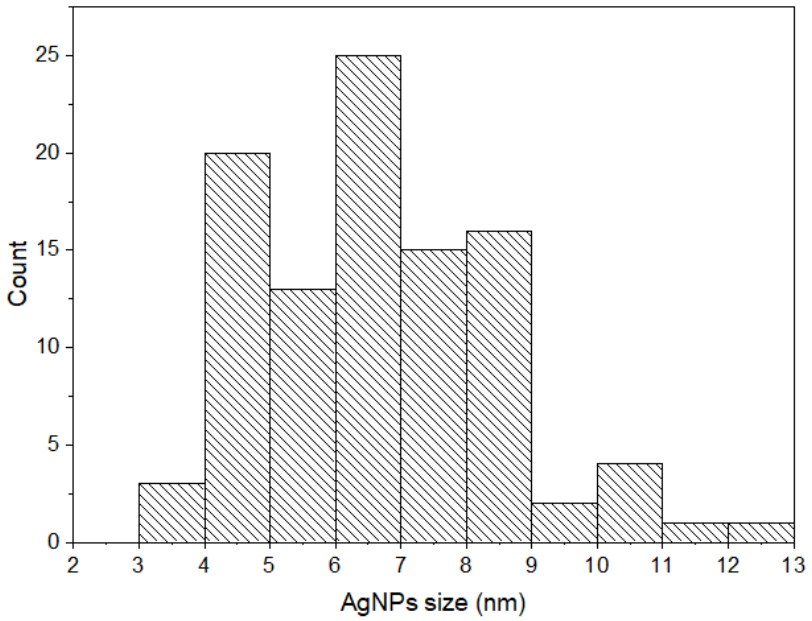

Figure 25 – Size distribution histogram of sample A

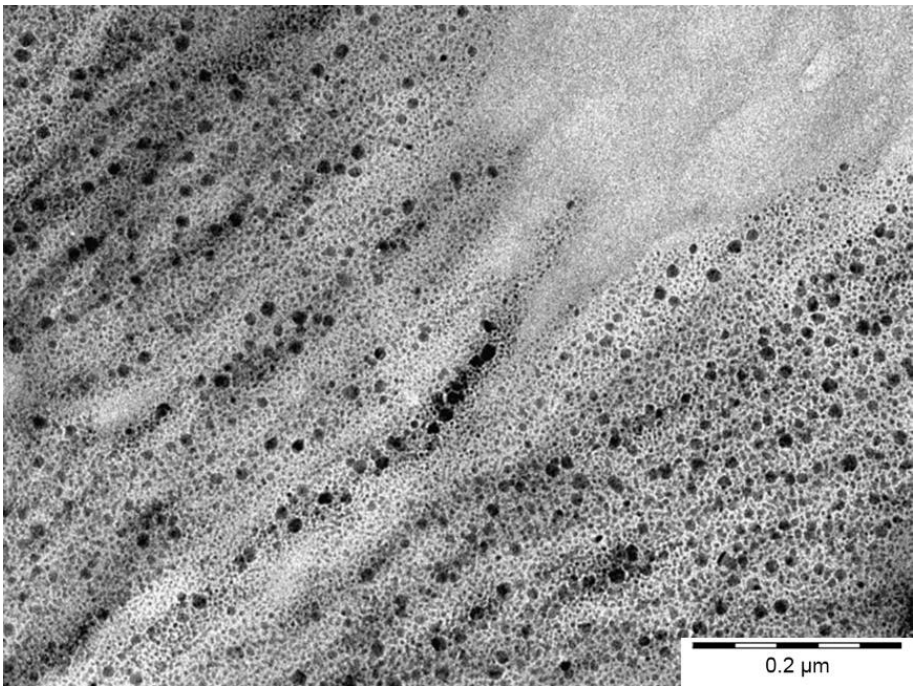

Figure 26 – Transmission electron microscopy micrograph of sample D

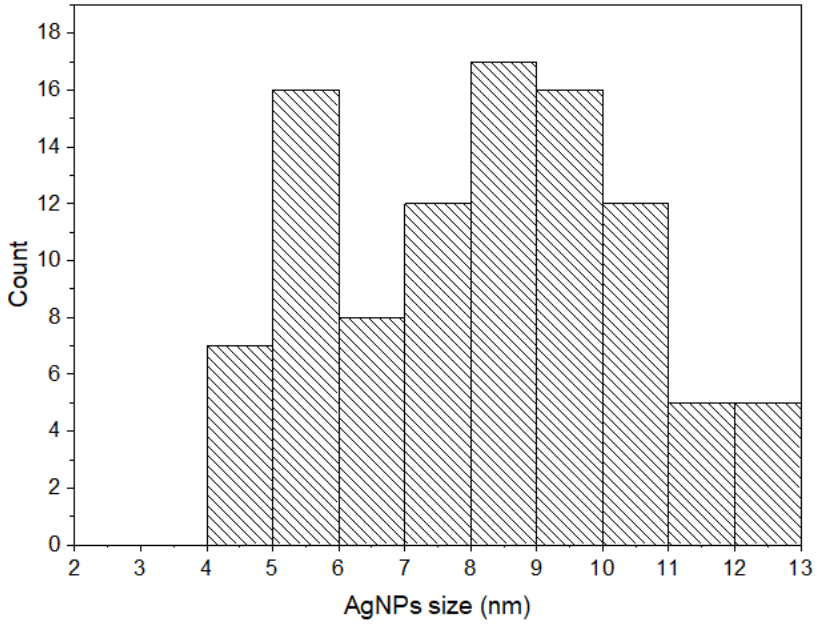

Figure 27 – Size distribution histogram of sample D

4.5 SAMPLE STERILIZATION

After sterilizing the samples with different exposure times to UV light, the Gram stain test showed the presence of Gram-negative and Gram-positive bacteria after 1 h. Gram-positive

bacteria were observed after 4 h and, at 8 h of exposure, no bacteria were observed. **Figure 28** shows the results of the sterilization test for sample A after 8 h. The medium does not show any turbidity when compared to the negative control, indicating successful sterilization.

Figure 28 – Sterilization test of sample A after 8 h under UV light

4.6 ANTIMICROBIAL ASSAYS

4.6.1 Semi-solid medium

The incorporation of AgNPs into PA6 microfibers exhibited both bactericidal and antiviral potential, enhancing the safety to users wearing facial respirators with these filter elements. On the other hand, the addition of GO did not achieve the expected results. **Figure 29** shows the results of the disc diffusion and striation test while **Figure 30** shows the results of the antimicrobial assays in a liquid medium with *E. coli*. The results of the assays with *S. aureus* are presented in **Figure 31** (disc diffusion and striation test) and **Figure 32** (liquid medium).

In the assays with *E. coli*, inhibition halos were observed around the samples containing AgNPs. Similarly, in the assays with *S. aureus*, halos formed around the samples D and E. The size of the inhibition halos was measured and is provided in **Table 4**. Notably, no bacterial growth was observed under any of the samples in the *E. coli* assays. While no inhibition halo

was formed around the samples A and B in the *S. aureus* assays, no bacterial growth was detected under these samples, as was the case with the samples C, F and G.

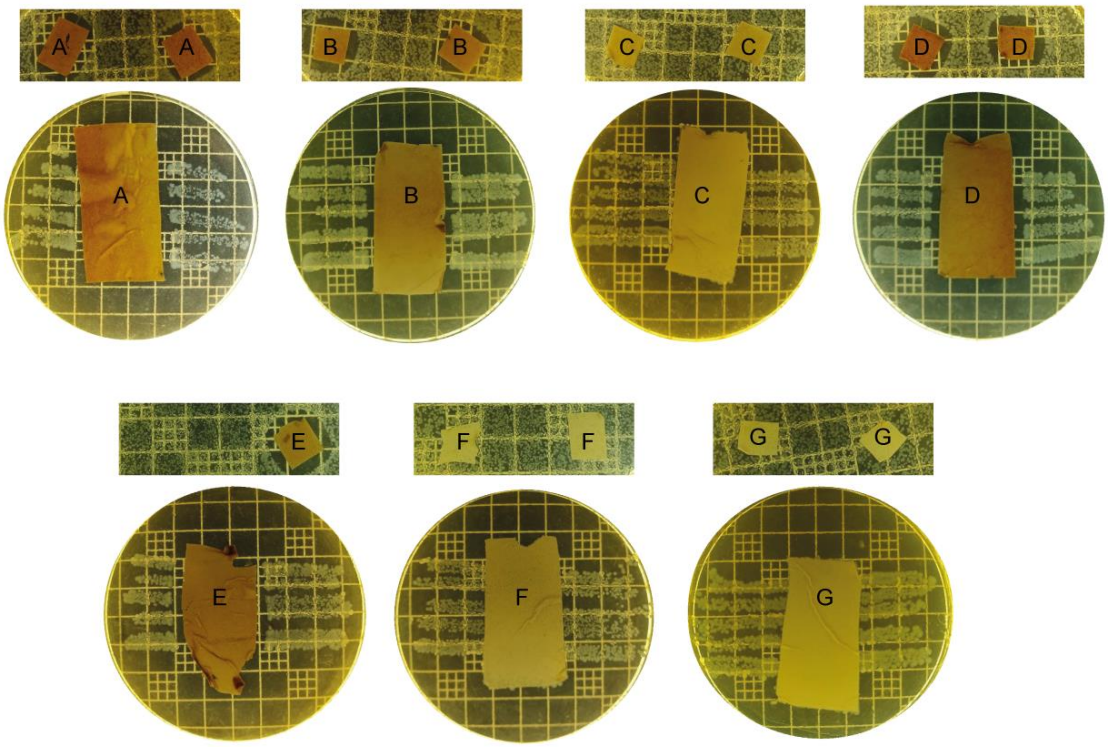

Figure 29 – Disc diffusion and striation antibacterial assays against *E. coli* with samples A, B, C, D, E, F and G

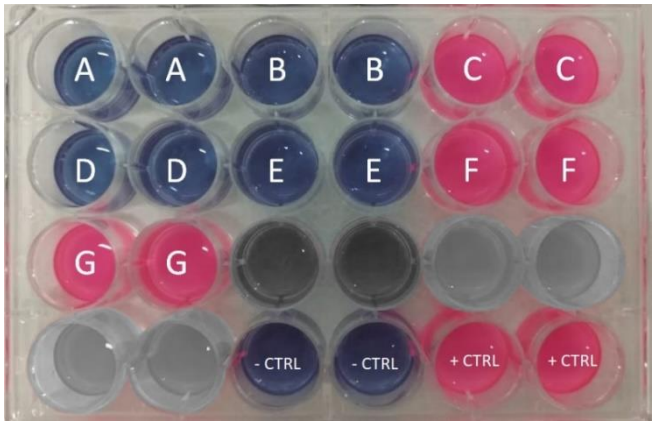

Figure 30 – Antibacterial assay in liquid medium against *S. aureus* with samples A, B, C, D, E, F and G

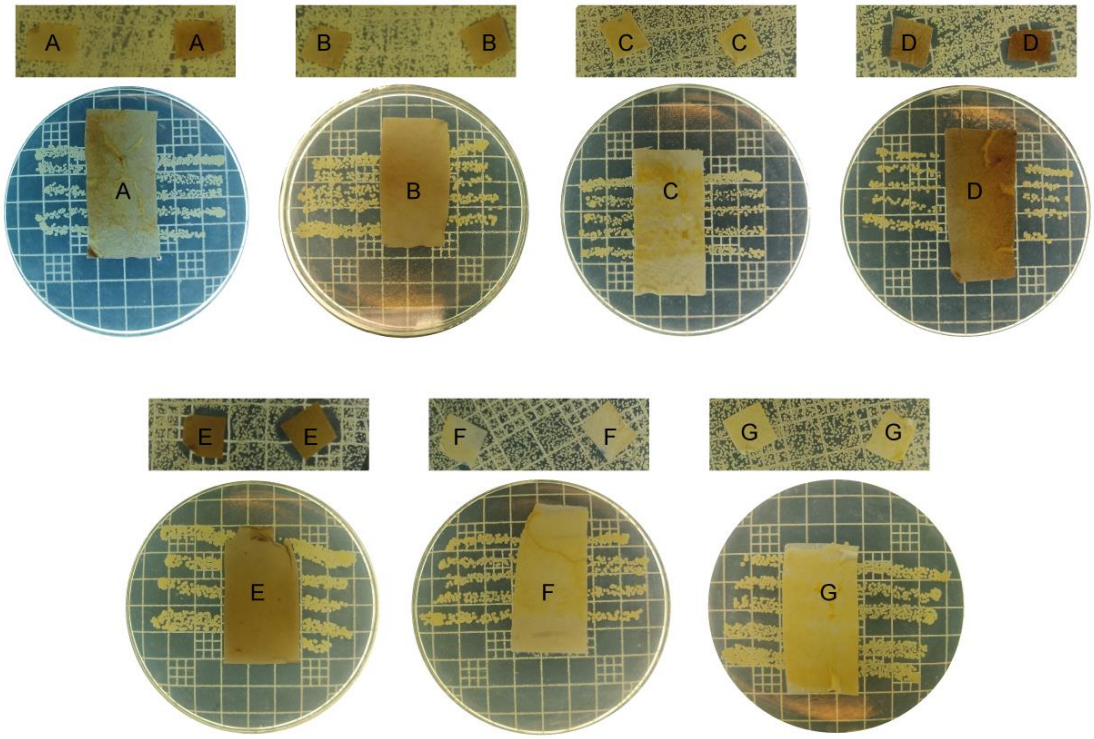

Figure 31 – Disc diffusion and striation antibacterial assays against *S. aureus* with samples A, B, C, D, E, F and G

Figure 32 – Antibacterial assay in liquid medium against *S. aureus* with samples A, B, C, D, E, F and G

Table 4 – Inhibition halos formed by the samples in antimicrobial assays

Sample	**Bacterium**	**Thickness of the inhibition halo in the disc diffusion assay** (mm)	**Thickness of the inhibition halo in the striation assay** (mm)
A	*E. coli*	3.0	2.0 – 3.0
B	*E. coli*	2.0 – 3.0	1.0 – 3.0
D	*E. coli*	3.0 – 4.0	3.0
E	*E. coli*	3.0	3.0
D	*S. aureus*	2.0 – 3.0	2.0 – 3.0
E	*S. aureus*	2.0 – 3.0	1.0

The results of the antimicrobial assays in liquid medium align with the findings from the bactericidal tests in the semi-solid medium. The solutions with *E. coli* containing the samples with AgNPs (A, B, D and E) remained blue, indicating bacterial growth inhibition. In contrast, the other solutions containing samples C, F and G turned pink, signifying aerobic respiration by the microorganisms in the solution. In the case of *S. aureus*, the solutions with samples A, D and E remained blue, while the solutions with samples B, C, F and G turned pink, that is, they indicated the presence of microorganisms.

Regarding the action of the samples, it was observed that *E. coli* grew on the Petri dish after inoculation with the solution containing samples A and E (**Figure 33**). This result indicates that these samples exhibit bacteriostatic properties. In contrast, sample D demonstrated bactericidal activity, as no bacterial growth was observed. All samples showed bacteriostatic effects against *S. aureus*.

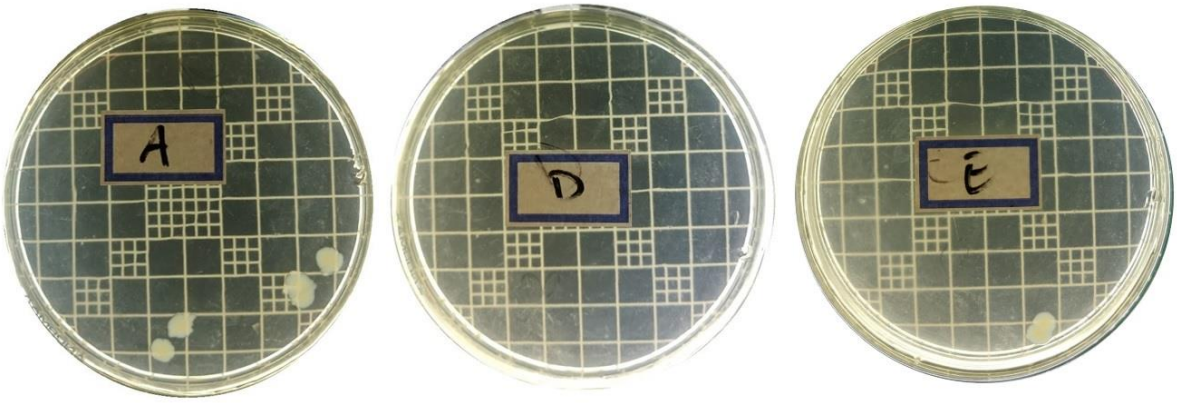

Figure 33 – Evaluation of the bactericidal or bacteriostatic character of PA6-Ag10 and PA6-Ag20 samples with *E. coli*

A study evaluating the antibacterial activity of AgNPs supported on starch nanofibers found that all tested concentrations (5-100 mg mL^{-1}) effectively inhibited the growth of *E. coli* and *S. aureus* (LV et *al*., 2021). The authors suggested that AgNPs interact with the bacterial cell wall, altering its permeability and ultimately leading to cell death. Tang and Zheng (2018) further explained that when AgNPs accumulate in the cell wall and membrane, they induce morphological changes, such as cytoplasm shrinkage, membrane detachment, and membrane disruption, which can be observed by TEM. Another study, conducted by Xu *et al.* (2020), investigated the antibacterial action of AgNPs supported on regenerated oxidized cellulose microfibers. In addition to observing inhibition halos in disk-diffusion assays with *E. coli* and *S. aureus*, the authors confirmed the activity of AgNPs through a fluorescent staining assay, where almost all bacteria were killed, highlighting the strong damaging effect of AgNPs on the bacterial membrane.

Anuar *et al.* (2024) observed antimicrobial activity of GO against Gram-positive bacteria, such as *S. aureus* and *B. subtilis*, and Gram-negative bacteria, such as *E. coli* and *P. aeruginosa*. In disk diffusion tests, the authors observed the formation of inhibition halos around the GO samples in tests with all these bacteria and found that the diameter of the halo

is directly dependent on the concentration of GO used. According to the authors, the mechanisms of elimination of bacteria from GO include ROS, the entry of GO into the cells, and the reaction between the epoxy groups of GO with the amino and carboxyl groups in the cell walls of the bacteria. Bentedlaouti, Belouatek and Kebaili (2024) evaluated the action of GO and GO with AgNPs against different Gram-positive and Gram-negative bacteria, as well as a fungus. The authors observed, in the disk diffusion test, the formation of inhibition zones around the samples with all the microorganisms evaluated. The GO-Ag samples showed significantly larger zones of inhibition than the GO samples, clearly indicating the occurrence of a synergistic effect between GO and AgNPs, increasing the antimicrobial capacity of the materials. Similar results were observed by Chaudhary *et al.* (2024), who also compared GO and GO-AgNPs samples against Gram-negative and Gram-positive bacteria. The authors believe that these nanocomposites are a potential alternative to common antibiotics.

Although the literature clearly presents results in which GO is used as an antimicrobial, this effect was not observed in our tests, in the same way that it was not possible to observe a synergistic effect with AgNPs. The previous characterization of GO showed that the material is not pure and it was not possible to evaluate its thickness. Thus, it can be speculated that this material is not a GO, which explains the results obtained in the antimicrobial tests. Thus, the samples containing GO were not further analyzed. The work continued with samples A and D, containing only AgNPs, and sample G, without any additive, which was used as a control sample.

4.6.2 Antiviral assays

Regarding the antiviral assays, samples A and D exhibited, respectively, a reduction of 99.0 and 99.9% of viral particles, demonstrating significant antiviral activity against betacoronavirus MHV-3. García-Serradilla and Risco (2021) evaluated the antiviral effects of

non-toxic concentrations of AgNPs against the Bunyamwera virus (BUNV), a group of pathogenic viruses affecting humans, animals, and plants. The authors reported that AgNPs could inhibit viral replication by up to three orders of magnitude (99.9% of viral reduction). In another study, Jeremiah *et al.* (2020) tested various concentrations and sizes of AgNPs and found that those with an average diameter of 10 nm and concentrations between 1.0 and 10 ppm were effective in inhibiting SARS-CoV-2. The authors noted that cytotoxicity was only observed at concentrations of 20 ppm and above, suggesting that AgNPs are highly potent against SARS-CoV-2 when used carefully to avoid potential harm to health and the environment.

Our results indicate that the antimicrobial and antiviral activities of the samples are directly correlated with the concentration of AgNPs. Medvedev *et al.* (2023) observed that both concentration and the size of AgNPs influence in the antimicrobial and antiviral effectiveness of melt blown PP fibers loaded with AgNPs. This finding is consistent with the work of Lv *et al.* (2021), who indicated these factors affect the cytotoxicity of the samples.

The antiviral activity of AgNPs can be explained by different mechanisms. One of them is that AgNPs can bind in the surface of RNA viruses, preventing the fusion of the virus and the host cell. AgNPs can also interact with the viral genome and block the replication inside the host cell (WIELER et al., 2023; ALLAWADHI et al., 2021).

4.7 CYTOTOXICITY ASSAYS

4.7.1 MTT assay

Although the filter elements do not come in direct contact with the skin of facial respirators users, it is essential that these materials pose no risk to users. The cell viability results for the L929 cell line exposed the pure extract and the diluted solutions (10, 50, and 90%) of A, D and G samples are shown in **Figure 34**.

It can be observed that after 1 and 2 days, all solutions inhibited cell growth by more than 30%, indicating a cytotoxic character. However, after 7 days, the 10 and 50% extracts did not exhibit cytotoxicity for any of the samples. Additionally, the 90% extract and the pure extract of sample G were not cytotoxic, as cell viability exceeded 70%, suggesting that the cells adapted to the experimental conditions. These results correlate with the antimicrobial and antiviral assays, showing that cytotoxicity increases with higher concentration of AgNPs.

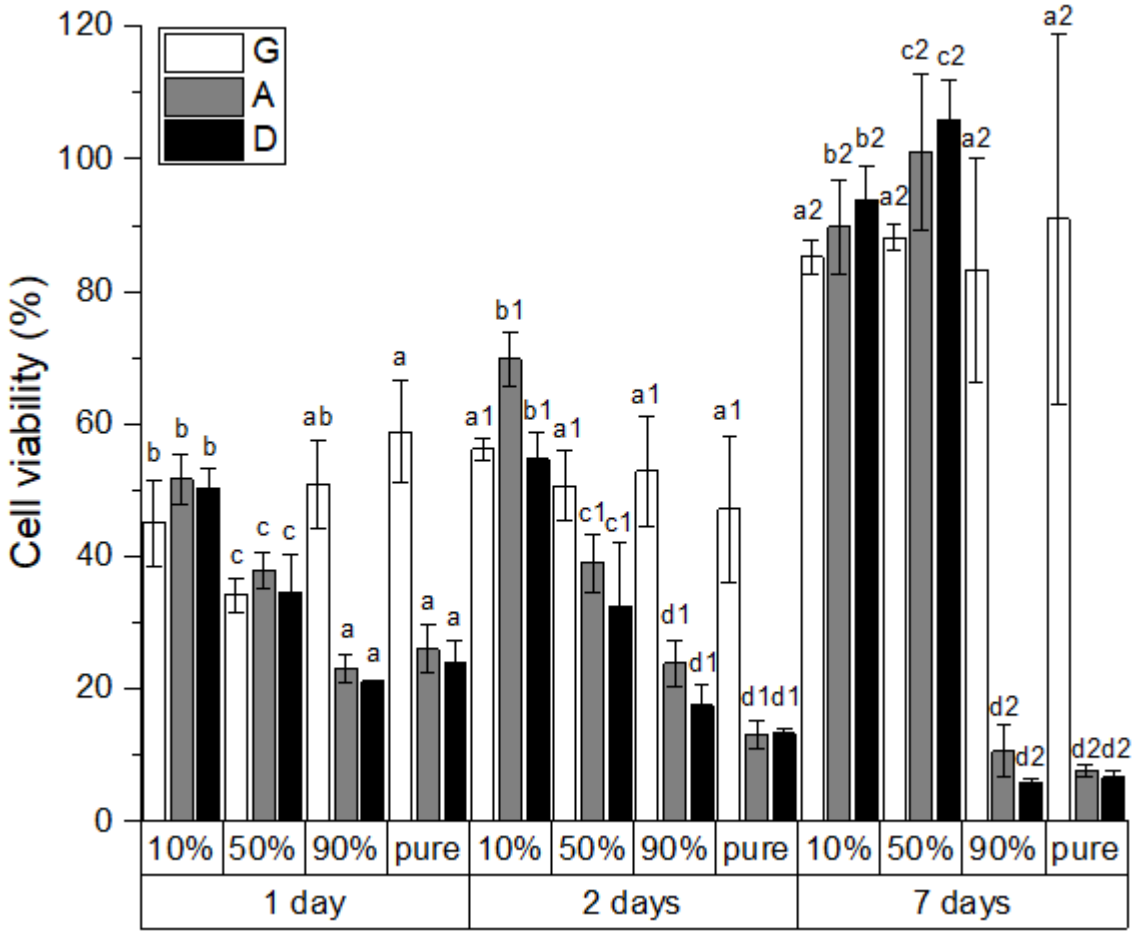

Figure 34 – Cell viability of L929 strain with PA6, PA6-Ag10, and PA6-Ag-20 samples (Equal letters indicate no statistical difference between the groups; different letters indicate statistically significant differences)

In vitro analyses, such as the MTT assay, are typically the first step in assessing the

toxicity of a material. Cytotoxicity data are essential for defining the concentrations used in subsequent in vivo assays (e.g., with guinea pigs). Although there is no standard method to directly translate vitro data into in vivo parameters, it is widely recognized that concentrations can often be scaled up significantly.

A guide published by the United States Health Service ((NATIONAL INSTITUTE OF HEALTH, 2015) indicated that linear regression can be employed to compare the concentration that kills 50% of cells (IC_{50}) in vitro with acute toxicity in vivo (LD_{50}). The guide emphasized the need for case-by-case evaluations, as the regression was applied to 347 chemical compounds, each yielding different results. Nevertheless, it is evident that for all compounds tested, LD_{50} values were higher than IC_{50} values.

In a similar approach, another study evaluated the minimum inhibitory concentration (MIC), total lethal concentration, and no observable adverse effects concentration (NOAEC) of AgNPs in different cell lines. These findings indicated that, depending on the cell line, the concentration could be 5 to 18 times higher (SAMBALE *et al.*, 2015), suggesting that the cytotoxicity of AgNPs varies according to the evaluated cell line.

A literature review (KRUSZEWSKI *et al.*, 2011) demonstrated that cell viability decreases with increasing concentrations of AgNPs. Beyond concentration, other factors such as the size and shape of the AgNPs, functionalization of the surface, exposure time, and the specific cell line being studied significantly influence the outcomes.

Souter *et al.* (2019) observed that even the culture medium used for L929 cell line cultivation affects the cytotoxicity of Ag^+ ions. According to Rajan *et al.* (2022), it is still not possible to have a conclusion about the cytotoxicity of AgNPs, a definitive conclusion on the cytotoxicity of AgNPs is not yet possible. Further studies with robust controls are necessary to expand the current understanding of AgNP cytotoxicity.

4.7.2 Cell adhesion

Figure 35 shows the FEG-SEM micrographs of samples A, D and G obtained in the cell adhesion assay. It is evident that cell adhesion occurred only on sample G. The cells, identifiable as small uniformly distributed spheres, can be observed on sample G. This result suggests that the samples A and D are cytotoxic to the L929 cell line, preventing cell growth and, consequently, adhesion to the microfibers.

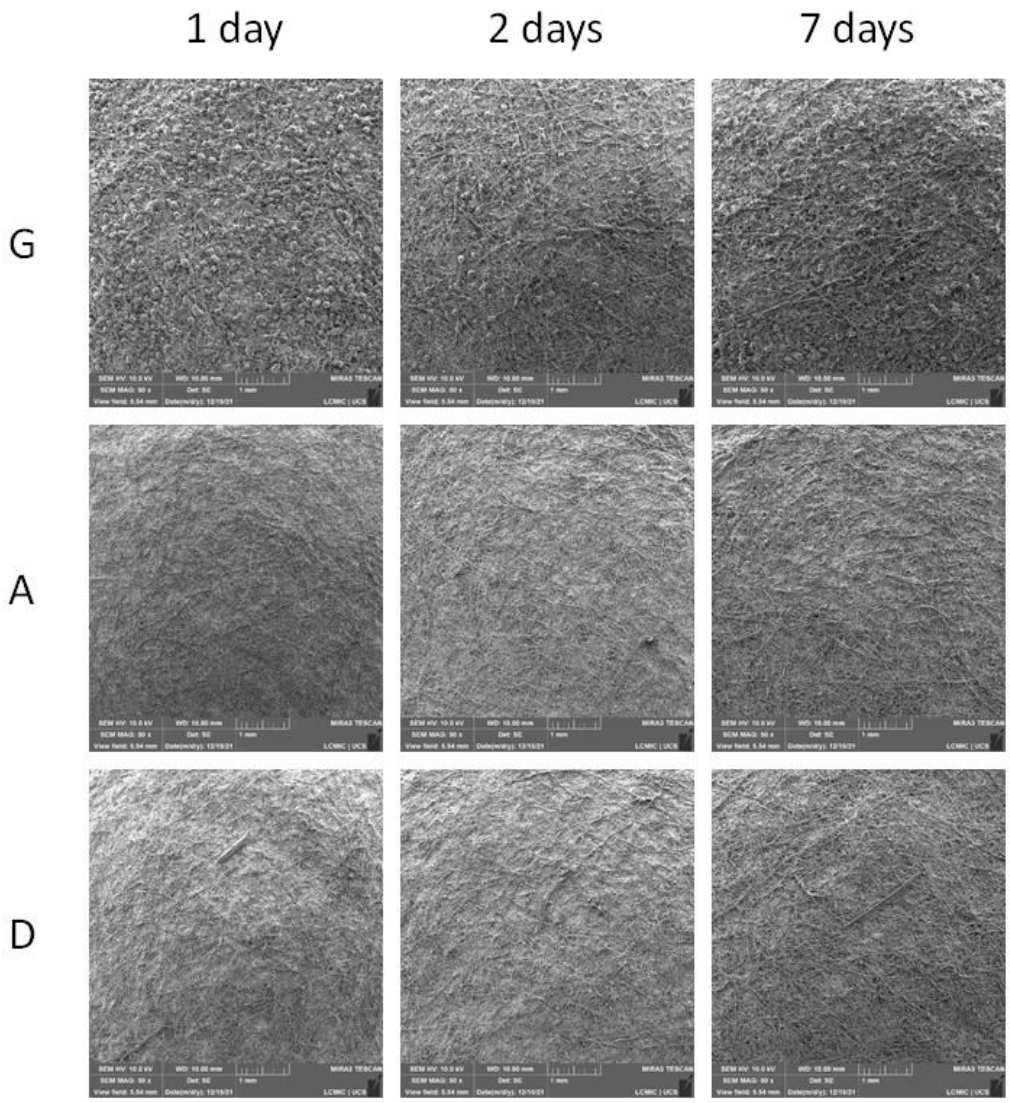

Figure 35 – FEG-SEM micrographs of PA6, PA6-Ag10 and PA6-Ag20 samples for evaluation of L929 cell adhesion

Martin *et al.* (2019) analyzed the effect of AgNPs on the basement membrane of epithelial cells. Their findings indicate that exposure to AgNPs disrupts the dynamics of the basement membrane and cell adhesion. The authors concluded that their data provide a foundation for future studies to investigate the effects of long-term exposure of cellular tissues to AgNPs.

4.8 CHARACTERIZATION OF PA6-AgNPs MICROFIBERS

The UV-Vis reflectance spectra of samples A and D (**Figure 36**) exhibited patterns similar to those reported by Alahmadi *et al.* (2018) and Zi-Qiang *et al.* (2018), confirming the reduction of $AgNO_3$ to AgNPs.

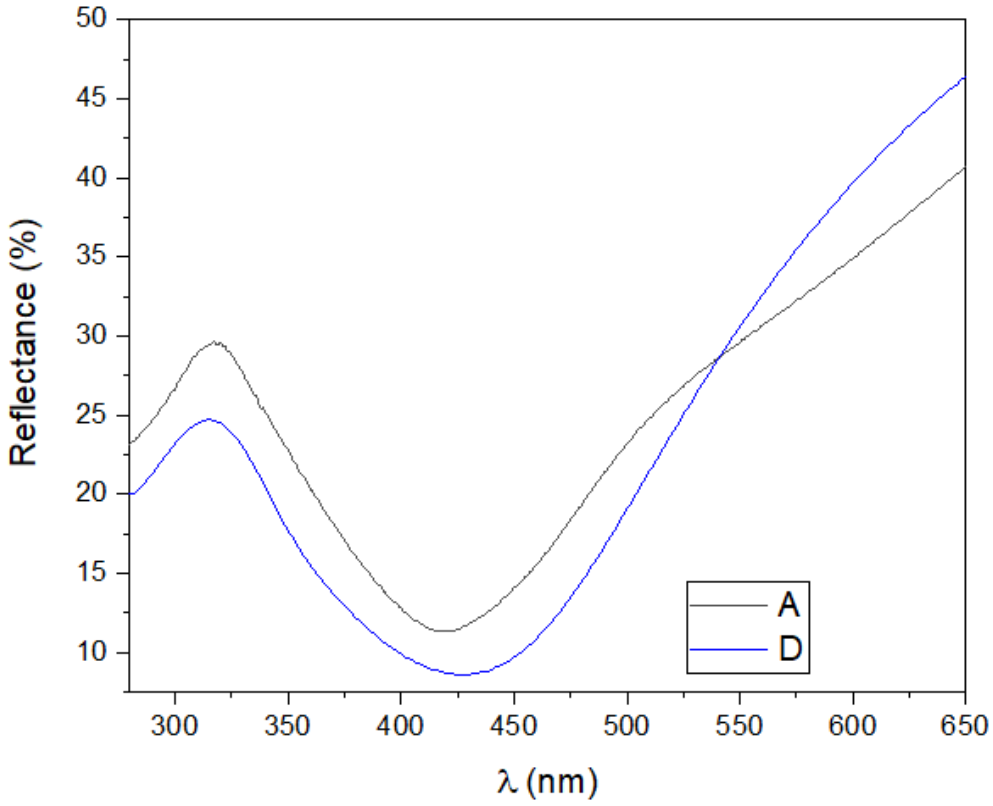

Figure 36 – UV-Vis diffuse reflectance spectra of samples A and D

The minimum reflectance, observed at 419 nm for PA6-Ag10 and at 425 nm for PA6-Ag20, is indicative of spherical AgNPs with an approximate size of 10 nm (ALAHMADI et al., 2018). The intensity of the peaks varies proportionally with the concentration of AgNPs in each sample confirming the stability of the AgNPs post-blow spinning, as also observed in the TEM micrographs. This assay confirms the stability of AgNPs after the blow spinning process.

Figures 37, 38 and **39** present the FEG-SEM micrographs and EDS composition maps of samples G, A and D, respectively. The microfibers in both A and G samples are randomly arranged, forming an interconnected network. Additionally, some beads were observed, which are well-distributed without aggregation or negative impact on the arrangement of the microfibers. In contrast, sample G shows a higher bead formation, which seems to affect the arrangement of the microfibers, leading to some agglomeration. Regarding the EDS composition maps, it was observed that AgNPs were distributed uniformly throughout both A and D samples.

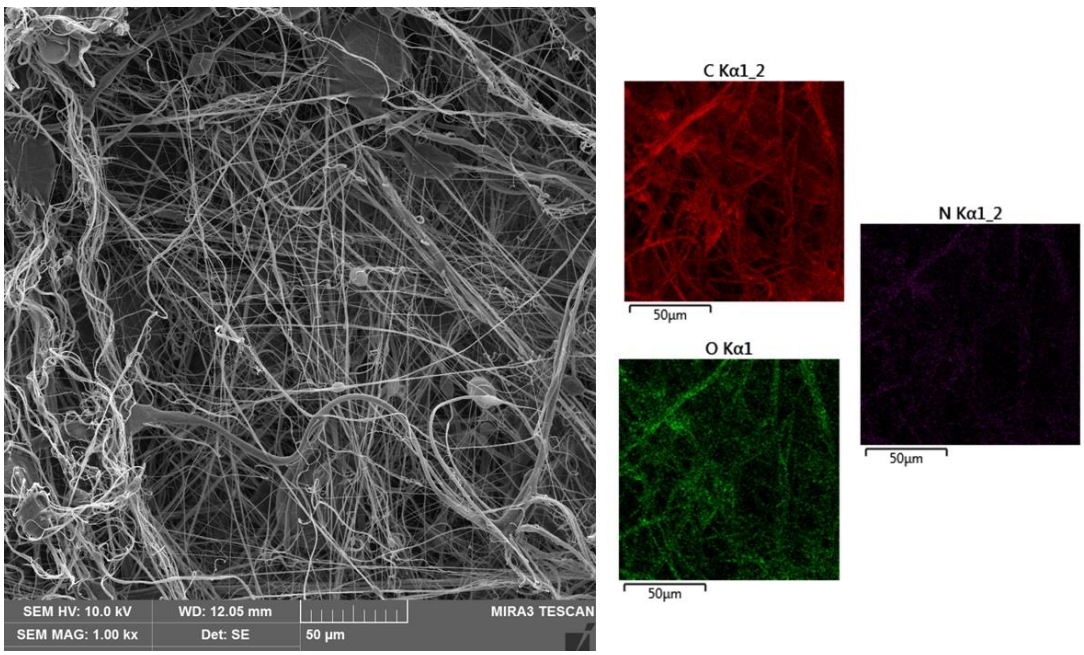

Figure 37 – FEG-SEM micrographs and EDS composition maps of sample G

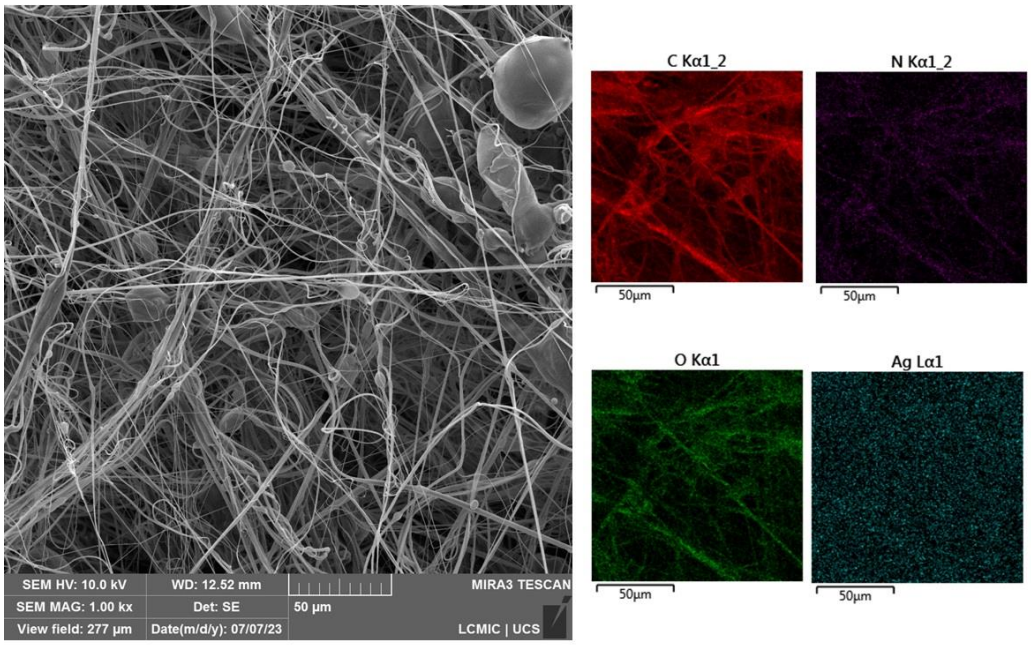

Figure 38 – FEG-SEM micrographs and EDS composition maps of sample A

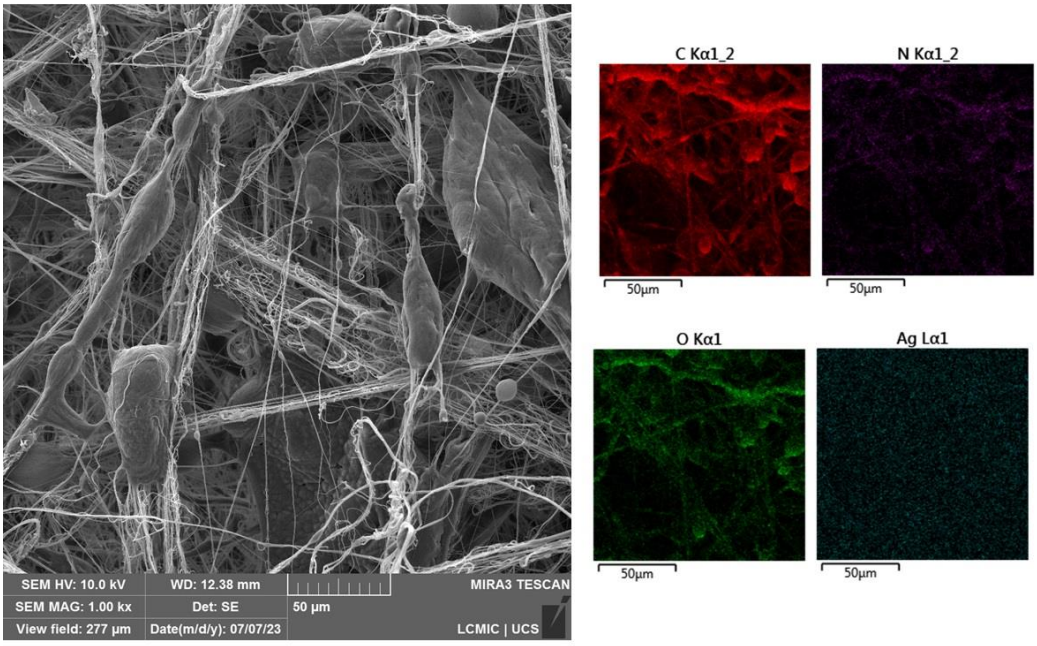

Figure 39 – FEG-SEM micrographs and EDS composition maps of sample D

Kasiri et al. (2020) also reported the presence of beads in polystyrene (PS) microfibers produced by solution blow spinning. The authors evaluated different processing conditions and

noted some variations in the samples; however, the general morphology was characterized by the presence of microfibers along with areas where PS accumulated in the form of beads. Zhang, Xu and Liu (2025) investigated the presence of beads in nanofibers structures for air filtration using computational fluid dynamics based on the parameters available on the literature. They concluded that the bead shape has minimal impact, but the presence of beads help reduce pressure drop and the presence of beads enhances filtration performance. The size of the beads, however, plays a significant impact in the quality, since as the size increases, efficiency decreases and affects the performance of the filtration.

The contact angles observed for the samples are presented in **Table 5**. Although both samples A and D showed an increase in hydrophobicity compared to sample G, as demonstrated in **Figure 40**, it was observed during testing that the water droplet was absorbed within a few seconds. This indicates that all the samples retain hydrophilic characteristics. PA6 nanofibers combined with soot pre and post-synthesis were analyzed by Alvarenga *et al.* (2023). They observed that the initial angles which indicated hydrophobic behavior turned to 0° in 2 min and a sample that was chemically activated with NaOH exhibited and angle of 0° in 20 s, therefore, indicating that even with high initial contact angles, all the samples present hydrophilic behavior.

Table 5 – Water contact angle for G, A and D samples

Sample	**Contact angle** (°)
G	83.9
A	111.6
D	104.3

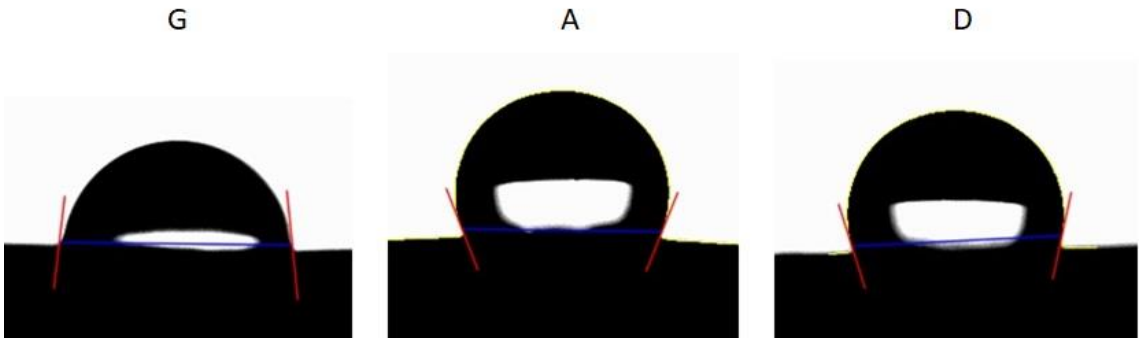

Figure 40 – Images obtained from the water contact angle test for samples G, A and D

Lv et al. (2021) observed a similar effect in starch nanofibers containing AgNPs compared to pure starch nanofibers. In nanofibers without AgNPs, the water drop was absorbed immediately, whereas in nanofibers with AgNPs, the contact angle increased proportionally with the concentration of AgNPs, although the water drops still took only 1.0 s to be absorbed. Zhang et al. (2023) conducted a study where they replaced the inner layer of a standard melt-blown mask with a composite membrane made from nylon-6 micro and nanofibers, which exhibited hydrophilic properties. They found that this modification allowed for better transfer of condensation generated during breathing to the outer layer of the mask, enhancing the wearer's comfort. Moreover, the filtration efficiency of the masks incorporating composite nanofibers remained consistently high, even under elevated humidity and temperature conditions, unlike conventional melt-blown masks. According to Niu *et al.* (2025), the formation of water droplets on the inside of masks due to the breathing process, especially in colder seasons, negatively impacts the breathability and comfort of the user. The authors developed Janus fibrous membranes, that is, membranes formed by layers of different materials with distinct wettability properties, forming a wettability gradient in which water droplets do not form on the inside of the mask, nor is it possible for moisture from the outside air to penetrate the mask. PAN-SiO_2 and PS-PU fibers were produced, which presented good performance, high filtration and low-pressure drop, in addition to ensuring comfort during use.

The thermal stability of filter elements is crucial to prevent deterioration of their properties during use or storage. **Figure 41** presents the TGA and DTG curves for all the samples. As observed, the first weight loss occurs within the temperature range of 50–100 °C, corresponding to the evaporation of water absorbed by the samples due to the hydrophilic nature of PA6 (OULIDI *et al.*, 2022). The recorded weight losses for G, A and D samples were 2.9, 2.2, and 1.7%, respectively. Overall, the curves display similar trends, with the addition of AgNPs increasing the thermal stability of the microfibers. Previous studies have shown that PA6 microfibers experience a significant weight loss around 350 °C, which is associated with the initial stage of PA6 decomposition due to scission of C–C bond (OULIDI *et al.*, 2022; VISCUSI *et al.*, 2023). Alvarenga *et al.* (2023) observed that PA6 nanofibers mats were completely decomposed before 450 °C.

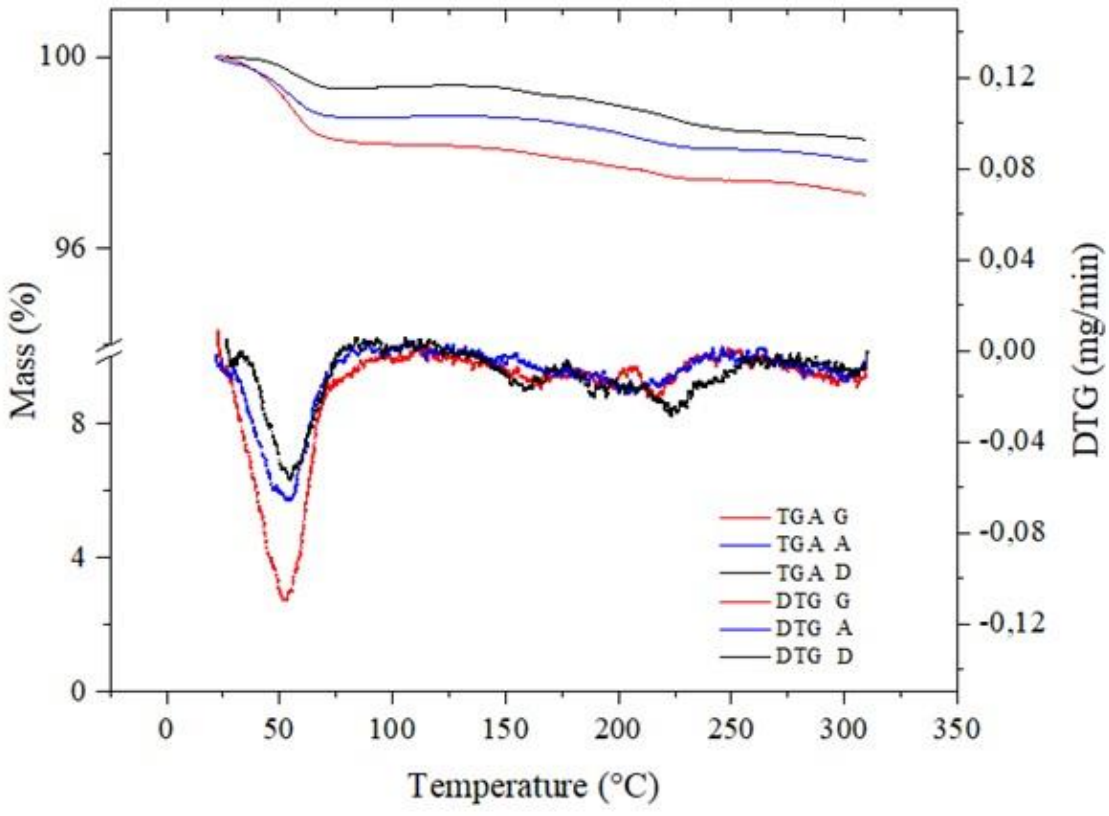

Figure 41 – TGA and DTG curves of samples A, D and G

To ensure optimal breathability, filter elements must minimize the pressure drop (RUSSO *et al.*, 2022). The Brazilian standard NBR 13698:2022 specifies the maximum allowable pressure drop for both inhalation and exhalation, which serves as a criterion for approving filter elements for practical use. **Table 6** presents the inhalation and exhalation pressure drops for each sample.

Table 6 – Resistance to inhalation and exhalation of A, D and G samples

Sample	**Airflow**	**Flow rate** (L min^{-1})	**Pressure drop** (Pa)
G	Inhalation	30	28 40 62
		95	71 98 168
	Exhalation	160	166 189 299
A	Inhalation	30	50 43 40
		95	135 113 105
	Exhalation	160	250 277 279
D	Inhalation	30	86 66 71
		95	235 178 192
	Exhalation	160	554 366 312

As shown, samples A and G exhibited pressure drops below the maximum allowed in all tests, indicating their suitability for use in facial respirators. In contrast, sample D showed pressure drop values exceeding the permissible limits during exhalation tests, indicating it does not meet the NBR 13698:2022 standard for facial respirators. This observation aligns with the FEG-SEM micrographs, where a higher bead formation was observed in sample D causing fiber agglomeration.

The PVDF nanofiber membranes obtained by Al-Attabi *et al.* (2023) demonstrated high filtration efficiency and greater durability and comfort when wearing compared to commercial masks, due to the low pressure drop, which was obtained by controlling the operational parameters of the electrospinning process. Other studies have also highlighted the potential of polymeric micro and nanofibers as filter elements due to their high filtration efficiency and low pressure drop (XU *et al.*, 2021; YAN *et al.*, 2019). For instance, Bortolassi *et al.* (2019) observed that silver nanoparticles in polyacrylonitrile (PAN) solutions increased the viscosity of the PAN solutions, leading to enhanced chain entanglement within the polymer. This, in turn, resulted in an increased pressure drop in the electro spun nanofibers produced from these solutions. The relationship between the thickness and porosity of PA6 nanofibers membranes produced by SBS was related to the pressure drop and filtration efficiency by Alvarenga *et al.* (2024). The authors found that the greater the thickness of the material, the greater the pressure drop and also the filtration efficiency. In general, a good filtration capacity was observed for nanoparticles with diameters between 30 and 300 nm, indicating that these nanofibers have great potential for application in filtration systems for nanoparticles and viruses, in addition to the possibility of being integrated into other types of membranes to achieve filtration efficiency similar to high efficiency particulate air (HEPA) filters. Alaeddin *et al.* (2025) evaluated the effect of nanofibers diameters with the efficiency of filtration and pressure drop. The authors used mathematical relationships and an experimental design model to predict optimal

conditions of electro spun PVDF nanofibers with different concentrations of the polymer and GO and cooper oxide nanoparticles (CuONPs). They observed that the addition of NP decreases the diameter of the nanofibers and, consequently, decreases the pressure drop and increases the filtration efficiency. Similar results were found by Hashmi, Ullah and Kim (2019), who concluded that the addition of CuONPs to PAN nanofibers improved the breathability of the samples.

4.9 EVALUATION OF THE AGING SAMPLES

In the antimicrobial assays with aged samples, no inhibition halos were observed around the samples in semi-solid medium (**Figure 42**). Conversely, in the liquid medium assay, the results were consistent with those observed in the initial tests: samples A and D inhibited bacterial growth (**Figure 43**). Additional analysis was performed to assess the action of the samples, and, once again, sample A demonstrated bacteriostatic behavior, while the sample D exhibited bactericidal behavior against *E. coli* (**Figure 44**).

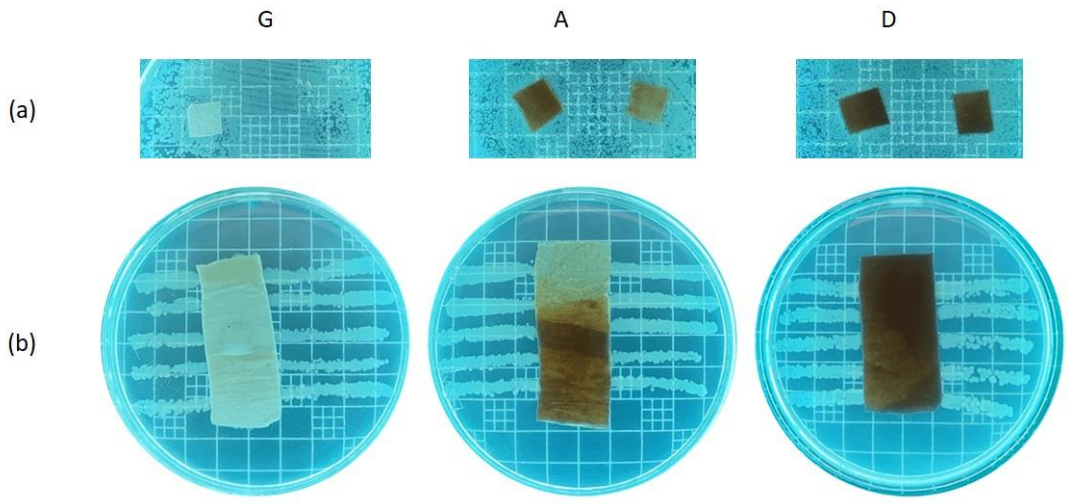

Figure 42 – (a) Disc diffusion and (b) striation antibacterial assays against *E. coli* with A, D and G samples

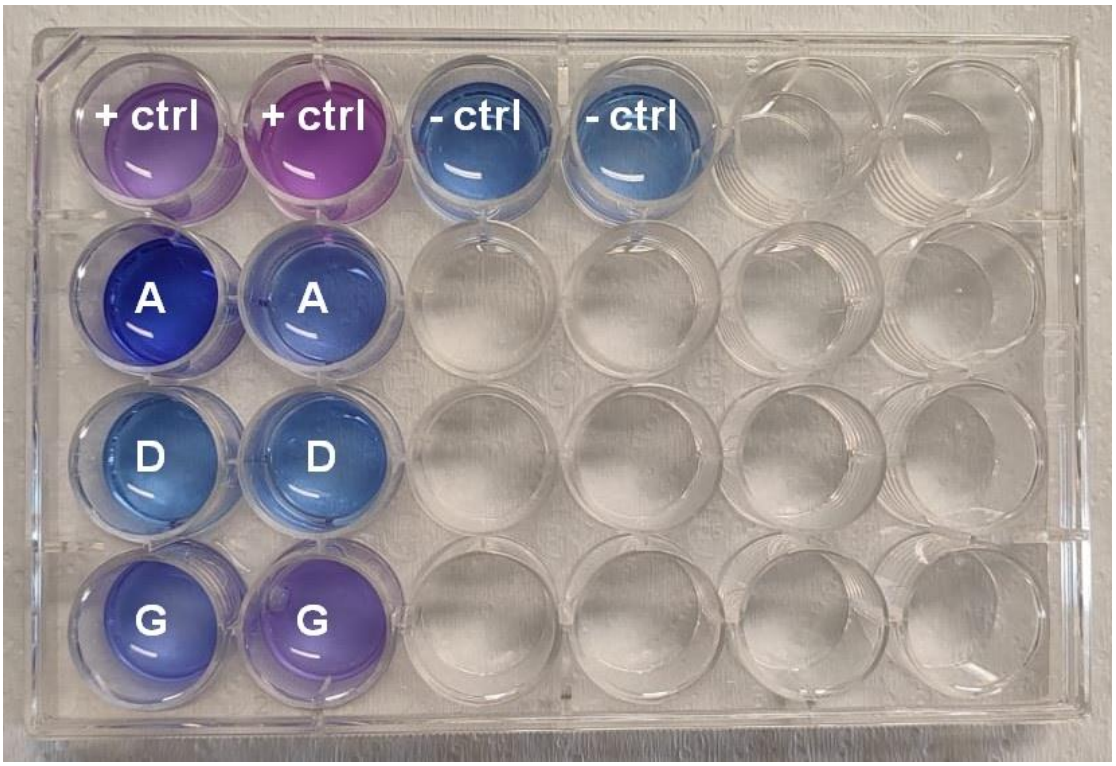

Figure 43 – Antibacterial assay in liquid medium against *E. coli* with aged A, D and G samples

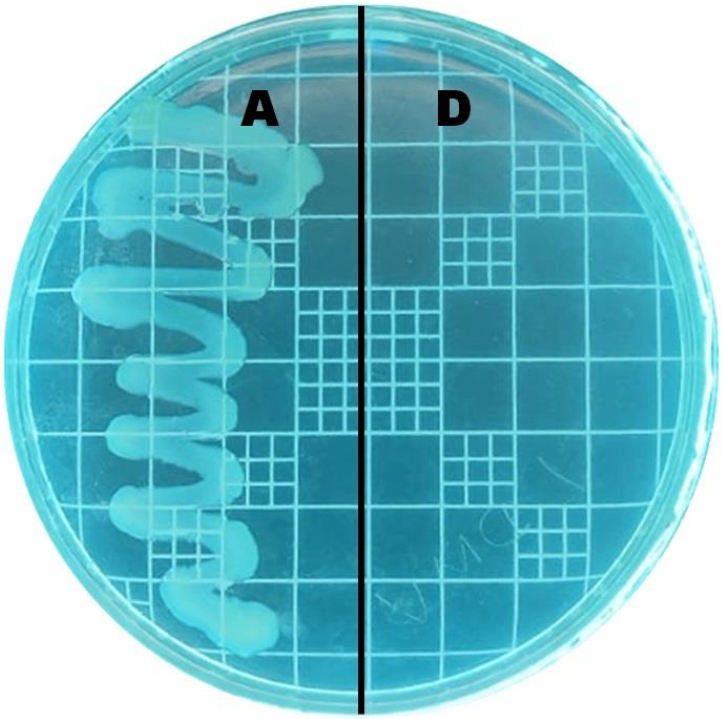

Figure 44 – Evaluation of the bactericidal or bacteriostatic character of aged A and D samples with *E. coli*

Regarding the MTT assay, the results presented in **Figure 45** demonstrate that the solutions exhibited lower cytotoxicity compared to the first assay, although cell viability remained below 70% on days 1 and 2. On day 7, as observed in the previous assay, the 10 and 50% solutions showed cell viability greater than 70%, whereas the 90% solutions and pure extract solution continued to exhibit cytotoxicity.

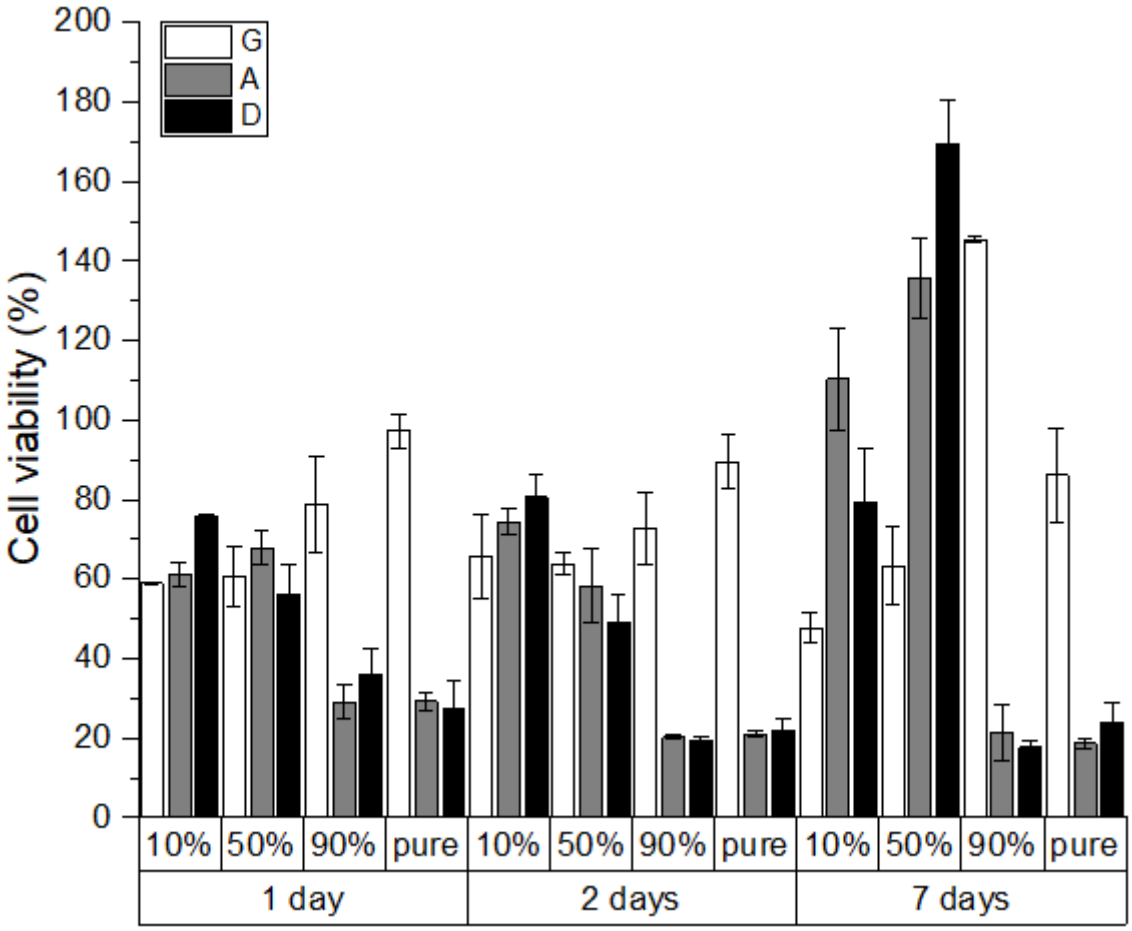

Figure 45 – Cell viability of L929 strain with one-year-old A, D and G samples

Although some properties of the aged samples remain similar to those of the new samples, it is evident that significant changes have occurred. Changes in the properties of AgNPs over time have also been observed in previous studies. Santos *et al.* (2024) observed that AgNPs lost their activity against *S. aureus* after 1 year of storage, regardless of the concentration used. The authors suggest that factors such as changes in the surface composition of AgNPs, silver

oxidation, and nanoparticle aggregation could explain this behavior. Wang *et al.* (2020) demonstrated that AgNPs undergo physicochemical transformations with aging. These changes include an increase in the dissolution of Ag^{+} ions, aggregation, and particle size growth, which ultimately result in reduced toxicity. However, over shorter periods AgNPs demonstrated stability, as presented in the work of Syukri et al. (2021), in which AgNPs were synthesized on a surgical nylon suture and maintained their properties against gram-positive and gram-negative bacteria for 12 weeks. This indicates that further studies must be carried out evaluating different periods to verify the shelf life of materials containing AgNPs.

5 CONCLUSIONS AND FUTURE PERSPECTIVES

This study demonstrated the feasibility of producing hybrid microfibers via the blow spinning process, incorporating additives with antiviral and antimicrobial properties that make them suitable for applications such as filter elements.

The characterization of commercial GO revealed discrepancies between its actual properties and those stated in its datasheet. This step proved crucial, as it provided insight into the unexpected behavior observed compared to the literature.

Silver nitrate synthesized from recovered silver exhibited high purity. Its incorporation into PA6 solutions enabled the in-situ synthesis of AgNPs directly within the polymer matrix.

Defining the blow spinning parameters was essential to obtaining microfibers with appropriate configurations for the intended application. For a 15 % *wt* PA6 solution with a 2:1 (v/v) solvent ratio, the optimal parameters were: airbrush opening of 0.3 mm, air pressure of 0.5 MPa, collector distance of 30 cm, and spinning duration of 20 minutes.

Microbiological assays showed that all samples containing AgNPs exhibited antibacterial activity against *E. coli* and *S. aureus*. The sample with the highest AgNP content demonstrated a bactericidal effect against *E. coli*, confirming that antimicrobial efficacy is directly related to AgNP concentration. In contrast, samples containing GO did not show antimicrobial activity, nor was a synergistic effect between AgNPs and GO observed. These unexpected results, contrary to the literature, were attributed to the characterization findings, which indicated that the commercial GO was a carbonaceous material with low carbon content and significant impurities. Consequently, GO-containing samples were excluded from further testing.

In antiviral assays, the samples showed a significant reduction in beta coronavirus particles. Sample A achieved a 99.0% reduction, while sample D achieved a 99.5% reduction,

both qualifying as antiviral.

Cytotoxicity assays indicated that the samples were cytotoxic to L929 cells on days 1 and 2. However, by day 7, some extracts demonstrated cell viability above 70%, suggesting possible cellular adaptation.

Morphological analysis showed that the microfibers formed randomly arranged, interconnected networks, except for sample D, where bead formation led to fiber agglomeration. All samples exhibited hydrophilic behavior and good thermal stability. While minor differences in properties were noted depending on AgNP concentration, no significant variations were observed in overall performance.

Breathability tests revealed that samples A and G met acceptable standards for inhalation and exhalation resistance. Sample D, however, failed the exhalation test due to a higher pressure drop.

Aging studies demonstrated that the properties of the materials are time-dependent, with AgNPs showing decreased stability over time.

In conclusion, PA6-AgNP microfibers present suitable properties for antibacterial and antiviral applications. Among the tested samples, sample A stands out as an effective candidate for use as a filter element in facial respirators.

The combination of in-situ AgNP synthesis and blow spinning proved to be a scalable and cost-effective approach, reducing the need for post-processing steps and enhancing material uniformity. The methodologies established and validated in this work also provide a solid foundation for future investigations into the development of advanced fibrous materials with tailored functionalities, including the incorporation of other nanomaterials or active compounds.

Although the COVID-19 pandemic was officially declared over by the WHO and mask-wearing is no longer mandatory or widely recommended, the work presented here contributes

to the advancement of scientific knowledge and could be applied as a preventive measure in future pandemics. In a broader context, these findings align with the growing global demand for functional materials capable of mitigating biological risks in healthcare, public transportation, and indoor environments. In addition, it holds potential for use in other applications that require antibacterial and antiviral materials. Notably, the in-situ synthesis of AgNPs in the polymeric solution is an efficient process that simplifies and accelerates microfiber production while ensuring sample homogenization.

In the short term, future studies could test a different sample of GO, with suitable characteristics, and evaluate whether the results obtained show improvements in relation to those observed to date. If a synergistic effect is observed between graphene oxide and silver nanoparticles, the possibility of reducing the concentration of AgNPs used could be evaluated.

Another evaluation that can be assessed in the short term is the production of fibers using exactly the same concentration of PA6 and AgNPs, but through the electrospinning method. Although the literature presents some review studies comparing the methods and, in general, presenting the SBS process as faster, simpler, and less expensive, there is still a lack of research studies comparing fibers obtained from exactly the same solutions using different techniques.

In the medium and long term, future studies should evaluate the stability of the samples to clearly determine their shelf life. Furthermore, the recyclability and/or correct disposal of the samples after use should be investigated to ensure user and environmental protection, especially considering the increasing focus on sustainable materials development.

PUBLICATIONS

SARTORI, PAULA; DELAMARE, ANA PAULA LONGARAY; MACHADO, GIOVANNA; DEVINE, DECLAN M.; CRESPO, JANAINA S.; GIOVANELA, MARCELO. Synthesis and Characterization of Silver Nanoparticles for the Preparation of Chitosan Pellets and Their Application in Industrial Wastewater Disinfection. Water, v. 15, p. 190, 2023.

SARTORI, PAULA; AGUZZOLI, CESAR; ROESCH-ELY, MARIANA; DEVINE, DECLAN M.; GIOVANELA, MARCELO; CRESPO, JANAINA S. Antibacterial and antiviral PA6-AgNPs microfibers for application as a filter element in facial respirators. INORGANIC CHEMISTRY COMMUNICATIONS, v. 165, p. 112511, 2024.

RESTELATTO, DANIELLE; BORTOLUZ, JORDANA; SARTORI, Paula; GUERRA, NAYRIM B.; CID, CRISTIANI C.P.; CRUZ, ROBINSON C.D.; GATELY, NOEL M.; DEVINE, DECLAN M; GIOVANELA, MARCELO; ROESCH-ELY, MARIANA; CRESPO, JANAINA S. Cosmetic gloves from natural rubber latex for upper limb prostheses: Preparation and physicochemical, mechanical and biological characterization. Biomedical Engineering Advances, v. 7, p. 100126, 2024.

SARTORI, P.; DEMORI, R.; SHEN, B. S. C.; TEIXEIRA, D.; STEFFEN, L. A.; CATAFESTA, J.; ELY, M. R.; GIOVANELA, MARCELO; CRESPO, J. S. Fibras poliméricas, elementos filtrantes, seus processos de produção e seus usos. 2022, Brasil. Patente: Privilégio de Inovação. Número do registro: BR1020220120048, título: "Fibras poliméricas, elementos filtrantes, seus processos de produção e seus usos", Instituição de registro: INPI - Instituto Nacional da Propriedade Industrial. **Filed: 17/06/2022**. Instituição(ões) financiadora(s): FINEP; CAPES; UCS; Indústria Mecânica NTC Ltda.

SARTORI, Paula; DEVINE, DECLAN M.; GIOVANELA, MARCELO; CRESPO, J. S. PA6-AgNPS microfibers for application as an antibacterial and antiviral filter element in facial respirators. In: Bioengineering in Ireland, 2024. BIOENGINEERING IN IRELAND, 2024.

SARTORI, P.; DEMORI, R.; CATAFESTA, J.; ELY, M. R.; GIOVANELA, MARCELO; CRESPO, J. S. Avaliação antimicrobiana de diferentes concentrações de nanopartículas de prata suportadas em uma matriz de microfibras poliméricas. In: II InovaBiotec - Congresso de Inovação e Biotecnologia, 2021, Lajeado. Anais do II Congresso de Inovação e Biotecnologia, 2021.

SARTORI, Paula. PA6-AgNPS microfibers for application as an antibacterial and antiviral filter element in facial respirators. (Poster presentation) In: PhD International Week, Hochschule Trier, German, 2024.

REFERENCES

AL-ATTABI, Riyadh *et al.* Durable and comfortable electrospun nanofiber membranes for face mask applications. **Separation and Purification Technology**, [*s. l.*], v. 322, n. June, 2023.

ALAEDDIN, Mohammad Mahdi *et al.* Development and optimization of electrospun respiratory face masks utilizing PVDF, graphene oxide, and copper oxide nanoparticles for enhanced efficiency and antiviral protection. **Carbon Trends**, [*s. l.*], v. 20, n. January, 2025.

ALAHMADI, N. S. *et al.* Synthesis and antimicrobial effects of highly dispersed, cellulose-stabilized silver/cellulose nanocomposites. **RSC Advances**, [*s. l.*], v. 8, n. 7, p. 3646–3656, 2018.

ALBUQUERQUE, D *et al.* Biosensors and Bioelectronics Combined detection of molecular and serological signatures of viral infections : The dual assay concept. [*s. l.*], v. 210, n. April, 2022.

ALIZADEH, Fahimeh; KHODAVANDI, Alireza. Systematic Review and Meta-Analysis of the Efficacy of Nanoscale Materials against Coronaviruses-Possible Potential Antiviral Agents for SARS-CoV-2. **IEEE Transactions on Nanobioscience**, [*s. l.*], v. 19, n. 3, p. 485–497, 2020.

ALJOHANI, Meshari *et al.* Electrospun AgNPs-polylactate nanofibers and their antimicrobial applications. **Reactive and Functional Polymers**, [*s. l.*], v. 167, n. July, p. 104999, 2021. Disponível em: https://doi.org/10.1016/j.reactfunctpolym.2021.104999.

ALLAWADHI, Prince *et al.* Silver nanoparticle based multifunctional approach for combating COVID-19. **Sensors International**, [*s. l.*], v. 2, n. May, p. 100101, 2021. Disponível em: https://doi.org/10.1016/j.sintl.2021.100101.

ALOSAIMI, Abeer M. *et al.* Review on Biomedical Advances of Hybrid

Nanocomposite Biopolymeric Materials. **Bioengineering**, [*s. l.*], v. 10, n. 3, p. 1–16, 2023.

ALTOMARE, Angela *et al.* QUALX2.0: A qualitative phase analysis software using the freely available database POW-COD. **Journal of Applied Crystallography**, [*s. l.*], v. 48, p. 598–603, 2015.

ALVARENGA, Augusto D. *et al.* Effect of static electricity and thickness of solution blow spun polyamide 6/AgNP nanofibrous membrane on nanoparticle filtration and microbiological activity. **Applied Surface Science**, [*s. l.*], v. 652, n. December 2023, 2024.

ALVARENGA, Augusto D. *et al.* Multifunctional and sustainable soot-modified nanofibrous membrane for adsorption, sensing and hydrogen peroxide electrogeneration. **Journal of Cleaner Production**, [*s. l.*], v. 422, n. May, 2023.

ALVARENGA, Augusto D. *et al.* Nanofibrous filtering membranes modified with sucrose-derived carbonaceous materials for adsorption in batch and fixed bed. **Chemical Engineering Journal**, [*s. l.*], v. 451, n. P1, p. 138557, 2023. Disponível em: https://doi.org/10.1016/j.cej.2022.138557.

ANUAR, Azra Umairah *et al.* Graphene oxide nanoparticles synthesized from waste tires: A multi-faceted analysis of structure, morphology and antibacterial behavior. **Nano-Structures and Nano-Objects**, [*s. l.*], v. 38, n. March, p. 101176, 2024. Disponível em: https://doi.org/10.1016/j.nanoso.2024.101176.

AZIZ, Shujahadeen B. *et al.* Polymer blending as a novel approach for tuning the SPR peaks of silver nanoparticles. **Polymers**, [*s. l.*], v. 9, n. 10, p. 486, 2017.

BADONI, Ayush; PRAKASH, Jai. Noble metal nanoparticles and graphene oxide based hybrid nanostructures for antibacterial applications: Recent advances, synergistic antibacterial activities, and mechanistic approaches. **Micro and Nano Engineering**, [*s. l.*], v. 22, n. August 2023, p. 100239, 2024. Disponível em: https://doi.org/10.1016/j.mne.2024.100239.

BAKR, Zeinab *et al.* Silver-Nanoparticle- and Silver-Nitrate-Induced Antioxidant

Disbalance, Molecular Damage, and Histochemical Change on the Land Slug (Lehmannia nyctelia) Using Multibiomarkers. **Frontiers in Physiology**, [*s. l.*], v. 13, n. August, p. 1–13, 2022.

BARTOSZKO, Jessica J. *et al.* Medical masks vs N95 respirators for preventing COVID-19 in healthcare workers: A systematic review and meta-analysis of randomized trials. **Influenza and other Respiratory Viruses**, [*s. l.*], v. 14, n. 4, p. 365–373, 2020.

BARTSCH, Sarah M *et al.* Maintaining face mask use before and after achieving different COVID-19 vaccination coverage levels: a modelling study. **The Lancet Public Health**, [*s. l.*], v. 2667, n. 22, 2022. Disponível em: http://dx.doi.org/10.1016/S2468-2667(22)00040-8.

BENTEDLAOUTI, Kaouter; BELOUATEK, Aissa; KEBAILI, Nouari. Antibacterial and antioxidant activities of graphene and graphene oxide synthesis coated silver nanoparticules. **Journal of Crystal Growth**, [*s. l.*], v. 627, n. September 2023, p. 127527, 2024. Disponível em: https://doi.org/10.1016/j.jcrysgro.2023.127527.

BORTOLASSI, Ana Claudia Canalli *et al.* Efficient nanoparticles removal and bactericidal action of electrospun nanofibers membranes for air filtration. **Materials Science and Engineering C**, [*s. l.*], v. 102, n. October 2018, p. 718–729, 2019.

CHAUDHARY, Rashi *et al.* Antibacterial activity of reduced graphene-silver oxide nanocomposite against gram-negative bacteria. **Microbe (Netherlands)**, [*s. l.*], v. 5, n. December, p. 100221, 2024. Disponível em: https://doi.org/10.1016/j.microb.2024.100221.

CHEAH, Yt Jun *et al.* Gelatin–chitosan–cellulose nanocrystals as an acellular scaffold for wound healing application: fabrication, characterisation and cytocompatibility towards primary human skin cells. **Cellulose**, [*s. l.*], v. 30, n. 8, p. 5071–5092, 2023. Disponível em: https://doi.org/10.1007/s10570-023-05212-w.

CHEN, Yi Ning *et al.* Antiviral activity of graphene–silver nanocomposites against non-

enveloped and enveloped viruses. **International Journal of Environmental Research and Public Health**, [*s. l.*], v. 13, n. 4, p. 4–6, 2016.

CHEN, Lu; LIANG, Jiangong. An overview of functional nanoparticles as novel emerging antiviral therapeutic agents. **Materials Science and Engineering C**, [*s. l.*], v. 112, n. January 2019, p. 110924, 2020. Disponível em: https://doi.org/10.1016/j.msec.2020.110924.

CHENG, Tien Hsin *et al.* Studies of the antimicrobial ability and silver ions migration from silver nitrate-incorporated electrospun nylon nanofibers. **Food Packaging and Shelf Life**, [*s. l.*], v. 16, n. October 2017, p. 129–137, 2018. Disponível em: https://doi.org/10.1016/j.fpsl.2018.03.003.

CHENG, Zi Qiang *et al.* Surface-enhanced Raman scattering effect of silver nanoparticles array. **Wuli Xuebao/Acta Physica Sinica**, [*s. l.*], v. 67, n. 19, 2018.

DADOL, Glebert C. *et al.* Solution blow spinning (SBS) and SBS-spun nanofibers: Materials, methods, and applications. **Materials Today Communications**, [*s. l.*], v. 25, n. September, p. 101656, 2020. Disponível em: https://doi.org/10.1016/j.mtcomm.2020.101656.

DARISTOTLE, John L. *et al.* A Review of the Fundamental Principles and Applications of Solution Blow Spinning. **ACS Applied Materials and Interfaces**, [*s. l.*], v. 8, n. 51, p. 34951–34963, 2016.

DOS SANTOS, Danilo M. *et al.* Advances in Functional Polymer Nanofibers: From Spinning Fabrication Techniques to Recent Biomedical Applications. **ACS applied materials & interfaces**, [*s. l.*], v. 12, n. 41, p. 45673–45701, 2020.

EL-ATAB, Nazek *et al.* Flexible Nanoporous Template for the Design and Development of Reusable Anti-COVID-19 Hydrophobic Face Masks. **ACS Nano**, [*s. l.*], v. 14, n. 6, p. 7659–7665, 2020.

EL-SEEDI, Hesham R. *et al.* Gelatin nanofibers: Recent insights in synthesis, bio-medical applications and limitations. **Heliyon**, [*s. l.*], v. 9, n. 5, p. e16228, 2023. Disponível

em: https://doi.org/10.1016/j.heliyon.2023.e16228.

FARIVAR, Farzaneh *et al.* Thermogravimetric Analysis (TGA) of Graphene Materials: Effect of Particle Size of Graphene, Graphene Oxide and Graphite on Thermal Parameters. **C**, [*s. l.*], v. 7, n. 2, p. 41, 2021. Disponível em: https://www.mdpi.com/2311-5629/7/2/41.

FORMENTINI, Giovanni *et al.* Challenging the engineering design process for the development of facial masks in the constraint of the COVID-19 pandemic. **Procedia CIRP**, [*s. l.*], v. 100, p. 660–665, 2021. Disponível em: https://doi.org/10.1016/j.procir.2021.05.140.

FU, Lung Ming *et al.* Process optimization of silver nanoparticle synthesis and its application in mercury detection. **Micromachines**, [*s. l.*], v. 12, n. 9, p. 1–16, 2021.

GAO, Yuan *et al.* Recent progress and challenges in solution blow spinning. **Materials Horizons**, [*s. l.*], v. 8, n. 2, p. 426–446, 2021.

HAN, Yongyue *et al.* Protein-based biomaterials for combating viral infections: Current status and future prospects for development. **Biosafety and Health**, [*s. l.*], v. 4, n. 2, p. 87–94, 2022. Disponível em: https://doi.org/10.1016/j.bsheal.2022.03.005.

HASAN, K. M.Faridul *et al.* Colorful and antibacterial nylon fabric via in-situ biosynthesis of chitosan mediated nanosilver. **Journal of Materials Research and Technology**, [*s. l.*], v. 9, n. 6, p. 16135–16145, 2020. Disponível em: https://doi.org/10.1016/j.jmrt.2020.11.056.

HASHMI, Motahira; ULLAH, Sana; KIM, Ick Soo. Copper oxide (CuO) loaded polyacrylonitrile (PAN) nanofiber membranes for antimicrobial breath mask applications. **Current Research in Biotechnology**, [*s. l.*], v. 1, p. 1–10, 2019. Disponível em: https://doi.org/10.1016/j.crbiot.2019.07.001.

HIRAGOND, Chaitanya B. *et al.* Enhanced anti-microbial response of commercial face mask using colloidal silver nanoparticles. **Vacuum**, [*s. l.*], v. 156, n. August, p. 475–482, 2018. Disponível em: https://doi.org/10.1016/j.vacuum.2018.08.007.

HUANG, Te Yang; LIN, Jr Ying; SU, Wen Ta. Coaxial nanofibers encapsulated with Ampelopsis brevipedunculata extract and green synthesized AgNPs for wound repair. **Colloids and Surfaces B: Biointerfaces**, [*s. l.*], v. 235, n. December 2023, p. 113771, 2024. Disponível em: https://doi.org/10.1016/j.colsurfb.2024.113771.

HUSSAIN, Zahid *et al.* **Silver nanoparticles: A promising nanoplatform for targeted delivery of therapeutics and optimized therapeutic efficacy**. [*S. l.*]: Elsevier Inc., 2019. *E-book*. Disponível em: http://dx.doi.org/10.1016/B978-0-12-816960-5.00009-4.

INTERNATIONAL ORGANIZATION FOR STANDARDIZATION. Nanotechnologies — Structural characterization of graphene — Part 1: Graphene from powders and dispersions. *In*: [*S. l.: s. n.*], 2021.

J GONZALEZ, Benito *et al.* Solution Blow Spinning and Obtaining Submicrometric Fibers of Different Polymers. **International Journal of Nanoparticles and Nanotechnology**, [*s. l.*], v. 3, n. 1, p. 1–10, 2017.

KRUSZEWSKI, Marcin *et al.* **Toxicity of Silver Nanomaterials in Higher Eukaryotes**. [*S. l.: s. n.*], 2011-. ISSN 18720854.v. 5

KUBO, Anna Liisa *et al.* Antibacterial and Antiviral Effects of Ag, Cu and Zn Metals, Respective Nanoparticles and Filter Materials Thereof against Coronavirus SARS-CoV-2 and Influenza A Virus. **Pharmaceutics**, [*s. l.*], v. 14, n. 12, p. 1–19, 2022.

KUMAR, Gul *et al.* Development of cellulose acetate/CuO/AgNP nanofibers based effective antimicrobial wound dressing. **Composites Communications**, [*s. l.*], v. 39, n. March, p. 101550, 2023. Disponível em: https://doi.org/10.1016/j.coco.2023.101550.

LAHOTI, Ronith; CARROLL, Dusty. Green Synthesis of Zinc Oxide Nanoparticles and their Applications - fisheriesindia.com. **Next Research**, [*s. l.*], v. 2, n. 1, p. 100164, 2025. Disponível em: https://www.fisheriesindia.com/2020/05/green-synthesis-of-zinc-oxide.html.

LEE, Seungsin. Developing UV-protective textiles based on electrospun zinc oxide

nanocomposite fibers. **Fibers and Polymers**, [*s. l.*], v. 10, n. 3, p. 295–301, 2009.

LI, Y. *et al.* Antimicrobial effect of surgical masks coated with nanoparticles. **Journal of Hospital Infection**, [*s. l.*], v. 62, n. 1, p. 58–63, 2006.

LI, D *et al.* Facial protection in the era of COVID-19: A narrative review. **Oral Dis.**, [*s. l.*], v. 27, n. 3, p. 665–673, 2021. Disponível em: https://onlinelibrary.wiley.com/doi/pdf/10.1111/odi.13460?src=getftr.

LV, Huaxin *et al.* AgNPs-incorporated nanofiber mats: Relationship between AgNPs size/content, silver release, cytotoxicity, and antibacterial activity. **Materials Science and Engineering C**, [*s. l.*], v. 118, n. July 2020, p. 111331, 2021. Disponível em: https://doi.org/10.1016/j.msec.2020.111331.

MA, Qing Xia *et al.* Potential utilities of mask-wearing and instant hand hygiene for fighting SARS-CoV-2. **Journal of Medical Virology**, [*s. l.*], v. 92, n. 9, p. 1567–1571, 2020.

MALISZEWSKA, Irena; CZAPKA, Tomasz. Electrospun Polymer Nanofibers with Antimicrobial Activity. **Polymers**, [*s. l.*], v. 14, n. 9, p. 1–32, 2022.

MARTIN, Megan E. *et al.* Silver nanoparticles alter epithelial basement membrane integrity, cell adhesion molecule expression, and TGF-β1 secretion. **Nanomedicine: Nanotechnology, Biology, and Medicine**, [*s. l.*], v. 21, p. 102070, 2019. Disponível em: https://doi.org/10.1016/j.nano.2019.102070.

MEDEIROS, Eliton S. *et al.* Solution blow spinning: A new method to produce micro- and nanofibers from polymer solutions. **Journal of Applied Polymer Science**, [*s. l.*], v. 113, n. 4, p. 2322–2330, 2009.

MILAZZO, Mario *et al.* Biodegradable polymeric micro/Nano-structures with intrinsic antifouling/antimicrobial properties: Relevance in damaged skin and other biomedical applications. **Journal of Functional Biomaterials**, [*s. l.*], v. 11, n. 3, p. 1–20, 2020.

MONSORES, Karollyne Gomes de Castro *et al.* Production of nanofibers from solution

blow spinning (SBS). **Journal of Materials Research and Technology**, [*s. l.*], v. 16, p. 1824–1831, 2022.

MORAIS, Fernando G. *et al.* Filtration efficiency of a large set of COVID-19 face masks commonly used in Brazil. **Aerosol Science and Technology**, [*s. l.*], v. 55, n. 9, p. 1028–1041, 2021. Disponível em: https://doi.org/10.1080/02786826.2021.1915466.

MORENO-SAMANIEGO, Mishell *et al.* Green synthesis of copper oxide nanoparticles using Eucalyptus globulus extract with effective bactericidal activity for river water treatment. **Results in Engineering**, [*s. l.*], v. 24, n. August, 2024.

NAQVI, Ahmad Abu Turab *et al.* Insights into SARS-CoV-2 genome, structure, evolution, pathogenesis and therapies: Structural genomics approach. **Biochimica et Biophysica Acta - Molecular Basis of Disease**, [*s. l.*], v. 1866, n. 10, p. 165878, 2020. Disponível em: https://doi.org/10.1016/j.bbadis.2020.165878.

NATIONAL INSTITUTES OF H; EALTH. Guidance Document on Using In Vitro Data to Estimate In Vivo Starting Doses for Acute Toxicity. **NIH Publication No: 01-4500**, [*s. l.*], v. 2015, n. 22/06/2015, p. 1–102, 2015.

NGUYEN, Lam Nhat; KANNEGANTI, Thirumala Devi. PANoptosis in Viral Infection: The Missing Puzzle Piece in the Cell Death Field. **Journal of Molecular Biology**, [*s. l.*], v. 434, n. 4, p. 167249, 2022. Disponível em: https://doi.org/10.1016/j.jmb.2021.167249.

NICOLAU, Géssica Da Silva *et al.* Influence of solution concentration on recycled polycarbonate nanofibers produced by solution blow-spinning process: A short communication. **Journal of Materials Research and Technology**, [*s. l.*], v. 21, p. 1454–1460, 2022.

NIKAEEN, Ghazal; ABBASZADEH, Sepideh; YOUSEFINEJAD, Saeed. Application of nanomaterials in treatment, anti-infection and detection of coronaviruses. **Nanomedicine**, [*s. l.*], v. 15, n. 15, p. 1501–1512, 2020.

NIU, Jianxing *et al.* Janus fibrous membrane with enhanced air filtration performance

and one-way water transport capability for advanced face mask filters. **Separation and Purification Technology**, [*s. l.*], v. 355, n. PA, p. 129539, 2025. Disponível em: https://doi.org/10.1016/j.seppur.2024.129539.

NOGUEIRA, T; PONCE, R. O vírus da Gripe. **Revista de Ciência Elementar**, [*s. l.*], v. 9, n. 2, 2021.

OULIDI, Oumayma *et al.* Incorporation of olive pomace as a natural filler in to the PA6 matrix: Effect on the structure and thermal properties of synthetic Polyamide 6. **Chemical Engineering Journal Advances**, [*s. l.*], v. 12, n. September, p. 100399, 2022. Disponível em: https://doi.org/10.1016/j.ceja.2022.100399.

PALANI, Naveen *et al.* Electrospun nanofibers synthesized from polymers incorporated with bioactive compounds for wound healing. **Journal of Nanobiotechnology**, [*s. l.*], v. 22, n. 1, p. 1–30, 2024. Disponível em: https://doi.org/10.1186/s12951-024-02491-8.

PALMIERI, Valentina *et al.* Face masks and nanotechnology: Keep the blue side up. **Nano Today**, [*s. l.*], v. 37, p. 101077, 2021. Disponível em: https://doi.org/10.1016/j.nantod.2021.101077.

PARK, Kyuhyun *et al.* Fabrication of silver nanowire coated fibrous air filter medium via a two-step process of electrospinning and electrospray for anti-bioaerosol treatment. **Journal of Hazardous Materials**, [*s. l.*], v. 411, n. January, p. 125043, 2021. Disponível em: https://doi.org/10.1016/j.jhazmat.2021.125043.

PELLETT, Philip E.; MITRA, Subhash; HOLLAND, Thomas C. **Basics of virology**. 1. ed. [*S. l.*]: Elsevier B.V., 2014-. ISSN 00729752.v. 123 Disponível em: http://dx.doi.org/10.1016/B978-0-444-53488-0.00002-X.

PERUMBILAVIL, Sreekanth *et al.* White light Z-scan measurements of ultrafast optical nonlinearity in reduced graphene oxide nanosheets in the 400–700 nm region. **Applied Physics Letters**, [*s. l.*], v. 107, n. 5, 2015. Disponível em:

https://pubs.aip.org/apl/article/107/5/051104/29691/White-light-Z-scan-measurements-of-ultrafast.

RAJAN, Ramachandran *et al.* A review on the toxicity of silver nanoparticles against different biosystems. **Chemosphere**, [*s. l.*], v. 292, n. October 2021, p. 133397, 2022. Disponível em: https://doi.org/10.1016/j.chemosphere.2021.133397.

RHAZOUANI, Asmaa *et al.* Can the application of graphene oxide contribute to the fight against COVID-19? Antiviral activity, diagnosis and prevention. **Current Research in Pharmacology and Drug Discovery**, [*s. l.*], v. 2, n. October, p. 100062, 2021. Disponível em: https://doi.org/10.1016/j.crphar.2021.100062.

RODRIGUES, Murilo Álison Vigilato *et al.* Comparing solution blow spinning and electrospinning methods to produce collagen and gelatin ultrathin fibers: A review. **International Journal of Biological Macromolecules**, [*s. l.*], v. 283, n. September, 2024.

RUSSO, Francesca *et al.* A review on electrospun membranes for potential air filtration application. **Journal of Environmental Chemical Engineering**, [*s. l.*], v. 10, n. 5, 2022.

SALAM, Abdul *et al.* Electrospun nanofiber-based viroblock/ZnO/PAN hybrid antiviral nanocomposite for personal protective applications. **Nanomaterials**, [*s. l.*], v. 11, n. 9, 2021.

SAMBALE, F. *et al.* Investigations of the toxic effect of silver nanoparticles on mammalian cell lines. **Journal of Nanomaterials**, [*s. l.*], v. 2015, 2015.

SARTORI, Paula *et al.* Silver Nitrate from Recovered Silver of Spent Ag2O Button Cells: Synthesis and Characterization. **Journal of Sustainable Metallurgy**, [*s. l.*], v. 6, n. 4, p. 557–562, 2020. Disponível em: https://doi.org/10.1007/s40831-020-00307-1.

SARTORI, Paula *et al.* Synthesis and Characterization of Silver Nanoparticles for the Preparation of Chitosan Pellets and Their Application in Industrial Wastewater Disinfection. **Water (Switzerland)**, [*s. l.*], v. 15, n. 1, 2023.

SEIFI, Tahereh; REZA KAMALI, Ali. Antiviral performance of graphene-based materials with emphasis on COVID-19: A review. **Medicine in Drug Discovery**, [*s. l.*], v. 11, n. May, 2021.

SHADI SAEIDI, Seyedeh *et al.* Synthesis and improving antibacterial effectiveness of Ag/Co3V2O8 nanocomposites by graphene oxide for biomedical applications. **Materials Science and Engineering: B**, [*s. l.*], v. 306, n. June, p. 117457, 2024. Disponível em: https://doi.org/10.1016/j.mseb.2024.117457.

SHANMUGAM, Rajeshkumar *et al.* Journal of the Indian Chemical Society Green synthesis of iron oxide nanoparticles using Cissus rotundifolia and its antibacterial activity against wound pathogens. **Journal of the Indian Chemical Society**, [*s. l.*], v. 102, n. 3, p. 101599, 2025. Disponível em: https://doi.org/10.1016/j.jics.2025.101599.

SHARMA, Abhishek *et al.* Graphene oxide/silver nanoparticle (GO/AgNP) impregnated polyacrylonitrile nanofibers for potential application in air filtration. **Nano-Structures and Nano-Objects**, [*s. l.*], v. 26, p. 100708, 2021. Disponível em: https://doi.org/10.1016/j.nanoso.2021.100708.

SHI, Quan *et al.* One-step synthesis of silver nanoparticle-filled nylon 6 nanofibers and their antibacterial properties. **Journal of Materials Chemistry**, [*s. l.*], v. 21, n. 28, p. 10330–10335, 2011.

SONI, Nupur; DINDA, Amit; KUMAR, Vipin. An integrative approach to harnessing the potential of Traditional Indian Medicinal plants for acute viral infections. **Journal of Herbal Medicine**, [*s. l.*], v. 33, n. April, p. 100559, 2022. Disponível em: https://doi.org/10.1016/j.hermed.2022.100559.

SOUTER, P *et al.* The variable toxicity of silver ions in cell culture media. **Toxicology in Vitro**, [*s. l.*], v. 60, p. 154–159, 2019.

SYED, S. Silver recovery aqueous techniques from diverse sources: Hydrometallurgy

in recycling. *In*: WASTE MANAGEMENT. [*S. l.*]: Elsevier Ltd, 2016. v. 50, p. 234–256. Disponível em: http://dx.doi.org/10.1016/j.wasman.2016.02.006.

TANG, Shaoheng; ZHENG, Jie. Antibacterial Activity of Silver Nanoparticles: Structural Effects. **Advanced Healthcare Materials**, [*s. l.*], v. 7, n. 13, p. 1–10, 2018.

TCHARKHTCHI, A. *et al.* An overview of filtration efficiency through the masks: Mechanisms of the aerosols penetration. **Bioactive Materials**, [*s. l.*], v. 6, n. 1, p. 106–122, 2021.

THE SILVER INSTITUTE. **World Silver Survey 2025**. [*S. l.: s. n.*], 2025.

UNNIKRISHNAN, Gayathri *et al.* Synthesis and analysis of multifunctional graphene oxide/Ag2O-PVA/chitosan hybrid polymeric composite for wound healing applications. **International Journal of Biological Macromolecules**, [*s. l.*], v. 277, n. P2, p. 134301, 2024. Disponível em: https://doi.org/10.1016/j.ijbiomac.2024.134301.

USKOKOVIĆ, Vuk. Why have nanotechnologies been underutilized in the global uprising against the coronavirus pandemic?. **Nanomedicine**, [*s. l.*], v. 15, n. 17, p. 1719–1734, 2020.

VISCUSI, Gianluca *et al.* Production of electrospun hybrid membranes based on polyamide 6 reinforced with hemp fibers dissolved in 1-ethyl-3-methylimidazolium dicyanamide ionic liquid. **Journal of Molecular Liquids**, [*s. l.*], v. 387, n. April, p. 122656, 2023. Disponível em: https://doi.org/10.1016/j.molliq.2023.122656.

VITCHULI, Narendiran *et al.* Electrospun Ultrathin Nylon Fibers for Protective Applications. **Journal ofAppliedPolymer Science**, [*s. l.*], v. 116, p. 2181–2187, 2010.

WANG, Ling *et al.* Biodegradable and high-performance multiscale structured nanofiber membrane as mask filter media via poly(lactic acid) electrospinning. **Journal of Colloid and Interface Science**, [*s. l.*], v. 606, p. 961–970, 2022. Disponível em: https://doi.org/10.1016/j.jcis.2021.08.079.

WHO. **Coronavirus disease (COVID-19): Masks**. [*S. l.*], 2022. Disponível em: https://www.who.int/emergencies/diseases/novel-coronavirus-2019/question-and-answers-hub/q-a-detail/coronavirus-disease-covid-19-masks. Acesso em: 16 mar. 2022.

WHO. **WHO Coronavirus (COVID-19) Dashboard**. [*S. l.*], 2022. Disponível em: https://covid19.who.int/table. Acesso em: 15 ago. 2023.

WIELER, Laura *et al.* Reduction in the COVID-19 pneumonia case fatality rate by silver nanoparticles: A randomized case study. **Heliyon**, [*s. l.*], v. 9, n. 3, p. e14419, 2023. Disponível em: https://doi.org/10.1016/j.heliyon.2023.e14419.

XU, Yuanqiang *et al.* Micro/nanofibrous nonwovens with high filtration performance and radiative heat dissipation property for personal protective face mask. **Chemical Engineering Journal**, [*s. l.*], v. 423, n. May, p. 130175, 2021. Disponível em: https://doi.org/10.1016/j.cej.2021.130175.

XU, Wenshi *et al.* Research progress of advanced polymer composite antibacterial materials based on electrospinning. **European Polymer Journal**, [*s. l.*], v. 222, n. November 2024, p. 113623, 2025. Disponível em: https://doi.org/10.1016/j.eurpolymj.2024.113623.

YAN, Shaole *et al.* The formation of ultrafine polyamide 6 nanofiber membranes with needleless electrospinning for air filtration. **Polymers for Advanced Technologies**, [*s. l.*], v. 30, n. 7, p. 1635–1643, 2019.

YE, Shiyi *et al.* Antiviral Activity of Graphene Oxide: How Sharp Edged Structure and Charge Matter. **ACS Applied Materials and Interfaces**, [*s. l.*], v. 7, n. 38, p. 21578–21579, 2015.

ZERAATI, Malihe *et al.* Optimization and predictive modelling for the diameter of nylon-6,6 nanofibers via electrospinning for coronavirus face masks. **Journal of Saudi Chemical Society**, [*s. l.*], v. 25, n. 11, p. 101348, 2021. Disponível em: https://doi.org/10.1016/j.jscs.2021.101348.

ZHANG, Lu *et al.* Multilayer electrospun nanofibrous membranes with antibacterial property for air filtration. **Applied Surface Science**, [*s. l.*], v. 515, n. March, 2020.

ZHANG, Xin; XU, Jing; LIU, Junjie. Nanoscale architecture: Enhancing the performance of nanofiber air filters with bead-on-string structures. **Separation and Purification Technology**, [*s. l.*], v. 360, n. P1, p. 131004, 2025. Disponível em: https://doi.org/10.1016/j.seppur.2024.131004.

ZIKALALA, Nkosingiphile E. *et al.* Green synthesis of reduced graphene oxide using Persea americana mill. extract: Characterization, oxygen reduction reaction and antibacterial application. **Diamond and Related Materials**, [*s. l.*], v. 149, n. September, 2024.

ANNEX A

Annex A – Graphene Oxide Datasheet, from BoomaTech Company.

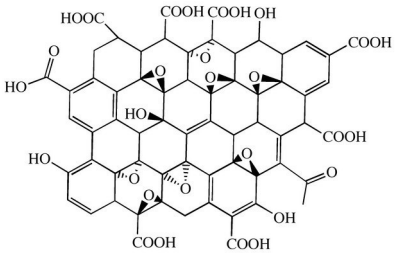

Product DataSheet

BoomaTech Graphene Oxide (GO)

Properties

Form	Liquid dispersion
Particle size (laser diffraction)	D90 25-28 µm
	D50 13-15 µm
	D10 6-7 µm
Color	Brown
Odor	Odorless
Dispersibility	Polar solvents
Apparent density	0.2-0.4 gr/mL
Humidity (TGA)	13-16%

Elemental Analysis

Carbon	49-56%
Hydrogen	1-2%
Nitrogen	0-1%
Sulfur	2-4%
Oxygen	41-50%

SEM image*

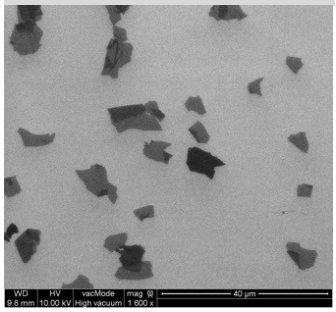

SEM image**

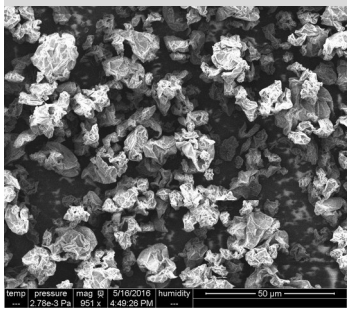

TGA

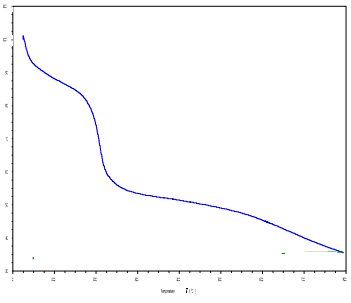

(*) 0.5mg/mL water dispersion (**) Powder format

www.booma-tech.com